2021

# The Identification of a Leptin Dependent Neural Pathway Regulating Adipose Tissue Innervation

Putianqi Wang


# THE IDENTIFICATION OF A LEPTIN DEPENDENT NEURAL PATHWAY REGULATING ADIPOSE TISSUE INNERVATION

A Thesis Presented to the Faculty of
The Rockefeller University
in Partial Fulfillment of the Requirements for
the degree of Doctor of Philosophy

by
Putianqi Wang
June 2021

# THE IDENTIFICATION OF A LEPTIN DEPENDENT NEURAL PATHWAY REGULATING ADIPOSE TISSUE INNERVATION

Putianqi Wang, Ph.D.
The Rockefeller University 2021

Leptin, secreted by the adipose tissue, is an afferent signal of a negative feedback loop that regulates body weight balance through its effects on feeding and energy expenditure. Mutations in the leptin gene or its cognate receptor result in severe obesity in both human and mice. My thesis work revealed a leptin-dependent, plastic pathway spanning the central to peripheral nervous system that is responsible for regulating energy homeostasis in mice.

Leptin deficient (*ob/ob*) mice accumulate excessive fat mass due to increased food intake, and decreased energy expenditure partially as a result of defective fat utilization. Chronic leptin delivery to *ob/ob* mice reverses both phenotypes and leads to drastic fat loss. In contrast, dietary restriction of *ob/ob* mice fails to increase energy expenditure and results in reduced lean body mass rather than fat mass. These findings indicate that leptin is necessary for mice to efficiently utilize fat as energy source, however, the underlying mechanism is not known. The sympathetic nervous system (SNS) is the major regulator of several critical steps involved in fat utilization, we therefore hypothesized that leptin might regulate the plasticity of SNS innervation of adipose tissue to promote fat usage.

We first visualized SNS innervation, using a whole-mount tissue clearing method (Adipo-Clear) paired with light sheet microscopy imaging, in both brown adipose tissue (BAT) and inguinal white adipose tissue (iWAT) of wild-type (WT) and *ob/ob* mice. Surprisingly, we found that *ob/ob* mice have a profound, around six-fold, reduction of SNS innervation density in both BAT and iWAT compared to age matched WT mice. The same phenotype was also observed in *db/db* mice which carry a mutation in leptin receptor. Furthermore, we showed that exogenous leptin delivery to adult *ob/ob* mice for 14 days through a subcutaneous osmotic pump normalizes their SNS innervation levels in both BAT and iWAT to WT level. This effect is independent of leptin-induced anorexia because *ob/ob* mice pair-fed to their leptin treated littermates fail to show any innervation increase in adipose tissues. These findings demonstrate that leptin regulates SNS innervation plasticity in adipose tissue.

We then tested whether restoring adipose tissue innervation structure in *ob/ob* mice is sufficient to correct their fat utilization defects, such as thermogenesis and lipolysis defects. Thermogenesis is the process that dissipates energy as heat from BAT in cold conditions; and lipolysis is the process that breaks down lipid storage from iWAT to meet energy demand of other organs in times of privation. We first exposed mice to cold challenge and found that *ob/ob* mice, having BAT innervation density restored but having no leptin in serum, can still activate BAT thermogenesis similarly as WT mice. In contrast, *ob/ob* mice, not having innervation restored but having high leptin level in serum, fail to activate thermogenesis and succumb to cold just like their *ob/ob* littermates given no leptin treatment. This experiment led us to the surprising finding that SNS structure, rather than active leptin signaling, is critical for thermogenesis. Additionally, we observed similar trends when we fasted *ob/ob* mice to induce lipolysis from iWAT. In aggregate,

these findings confirm our hypothesis that leptin regulates structural plasticity of SNS in adipose tissue, which in turn promotes fat utilization and energy expenditure.

We next uncovered the neural mechanism underlying leptin dependent innervation regulation. We identified LepR expressing neurons in the arcuate nucleus of hypothalamus (ARC) as regulators of SNS innervation. In WT mice, either genetic deletion of LepR in ARC or diet induced leptin signaling loss in ARC leads to dramatic SNS innervation reduction in both BAT and iWAT. There are two major LepR expressing neuron populations in the ARC, agouti related peptide (AGRP) neurons and pro-opiomelanocortin (POMC) neurons. We employed a CRISPR-based gene editing strategy to selectively delete LepR in either AGRP or POMC neurons and found that leptin signaling loss in either population leads to same level of SNS innervation reduction in adipose tissue. Moreover, the magnitude of SNS innervation reduction resulted from ablating LepR in either AGRP or POMC is halved comparing to that from ablating LepR in the entire ARC region. These data suggest that AGRP and POMC neurons act synergistically in regulating leptin dependent SNS innervation.

In order to regulate SNS plasticity in adipose tissue, leptin signaling needs to reach sympathetic preganglionic neurons in the spinal cord which act as the conduit between the brain and target-innervating sympathetic neurons in the periphery. However, AGRP and POMC neurons send efferents mostly within the brain, indicating the existence of downstream central populations that mediate leptin's effects on innervation. We identified a group of brain-derived neurotropic factor (BDNF) expressing neurons in the paraventricular nucleus of hypothalamus (PVH) that 1) project directly to the sympathetic preganglionic neurons in the spinal cord, 2) are activated by leptin signaling and receive inputs from both AGPR and POMC neurons, and 3) are necessary for leptin to regulate SNS innervation. In conclusion, leptin requires downstream BDNF signaling to regulate sympathetic plasticity in adipose tissue. These downstream neurons may present therapeutic potentials for treating obesity associated with leptin resistance.

The work mentioned above revealed a novel role of leptin in bidirectionally regulating sympathetic neural plasticity in adipose tissues and its underlying neural mechanism. Large-scale sympathetic neural plasticity is normally only observed during organ development or tissue injuries; therefore, it is important to understand how leptin turns on this process in adult animals. Since little is known about the connectivity between the brain and adipose tissue, we first used retrograde circuit tracing approaches to anatomically characterize the locations of the sympathetic pre- and postganglionic neurons innervating both iWAT and BAT. Interestingly, we found little overlap between iWAT and BAT innervating pre-ganglionic neurons, and zero overlap between post-ganglionic neurons, suggesting that the sympathetic neurons are highly specific to target organs. Furthermore, we revealed that there are similar number of fat innervating postganglionic neurons between WT and *ob/ob* mice, despite the drastic differences in adipose tissue SNS innervation density between these two mouse lines. These results suggest that the gene expression profiles of the fat innervating postganglionic neurons in WT and *ob/ob* mice are distinct. Therefore, we are currently conducting single cell sequencing experiments to uncover the molecular identities of the sympathetic postganglionic neurons in WT and *ob/ob* mice; we also hope to reveal the molecular mechanisms underlying leptin dependent plasticity in these neurons. We believe that targeting fat innervating postganglionic neurons might be a good strategy to treat metabolic diseases, and these experiments might help identify potential therapeutic targets.

*Dedicated to my family members who support me throughout my academic journey.*

**ACKNOWLEDGMENTS**

I would first like to express my deepest gratitude towards my thesis advisor Professor Jeffery Friedman who provided tremendous support and guidance on my graduate work. I really appreciate that Jeff is supportive on new ideas and gives people freedom to explore their own scientific interests, while always providing the strongest scientific and emotional support to his lab members. In my first year working in his laboratory, Jeff told me, "It is more important that you work on something that makes you happy. This is how I started my work on a sympathetic nervous system and obesity. Throughout my graduate training in his lab, Jeff devoted a lot of time sitting down with me to review the data and give me valuable inputs on experimental designs. In addition to being a great scientific advisor, Jeff has always been supportive for my career choices. In my fourth year of graduate school, I had discussions about career options with Jeff and I remember he told me that he will support me on whatever I choose to do, and I feel very grateful about his generosity.

Next, I would like to express my special thanks to my thesis committee members Professor Paul Cohen and Professor Robert Darnell who have provided insightful guidance on my thesis work and been extremely supportive on my career development.

In addition to my mentors, I would like to express my gratitude towards the great people I work with in the Friedman lab. Firstly, the person I need to thank is Ken Loh, who I collaborated with on the first part of my thesis project. We spent numerous hours brainstorming, designing and conducting experiments together, and I learned a lot from him. Besides being a great scientific collaborator, Ken is also a great friend. I enjoyed having meal with him because he has such strong passion about food and desserts. Next, I would like to express my gratitude towards Anoj Ilanges, who is the best bay-mate for the past three years. We worked together developing the single cell sequencing approaches for sympathetic postganglionic neurons. I really enjoy talking about science with him and hearing about his ideas.

I would also like to thank Tan Han for providing generous help with the single cell sequencing experiments; Michelle Wu for her hard work on many experiments included in Chapter 2-4; Marc Schneeberger for helping with thermogenesis experiments in Chapter 2; Xiaofei Yu for designing and cloning the guide RNAs for CRISPR; Christin Kosse for helping with BDNF mouse experiments; Lisa Pomeranz for providing the PRV for tracing; Kristina Hedbacker for generating *ob/ob* mice; Jingyi Chi for advising on AdipoClear imaging, quantification and ex-vivo sympathetic ganglion culture; Zhuhao Wu for providing critical suggestions on data and experimental designs; Paul Muller for advising on sympathetic ganglion dissections and experimental designs; C.H. Choi and François Marchildon for their generous help setting up the metabolic home cages and Clark Electrode measurement; and all other members from the Friedman Laboratory for being great lab-mates. In addition to my lab-mates and collaborators, I also want to thank the staffs at BIRC, FCRC, and Genomic Core who provided excellent equipment training and services. Especially I would like to express my gratitude towards Helen Hong Duan at the Genomic Core, who provided great help and guidance on the single cell sequencing library preparation; Stanka Semova and Songyan Han at the Flow Core, who patiently helped us identify live cell populations and greatly improved our sample quality. Without their patient assistance and expertise, we would not be able to do the single cell sequencing experiments.

Beside the people at Rockefeller University, I also need to thank Donald A. Morgan and Kamal Rahmouni, our collaborators from University of Iowa, who helped conduct sympathetic nerve activity recording in Chapter 2.

Apart from the people I need to acknowledge from work, I also want to express my special and deepest gratitude towards my boyfriend, Cheng Lyu, who has been a great life companion and has provided me with countless emotional supports during our time in graduate school. Lastly, I need to thank my father, Xiaoxiang Wang, and my mother, Yu Tao, as well as my grandparents, who always love and believe in me and support my life and career choices unconditionally. Without these people, I will not be the person I am today.

**TABLE OF CONTENTS**

## LIST OF FIGURES

## LIST OF TABLES

# Chapter 1. Introduction

## 1.1. Leptin and body weight balance

### 1.1.1. Obesity and energy balance

Obesity is a one of the biggest global health issues nowadays. The prevalence of obesity grows continuously over the past decades. Currently in the U.S., more than 42.4% adult, 18.5% children and adolescents are considered obese according to CDC (CDC 2019). Obesity and its comorbidities, such as type II diabetes, cardiovascular diseases and some types of cancer, are causing tremendous burdens to the healthcare system and the society. Despite its accelerating prevalence, the treatment options of obesity are still limited to life-style intervention, bariatric surgery and only a few approved medications (Mayoclinic 2020).

Obesity is a result of imbalance between an organism's energy intake and energy expenditure. Energy intake is usually in the form of food intake, whereas energy expenditure takes is composed of basal metabolic rate, physical activity and adaptive thermogenesis (Spiegelman and Flier 2001, Figure 1.1). Physiological or cellular events that perturb the energy balance equation will lead to or prevent obesity formation. For example, when food is abundant and physical activity is limited, the animal will gradually increase fat storage and become obese eventually. Obesity drugs are being designed to either reduce energy intake or increase one or more components of energy expenditure. However, the efficacy of the currently available anti-obesity drugs is far from satisfying, highlighting the need for new therapeutics.

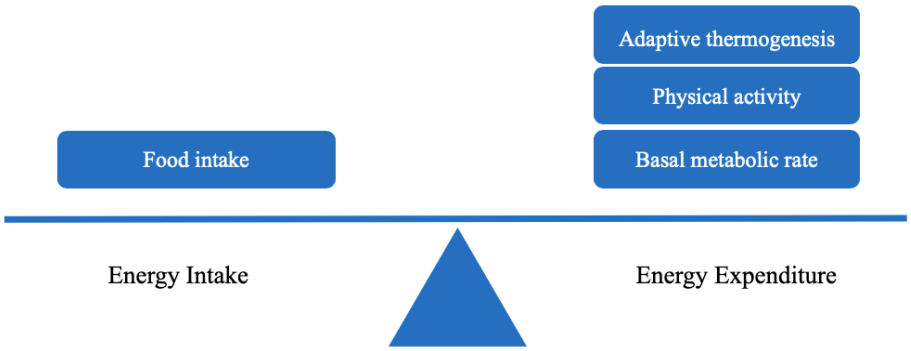


**Figure 1.1 Body weight balance equation**

The two arms of the body weight balance equation are energy intake and energy expenditure. Energy intake is in the form of food intake. Energy expenditure is composed of basal metabolic rate, physical activity and adaptive thermogenesis. Body weight will stay constant only when the two arms are balance.

### 1.1.2. Leptin gene and obesity

The last few decades witnessed the discovery of many obesity-related genes, among which leptin and its receptor are probably the most import ligand-receptor pair responsible for monogenetic obesity syndrome. Loss of function mutations in leptin or leptin receptor leads to server obesity in both humans (Montague et al. 1997; Clément et al. 1998) and mice (Yiying Zhang et al. 1994; Chen et al. 1996). Exogenous leptin delivery to leptin deficient (*ob/ob*) subjects can correct their obese phenotype (Halaas et al. 1995; Farooqi et al. 2002; Pelleymounter et al. 1995). However, obesity resulted from leptin deficiency only account for a small percentage of human obesity. In fact, most obese patients have high level of circulating leptin due to massive fat storage but with impaired responsiveness to leptin signaling, which is leptin resistance. Due to this reason, leptin cannot be used directly as a treatment for most forms of obesity in clinic.

## 1.2. Physiological functions of leptin

### 1.2.1. Leptin as a master regulator of energy homeostasis

Leptin, encoded by the *ob* gene, is an adipose tissue secreted afferent signal that circulates in the blood stream and signals through leptin receptor (LepR), mostly located in brain, to inform the brain about the energy state of an organism. The brain then maintains body weight homeostasis through regulating the organism's feeding behavior and energy expenditure, which are the two arms of the body weight balance equation mentioned above. When animal is in low energy state (eg. starvation), leptin level drops sharply which triggers food seeking behavior and neuroendocrine responses to help conserve energy (Ahima et al. 1996). Conversely when animal's energy storage increases, leptin level goes up to restrict feeding and promote utilization of energy. Leptin operates in such negative feedback loop to maintain energy balance. Leptin deficient *ob/ob* mice accumulate excessive fat mass as results of both excessive overeating and reduced energy expenditure. Leptin delivery to these mice normalizes both phenotype and re-establishes body weight balance. Next we will discuss how leptin carries out its effects.

### 1.2.2. Leptin action in the central nervous system (CNS)

Leptin binds with high affinity with its receptor LepR, which mainly expresses in the CNS. LepR presents in six different isoforms, among which only the long isoform LepRb has intracellular domain capable of activating Jak-STAT signaling pathway. Leptin exerts its behavioral and metabolic functions mainly through the signaling pathways downstream of LepRb (Elmquist et al. 1998). LepRb is present in many regions of the brain but concentrated in the hypothalamus, including the arcuate (ARC), ventromedial (VMH), dorsomedial (DMH) and lateral hypothalamic nuclei. Since leptin was discovered in 1994, our understanding of the how these nuclei mediate leptin's effect has been largely advanced, and summarized below.

### 1.2.3. Role of leptin in appetite control

In the arcuate nucleus of hypothalamus (ARC), LepRb colocalizes with multiple neuropeptides, such as agouti related peptide (AGRP), neuropeptide Y (NPY), pro-opiomelanocortin (POMC), a precursor of α-melanocyte stimulating hormone (α-MSH), and cocaine- and amphetamine-regulated transcript (CART) (Håkansson et al. 1998). In the ARC, AGRP and NPY are expressed in the same neurons (we will refer to the population as AGRP neurons), and POMC and CART are expressed in a separate neuron population (referred as POMC neurons). These two neuron populations have antagonizing roles in regulating feeding-NPY promotes feeding, whereas α-MSH inhibits feeding (Ahima and Flier 2000). Moreover, AGRP neurons co-express neurotransmitter GABA, which can be used to inhibit the activity of anorexic POMC neurons to promote feeding.

Leptin's effects on feeding are mainly controlled by these two neuron populations. Electrophysiological studies have confirmed that leptin directly modulates the activity of AGRP and POMC neurons, but in opposite directions. On one hand, leptin hyperpolarizes AGRP neurons through activating a potassium channel (J. Xu et al. 2018; Spanswick et al. 1997). On the other hand, leptin depolarizes POMC neurons by direct action through a non-specific cation channel, and by indirectly action through releasing local inhibition from AGRP neurons (Cowley et al. 2001). Moreover, functional studies reveal that leptin regulates feeding mostly through AGRP neurons, and to a less extent through POMC neurons. Ablation of leptin receptor in AGRP neurons of adult mice using a CRISPR-Cas9 mediated technology leads to a significant increase in feeding and body weight, whereas ablation of LepR in POMC neurons leads to a modest increase in body weight but not food intake (J. Xu et al. 2018). In a separate study, leptin is shown to reduce feeding through activating melanocortin-4 (MC4) receptors, which is the target of α-MSH secreted by POMC neurons (Seeley et al. 1997).

### 1.2.4. Role of leptin in energy expenditure

The initial evidence suggesting that leptin regulates more than food intake comes from a pair feeding study (Levin et al. 1996). In this study, leptin deficient *ob/ob* mice were treated with vehicle control, leptin or pair-fed to leptin treated littermates. It is obvious that pair-fed *ob/ob* mice lost weight much slower compared to leptin treated one; more importantly, they lost much lean mass rather than fat mass. This study indicates that leptin has a role in promoting fat utilization, independent of its role in feeding. In addition, Ahima et al. showed the drop of leptin level during starvation mainly impacts neuroendocrine axis to conserve energy rather than controlling feeding (Ahima et al. 1996).

In comparison with well-defined neuron populations mediating leptin's effect on feeding, our understanding of the neural mechanisms underlying the role of leptin on energy expenditure are limited. Some hypothalamic regions, including ARC, DMH and VMH, have been shown to regulate energy expenditure in a leptin dependent manner (summarized in (Pandit, Beerens, and Adan 2017b)). For example, AGRP and POMC neurons in the ARC converge onto the melanocortin system to mediate leptin-dependent effects on energy expenditure (Cone 1999). Beside ARC, LepR neurons in the DMH and median preoptic area (MPO) have been shown to regulate brown adipose tissue thermogenesis through the sympathetic nervous system (Enriori et

al. 2011; Y. Zhang et al. 2011). Leptin's action in the VMH also regulates energy expenditure, but the downstream mechanism remains to be defined (Dhillon et al. 2006).

### 1.2.5. Energy expenditure defects of *ob/ob* mice

Leptin deficient *ob/ob* mice are massively obese as a result of both hyperphagia and decreased energy expenditure (Friedman and Halaas 1998) secondary to reduced locomotion and impaired fat utilization (Breslow et al. 1999), such as defective thermogenesis (Himms-Hagen 1985) and lipolysis processes (Steinmetz, Loway, and Yen 1969). Our preliminary results below also confirm these findings.

*Thermogenesis defect*

Thermogenesis is a process that produces heat and takes place in the brown adipose tissue (BAT). Thermogenesis is critical for survival of mice in places where temperature is below thermoneutrality, and for raising body temperature in certain behavior states, such as fever and stress. Thermogenesis utilizes metabolic fuels, therefore is a critical component of energy expenditure (Morrison, Madden, and Tupone 2014). Uncoupling protein 1 (UCP1), expressed in thermogenic tissues, is an important protein for thermogenesis. UCP1 protein is concentrated in the inner mitochondrial membrane of BAT, where it uncouples mitochondrial proton gradients from ATP production to heat release (Feldmann et al. 2009). Since thermogenesis requires availability of metabolic fuels, *ob/ob* mice, whose metabolism resembles mice in starvation state, have impaired thermogenesis. At a baseline level, *ob/ob* mice have lower brown fat temperature and lower level of thermogenic gene expression, including UCP1, compared to age matched WT mice (Figure 1.2 a, d).

*Lipolysis defect*

Lipolysis, which takes place in white adipose tissue (WAT), is the process that hydrolyzes triglycerides into free fatty acids (FFAs). In times of energy shortage, FFAs released through lipolysis are used to meet energy demand of other organs. After being food restricted for extended period, WT mice activate lipolysis, as indicated by elevated phosphorylated hormone sensitive lipase (p-HSL) level, to release FFAs from inguinal white adipose tissue (iWAT) (Figure 1.2 b). In contrast, *ob/ob* mice fail to activate lipolysis despite that they have larger fat storage than WT mice (Figure 1.2 c, e). These data indicate that *ob/ob* mice cannot efficiently utilize their fat storage, that leads to severe energy expenditure defects.

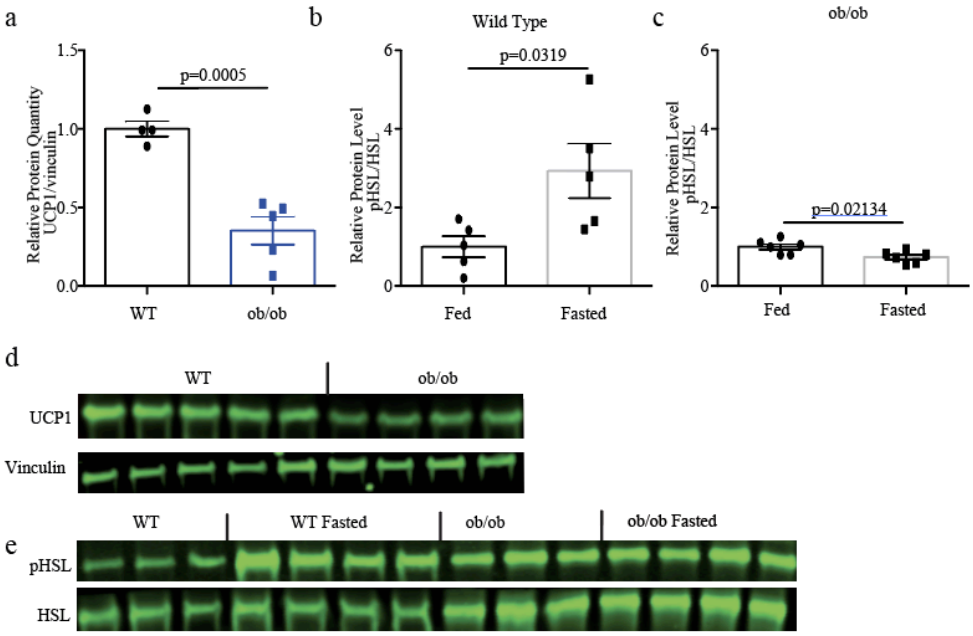


**Figure 1.2. *ob/ob* mice have thermogenesis and lipolysis defects**

(a) Relative basal UCP1 protein levels in BAT of *ob/ob* mice compared to WT age matched control animals by western blotting. Protein levels are normalized to vinculin protein (n=4 for WT, n=5 for *ob/ob*). (b) Relative basal p-HSL to HSL protein levels before and after 36 hours fast in WT mice (b, n=5 per group), *ob/ob* mice (c, n=6 per group). Western blot quantified in (a) is shown in (d), (b, c) in (e). Data shows mean ± SEM. Significant differences between treatments calculated using Student's two-tailed, unpaired t test. Gels are cropped to show representative lanes used for quantification.

### 1.2.6. Controversy regarding leptin's role in energy expenditure

It is known that exogenous leptin delivery to *ob/ob* mice for weeks corrects all the metabolic defects (Pelleymounter et al. 1995; Farooqi et al. 2002). However, recent studies demonstrated that acute leptin injection to *ob/ob* mice fails to activate thermogenesis (Kaiyala et al. 2016; Fischer et al. 2016), but rather helps conserve heat loss through the tail. In this thesis, we performed experiments to understand the basis of this discrepancy.

## 1.3. Sympathetic nervous system (SNS) and energy expenditure

### 1.3.1. Background of the SNS

The autonomic nervous system, conveys signals from the brain to the rest of the body, is an indispensable component in the maintenance of energy homeostasis in mammals. The autonomic nervous system is composed of two antagonizing branches - sympathetic nervous system (SNS) and parasympathetic nervous system (PNS). SNS controls "fight or flight" responses, whereas PNS controls "rest and digest" activities. The dysfunctions of the autonomic nervous system have been shown to cause many diseases (Guarino et al. 2017). In this dissertation, we will be focusing on studying the roles of SNS in energy homeostasis and its regulation by leptin.

The SNS activation leads to increased energy expenditure, including increased basal metabolic rate and thermogenesis. During "fight or flight" reactions or exercises, the SNS activity induces heart rate acceleration, heat production, periphery vasoconstriction and lipolysis enhancement to support the body for strenuous physical activities (McCorry 2007). Since the SNS plays a role in regulating energy balance, dysregulation of the SNS is often associated with obesity and other metabolic syndromes.

### 1.3.2. SNS in obesity

Sympathetic nervous activities (SNA) are increased with body weight gain, as an adaptive mechanism to enhance energy expenditure in order to combat the increased weight (summarized in Guarino et al. 2017). Elevated SNA results in increased BAT thermogenesis and lipid metabolism in normal animals, leading to efficient energy utilization. However, in obese subjects the adipose tissue responses to SNA are much blunted possibly due to local catecholamine resistance in fat, possibly mediated by downregulation of β-adrenergic receptors on adipocytes (summarized in Guarino et al. 2017). In the meanwhile, elevated SNA in obesity often leads to increased hypertension and risks over cardiovascular diseases, suggesting that sympathetic ganglionic blockers, as well as β-blockers might be advantageous to obese patients. Due to the double-edged effects of SNS in obesity, initial clinical studies modulating SNS in treating obesity reached contradicting results. In order to reveal the full therapeutic potential of SNS in the treatment of obesity, more mechanistic studies need to be done in the future. In particular, understanding the molecular diversities of the sympathetic nervous system, as well as the underlying mechanisms of the target-specific recruitment of sympathetic activity, will provide valuable insights for disease treatments. For example, being able to target sympathetic nervous system to specifically drive lipolysis or thermogenesis in adipose tissue while sparing the cardiovascular system will be a unique approach for the treatment of obesity.

### 1.3.3. Role of SNS in thermogenesis

The brown adipose tissue is densely innervated by the SNS. SNS innervates both brown adipocytes and the bloods vassals in the tissue (summarized in Bartness and Song 2005). The necessity of SNS for thermogenesis was proven by denervation study. Unilateral BAT denervation leads to reduced UCP1 level, norepinephrine (NE) content, the neurotransmitter of SNS, and BAT mass in the denervated side comparing to the contralateral side, (summarized in Bartness and

Song 2005). The reduction of thermogenesis profiles in the denervated BAT can be fully restored by NE treatment, further confirming that SNS activation is sufficient to drive thermogenesis in BAT. Bilateral BAT denervation leads to whitening of brown fat and mild body weight gain due to impaired energy expenditure (Bartness and Wade 1984). Moreover, increased sympathetic activity to WAT, under chronic cold exposure, causes browning of white adipocytes, featured by increased mitochondrial content and UCP1 level (summarized in Bartness and Song 2005).

### 1.3.4. Role of SNS in lipolysis

In comparison to the well-established role in BAT thermogenesis, the function of SNS in WAT lipolysis has only been confirmed recently. The laboratory of Tim Bartness has made extensive contributions to our understanding of SNS in WAT. By studying the interesting phenotype of seasonal obesity in Siberian Hamsters, the Bartness group revealed that it is a neural rather than circulating factor responsible for regulating lipolysis (summarized in Bartness et al. 2014). In the past few years, advancement in imaging technology made it possible for us to visualize dense SNS innervation in WAT (Chi et al. 2018; Zeng et al. 2015). Similarly as in BAT, there are both SNS fibers innervating white adipocytes and blood vessels in the tissue. Initial denervation studies showed that fasting induced lipolysis is attenuated in denervated white fat (summarized in Bartness et al. 2014). Recently, our lab provided the direct evidence that SNS is sufficient to drive lipolysis in inguinal WAT (iWAT). Zeng et al. showed that optogenetic activation of SNS innervating iWAT led to increased p-HSL, the lipoylsis marker, and eventually depletion of fat pad (Zeng et al. 2015).

### 1.3.5. Leptin's effect on SNS

Previous studies showed that leptin modulate heart rate, renal sympathetic tone and blood pressure through the SNS, suggesting that high leptin level in obese subjects is the cause of hypertension (summarized in Pandit, Beerens, and Adan 2017). Leptin was also shown to inhibit bone formation through the SNS (Takeda et al. 2002). More importantly, leptin regulates thermogenesis and lipolysis in a SNS dependent manner.

Leptin delivery to WT mice increases sympathetic tone to both BAT and iWAT, measured by electrophysiological recordings (Rahmouni and Morgan 2007; Harlan et al. 2011a; Bell et al. 2018). Moreover, ablation of LepR in the actuate nuclei abolishes leptin-induced sympathetic activity to fat depots (Harlan et al. 2011a; Bell et al. 2018). Despite electrophysiological studies, many functional studies also demonstrated the importance of SNS in adipose tissue functions. Work from our lab showed that leptin-induced lipolysis in iWAT is blocked by SNS denervation or β-adrenergic receptor blockade (Zeng et al. 2015). BAT temperature change induced by leptin treatment or LepR neuron activity is also blocked by β-adrenergic receptor blockade in BAT (Y. Zhang et al. 2011; Enriori et al. 2011). However, most of these experiments were done on WT mice where there are no developmental defects in adipose tissue functions or energy expenditure. The role of leptin on SNS in *ob/ob* mice, who have defects in thermogenesis and lipolysis as described above in 1.2.5, is yet to be discovered. This will possibly help explain the discrepancy between function of chronic vs. acute leptin treatment on thermogenesis in *ob/ob* mice.

### 1.3.6. CNS origins of SNS

The SNS serve as the signal conductor between the brain and the rest of the body, therefore, anatomically and functionally characterizing the brain regions regulating SNS outflow have always been of great interests to the field. The development of pseudorabies virus (PRV), a polysynaptic neural circuit tracer, largely advanced our understanding of the CNS origins of sympathetic outflow to a variety of tissues, including BAT and WAT (summarized in Callaway 2008).

Once injected into the adipose tissue, PRV is uptaken by the sympathetic axons and further propagates to label a series of presynaptic neurons, including the sympathetic postganglionic neurons in the sympathetic chain and the preganglionic neurons in the spinal cord, before reaching the brain. PRV tracing experiments have revealed many brain regions sending efferents to the both WAT and BAT, including PVH, raphe pallidus (RPa), ARC, DMH, etc. (Ly et al. n.d.). Among these regions, the PVH (Biag et al. 2012; Sutton, Myers, and Olson 2016) and RPa (Nakamura et al. 2004) are two known sympathetic premotor regions that directly project to the preganglionic neurons in the spinal cord. Factors acting centrally to regulate SNS-mediated effects on energy expenditure, such as leptin-mediated thermogenesis and lipolysis effects, would mostly likely pass through one of these two regions. However, how leptin signaling interacts with these sympathetic premotor neurons has not been shown yet.

## 1.4. Brain-derived neurotropic factor (BDNF) and body weight regulation

### 1.4.1. BDNF signaling and obesity

Brain-derived neurotropic factor (BDNF) is broadly distribution in the central nervous system and has significant roles in neuron growth and survival. BDNF binds to its receptor, tropomyosin-related kinase B (TrkB), and induces the activation of a serious of signaling cascade in its target cells. BDNF signaling pathway, together with leptin and melanocortin signaling pathways, are the most important systems in regulating energy homeostasis. Similarly as in the other two systems, BDNF or TrkB gene mutations result in severe obesity in both humans (Yeo et al. 2004; Han et al. 2008) and mice (B. Xu et al. 2003; Rios et al. 2001). Intracerebroventricular (i.c.v.) infusion of recombinant BDNF reduces food intake and body weight in rodents. There are evidence suggesting that the BDNF expressing neurons in the VMH and paraventricular nucleus of hypothalamus (PVH) are responsible for the feeding effects of BDNF (summarized in B. Xu and Xie 2016).

### 1.4.2. BDNF and energy expenditure

The initial evidence supporting that BDNF regulates energy expenditure comes from study in *db/db* mice. In this study, both peripheral and central BDNF delivery led to increased NE turnover and UCP1 upregulation in *db/db* mice (Nonomura et al. 2001), suggesting that BDNF regulates thermogenesis through the SNS. Following that, more studies show that BDNF delivery directly into the VMH and PVH modulate energy expenditure (summarized in B. Xu and Xie 2016). More recently, study showed that genetic or viral mediated deletion of BDNF gene from PVH resulted in dramatic weight gain and BAT temperature decrease (An et al. 2015). Moreover, PVH

is a sympathetic premotor region in the brain, as described in 1.3.6, raising the possibility that BDNF neurons in this region might regulate energy expenditure through SNS. More studies need to be done to confirm this hypothesis.

### 1.4.3. Leptin and BDNF signaling

Although both central leptin and BDNF signaling pathways have strong implications in regulating energy balance, the interaction between the two systems is not well understood. The lack of colocalization between LepR and BDNF gene suggest that leptin does not regulate BDNF expression directly. Previous study suggested that leptin indirectly upregulates BDNF mRNA levels in the VMH (Liao et al. 2012). However, more precise mechanism of interaction between these two systems remains to be discovered.

## 1.5. Dissertation summary

This dissertation includes all my work in the Friedman lab from 2015-2020, with the aim to further understand leptin's role in the regulating sympathetic nervous system and energy expenditure. In particular, we would like to explore how leptin regulates the SNS structure and function in the adipose tissues, and the underlying neural mechanisms both at the circuit and molecular level. Starting from Chapter 2, each chapter summarizes one component of this project.

Chapter 2 focuses on studying the functional role of leptin on energy expenditure. As stated above in 1.2.6, there's a long-standing controversy between the function of chronic vs. acute leptin treatment on *ob/ob* mice. In this chapter, we aim to revisits this issue by exploring how chronic and acute leptin impact thermogenesis and lipolysis. This led us to an unexpected discovery that *ob/ob* mice have a profound loss of sympathetic nervous system innervation in the adipose tissue compared to the WT mice, and chronic leptin treatment can restore the innervation defects in *ob/ob* mice. Our results also show that chronic, but not acute, leptin treatment of *ob/ob* mice upregulates thermogenesis in BAT and lipolysis in iWAT, suggesting that SNS structure in the adipose tissues is critical for their functions.

Chapter 3 and 4 reveal the central neural mechanisms underlying leptin dependent regulation of SNS innervation in adipose tissue. In Chapter 3, we revealed the first order leptin-responsive neurons in the ARC that are necessary for leptin to regulate innervation. In Chapter 4, we found a BDNF expressing neuron population in the PVH that is downstream of leptin signaling and is necessary for leptin to induce innervation change in adipose tissues. These results show that leptin dependents on BDNF signaling pathway to regulate energy expenditure, providing a possible mechanism of how leptin and BDNF signaling pathways, two of the important singling pathways in regulating energy homeostasis, interact to maintain body weight balance. Results from Chapter 2-4 have been published (P. Wang et al. 2020).

Chapter 5 and 6 describe a follow up study based on the above-mentioned discoveries. In Chapter 5, we focused on characterizing the anatomy of the sympathetic pre- and postganglionic neurons innervating both BAT and iWAT. We first revealed the anatomical locations of the sympathetic postganglionic and preganglionic neurons innervating BAT and iWAT. Then we compared the anatomy of fat innervating neurons between WT and *ob/ob* mice, and found that the location and cell number of fat innervating postganglionic neurons are similar between these two mouse lines. These data imply that the gene expression profiles in these postganglionic neurons between WT and *ob/ob* are very different. Therefore, in Chapter 6, we optimized single cell sequencing protocol and applied to the sympathetic postganglionic neurons. We hope to reveal the cell type diversities of the sympathetic postganglionic neurons in both WT and *ob/ob* mice, and the molecular identities of the adipose tissue innervating neurons. Lastly, we are interested in comparing the cell state differences between WT, *ob/ob* and leptin treated *ob/ob* mice, and identifying the cellular and molecular mechanism underlying leptin-dependent neural plasticity at the level of adipose innervating sympathetic postganglionic neurons.

## Chapter 2. Leptin's role on SNS innervation in adipose tissue and its functional implications

### 2.1. Chronic leptin treatment to *ob/ob* mice promotes energy expenditure

In order to test what role leptin plays in regulates energy expenditure, the first experiment we did was to treat leptin deficient *ob/ob* animals with chronic leptin and placed them in metabolic chamber (TSE systems) to record their metabolic activities. Mice were given either PBS (blue line) or leptin at a rate of 400 ng/hr (red line) through an osmotic pump for 14 days. Oxygen consumption, carbon dioxide production and physical activities were recorded for individual animal inside the metabolic chamber. Energy expenditure of the animals were calculated based on the oxygen consumption and carbon dioxide production values. From this experiment, we found that leptin treated *ob/ob* mice increased energy expenditure both in dark and light cycle continuously over the period of 14 days (

Figure 2.1 a-b), which was only partially due to an increase in physical activity (Figure 1.1 c-d). During the daytime, energy expenditure of the leptin treated mice increases while there is no significant upregulation of physical activities (

Figure 2.1 a, c). During the night cycle, physical activity of the leptin treated animals increases and plateaus at after 7 days of treatment (

Figure 2.1 d). However, the energy expenditure of the leptin treated animals keeps increasing over the 14-day treatment period (

Figure 2.1 b). This data imply that leptin might have prominent roles in upregulating basal metabolic rate or adaptive thermogenesis, which might contribute to the rising total energy expenditure. In the following sections of this chapter, we will focus on exploring how leptin affects two of the critical process involved in energy expenditure-thermogenesis and lipolysis.

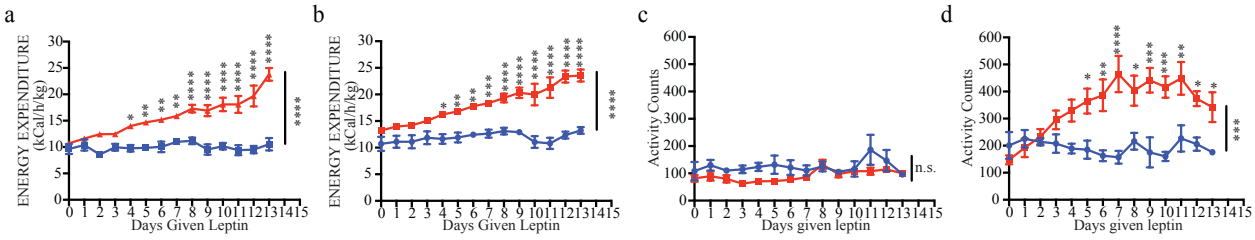


**Figure 2.1. Leptin regulates energy expenditure through its effects on physical activity and beyond.**

*(a) ob/ob* mice were treated with leptin (400ng/hr, red line) or PBS (blue line) through a subcutaneous osmotic pump. (a) Day cycle and (b) night cycle energy expenditure was recorded throughout the treatment. (c) Day cycle and (d) night cycle activity counts were recorded. Data shows mean ± SEM, significant differences between treatments calculated using two-way ANOVA followed by Bonferroni post-hoc test.

## 2.2. Chronic, not acute leptin treatment of *ob/ob* mice corrects defects in energy expenditure

As discussed in 1.2.6, chronic leptin delivery to *ob/ob* mice reverses thermogenesis and lipolysis defects. In contrast, acute leptin treatment of *ob/ob* fails to stimulate either of process. The basis for discrepancy between the effects of chronic vs. acute leptin treatment is not well established. In order to understand this, we first designed an experiment to quantitate the effects of chronic vs. acute leptin treatment on thermogenesis and lipolysis. Four groups of animals were included: 1) *ob/ob* PBS. *ob/ob* mice receiving PBS via osmotic pumps for 14 days, 2) Chronic Leptin. *ob/ob* animals receiving leptin for 14 days, 3) Acute Leptin. *ob/ob* mice receiving PBS for 14 days followed by an acute dose (3mg/kg) of leptin on day 16, 4) Wild Type (WT) Control. Wild type mice receiving PBS. On Day 14, pumps were removed, and on Day 16 the other three groups, besides the *Acute Leptin* group that received leptin, received a single dose of PBS injection. Two days after pump removal (Day 16), only the *Acute Leptin* group had high circulating levels of leptin. Afterwards, animals were placed in a 4 °C chamber to measure brown adipose tissue (BAT) thermogenesis; or food restricted to induce lipolysis in iWAT in a separate experiment. The experimental design is summarized in Figure 2.2.

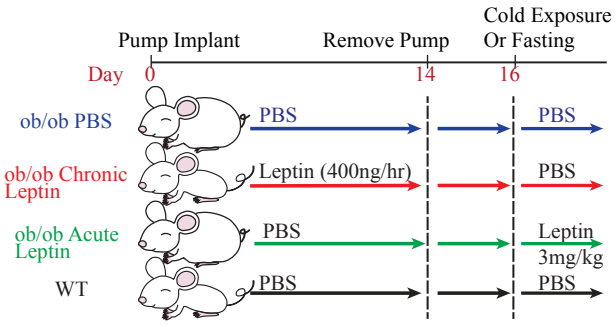


**Figure 2.2. Scheme for chronic and acute leptin treatment of *ob/ob* mice.**

At day 0, osmotic pumps delivering 400 ng/hr of leptin or PBS control were implanted subcutaneously into *ob/ob* or WT mice. On day 14, pumps were surgically removed leading to leptin turnover. On day 16, mice received intraperitoneal (i.p.) injections of either 3 mg/kg leptin (Acute Leptin) or PBS (all other groups) 2 hours prior to either of the following interventions: 1) cold challenged by a 4°C environment for 4 hours or 2) fasted for 36 hours (in this case, the "Acute Leptin" group also received additional injections of leptin at 12 and 24 hours post fasting while all other groups receive PBS).

In the cold exposure experiment, consistent with previous observations, WT mice (black line) maintained core and BAT temperature after cold exposure, while the *ob/ob* PBS (blue line) and the Acute Leptin groups (green line) became profoundly hypothermic (Figure 2.3 a-c). In contrast, the Chronic Leptin group (red line) defended core and BAT temperatures similarly to WT mice. Protein and RNA levels of thermogenic genes, including UCP1, were significantly higher in BAT of Chronic Leptin group compared to the PBS or Acute Leptin groups (Figure 2.3 d-f). Tail temperature of animals from WT and Chronic leptin were lower than those from PBS or Acute Leptin group both before and after cold exposure (Figure 2.3 g). The opposite trend we saw comparing tail temperature to BAT or core temperature was expected. Since tail is a heat dissipating organ, lower tail temperature of mice in WT or Chronic Leptin group helped to retain their body temperature under cold exposure, whereas higher tail temperature of mice in Acute Leptin or PBS group led to more heat dissipation. Additionally, it is important to note that animals in Chronic Leptin group, followed by pump removal, had no leptin in their blood serum and lacked active leptin signaling confirmed by the absence of phosphorylated STAT3 in the hypothalamus (Figure 2.3 h-i). Animals in Acute leptin group, on the other hand, had high level of leptin in blood serum and active leptin signaling in the hypothalamus (Figure 2.3 h-i).

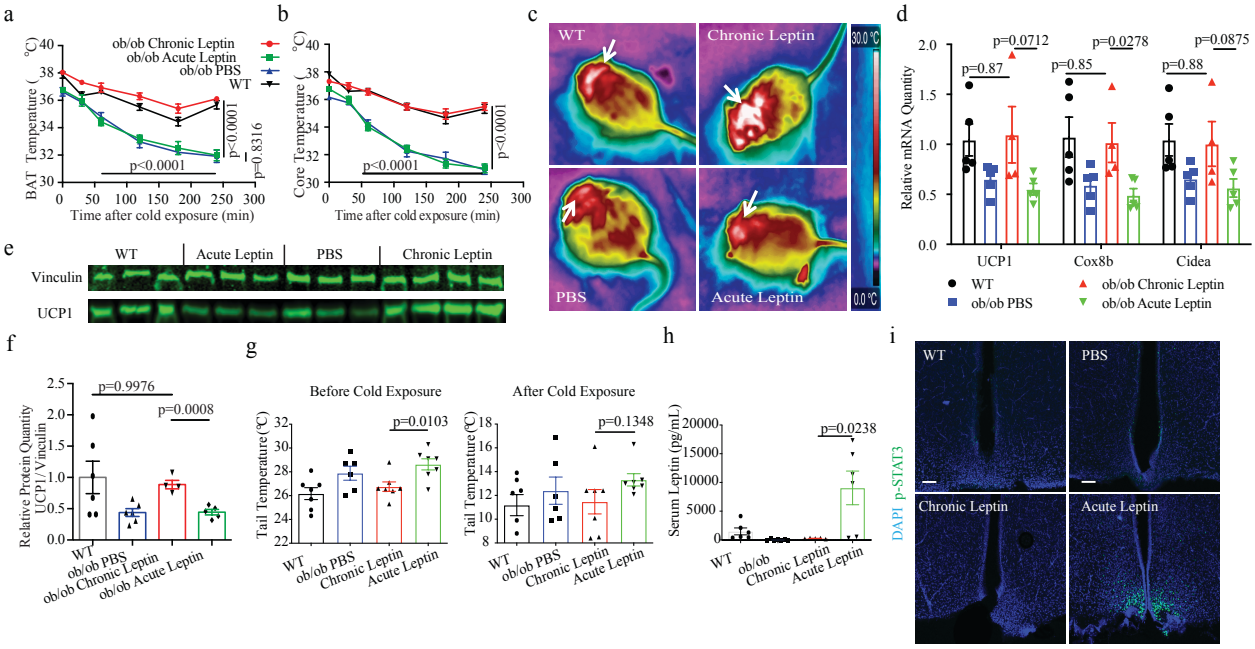


**Figure 2.3. Chronic, not acute leptin, treatment of *ob/ob* mice corrects thermogenesis defect.**

(a) BAT temperature and (b) core temperature of mice treated as shown in Fig. 1.2 following cold challenge (n=7 for all groups except *ob/ob* PBS n=6). (c) Thermographic camera images of mice following cold challenge for 2 hours. White arrow indicates BAT. (d) Relative mRNA levels of known thermogenesis genes in BAT following 4 hours of cold exposure, as measured by qPCR (n=4 for *ob/ob* PBS, n=5 for all other groups). (e) Western blots showing UCP1 and vinculin levels after cold exposure for 4 hours. (f) Quantification of (e). Relative UCP1/vinculin protein levels in BAT of mice (n=6 for WT and *ob/ob* PBS; n=4 for Chronic Leptin; n=5 for Acute Leptin). (g) Tail temperature as measured by thermographic camera, of mice treated as in Fig. 1b-c before (left panel) and after cold exposure for 2 hours (right panel). Both WT and chronic leptin treated *ob/ob* mice exhibit lower tail temperatures, consistent with findings by Fischer et al.(Fischer et al. 2016) (n=6 for *ob/ob* PBS, n=7 for all other groups). (h) Serum leptin levels measured by leptin ELISA from mice treated as in Fig. 1b-d (n=6 for WT and Acute leptin, n=7 for *ob/ob*, n=5 for Chronic leptin). (i) Representative coronal hypothalamic arcuate nucleus brain sections of mice from groups shown in (Fig. 1a), immunolabeled for p-STAT3 (in green) and DAPI (in blue). Scale bar, 100 µm. Data shows mean ± SEM, significant differences between treatments calculated using two-way ANOVA (a-b) or Student's two-tailed, unpaired t test (d-h).

Similar finding in lipolysis was observed in a separate experiment when animals treated as in Figure 2.2 were food restricted for 36 hours. Animals in Chronic Leptin group had significantly higher levels of lipolysis marker, pHSL, in their iWAT compared to those in PBS or Acute Leptin group (Figure 2.4 a-b). In this experiment, animals in Acute Leptin group received 2 additional doses of leptin every 12 hours to further sustain high plasma levels of leptin throughout the 36-hour fast period.

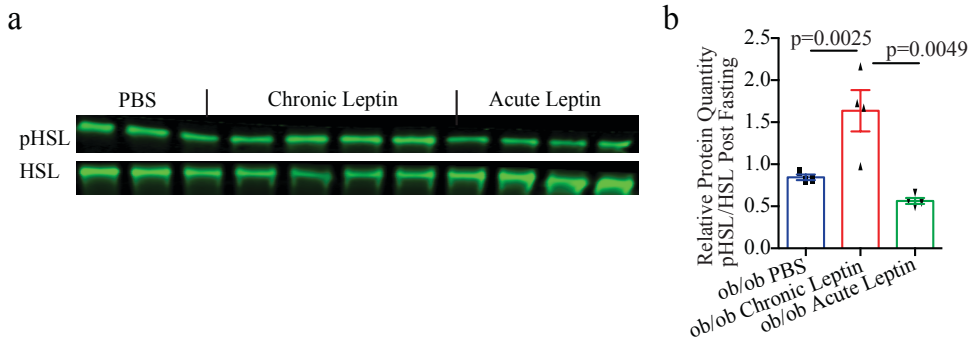


**Figure 2.4. Chronic, not acute leptin, treatment of *ob/ob* mice corrects lipolysis defect.**

(a) Western blots showing pHSL and HSL levels after fasting for 36 hours. (b) Quantification of (a). Relative p-HSL/HSL levels in inguinal WAT of fasted mice by Western Blots (n=4 per group). Data shows mean ± SEM, significant differences between treatments calculated using Student's two-tailed, unpaired t test.

In conclusion, we demonstrated that chronic, but not acute, leptin treatment of *ob/ob* mice restores thermogenesis and lipolysis defects, and thus promotes utilization of fat storage in *ob/ob* mice. More importantly the effects of chronic leptin on thermogenesis and lipolysis persist for days after circulating leptin has turned over, suggesting that chronic leptin induces plasticity of the pathways regulating these processes.

### 2.3. *ob/ob* mice have low sympathetic innervation in adipose tissue which can be restored by chronic leptin treatment

Thermogenesis in BAT and lipolysis in iWAT are both regulated by the sympathetic nervous system (SNS). Therefore, we hypothesized that leptin might regulate the plasticity of SNS innervation of adipose tissue to promote these processes. To test this, we visualized SNS innervation of iWAT in *ob/ob* and WT mice, using whole-mount tissue clearing method (Adipo-Clear, Chi et al. 2018) followed by light sheet microscopy imaging (Figure 2.5 a). The SNS was immunolabeled for tyrosine hydroxylase (TH), which is an essential enzyme for catecholamine production and therefore a marker for SNS. Surprisingly, we observed that *ob/ob* mice have a profound, around six-fold decrease in SNS innervation in iWAT comparing to age-matched WT mice (Figure 2.5 b). We also visualized SNS innervation in BAT. Due to technical difficulties in clearing brown fat, we delipidated BAT, cut it into 30um sections under cryoprotection, immunolabeled for TH and visualized by confocal microscopy. Similarly, we observed a drastic reduction of SNS innervation of *ob/*ob mice in BAT (Figure 2.5 c). The same phenotype was also

observed in *db/db* mice which carry a mutation in leptin receptor (Figure 2.5 b-c). This SNS innervation defects in *ob/ob* mice are developmental. We imaged SNS in iWAT and BAT of adolescent *ob/ob* mice, and found that they have lower innervation level comparing to age match WT mice at week three and week five (Figure 2.5 d-g).

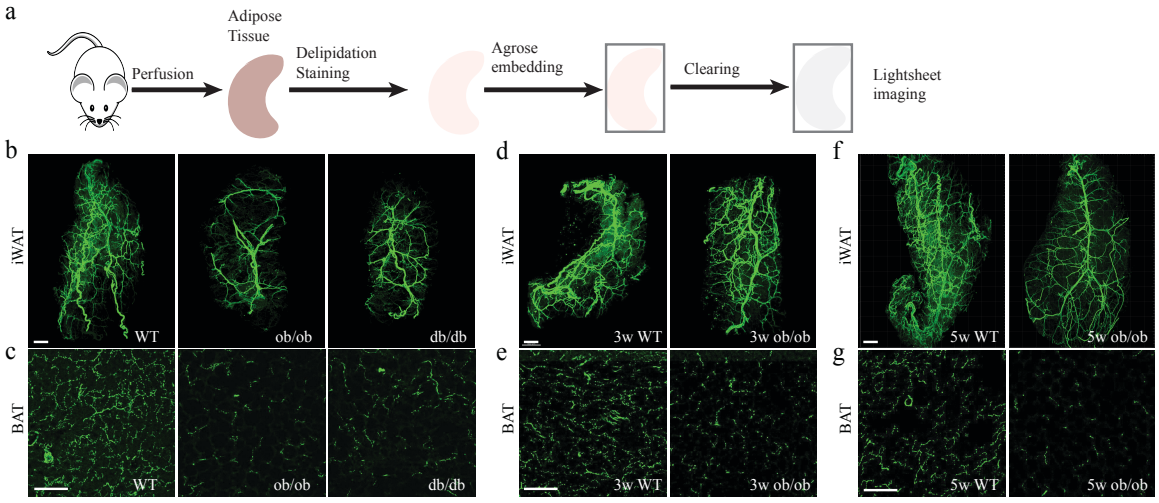


**Figure 2.5. *ob/ob* mice have profound reduction of SNS innervation in adipose tissues.**

(a) Scheme describing Adipo-Clear protocol for whole mount imaging of innervation in adipose tissue. (b) Tyrosine hydroxylase (TH) immunolabeling in cleared iWAT from WT, *ob/ob* and *db/db* mice visualized by fluorescence light-sheet microscopy imaging. (c) same as (b) but TH immunolabeling of delipidated 30 μm sections of BAT. TH immunolabeling in iWAT and BAT, of 3-week old *ob/ob* (d-e) or 5-week old *ob/ob* (f-g) mice with age matched WT controls shown on left. Scale bar, 1mm (b, d, f); 100 μm (c, e, g).

We next treated *ob/ob* mice with chronic, exogenous leptin for 14 days through subcutaneous osmotic pumps and found that it dramatically increased the level of SNS innervation in both iWAT and BAT (Figure 2.6 a-b). The dynamics of leptin induced innervation in iWAT and BAT are slightly different. It takes 7 days for leptin to restore BAT innervation to WT level, whereas it takes 14 days in iWAT (Figure 2.6 a-b). Protein levels of tyrosine hydroxylase (TH) are also increased in leptin treated *ob/ob* mice comparing to their PBS treated littermates, shown by Western blots (Figure 2.6 c-d). We next stained delipidated BAT section of *ob/ob* mice with TH antibody together with b3 tubulin antibody (a pan-neuronal marker), and found that leptin also induces generation of more neural fibers inside BAT (Figure 2.6 e). Similarly, there are more neural fibers in iWAT, stained by PGP9.5, another pan-neuronal marker, of leptin treated *ob/ob* mice comparing to their PBS treated littermates (Figure 2.6 c). These findings demonstrate that leptin induces axonogenesis in adipose tissues of *ob/ob* mice rather than simply upregulates TH expression levels in existing neural fibers. Chi et al revealed in their study that there are three major patterns of SNS innervation in adipose tissue, along blood vessels, nerve bundles and neurites directly project to fat cells, or parenchymal innervation (Chi et al. 2018). We found that *ob/ob* mice, compared to WT mice, have low levels of fibers directly innervating fat cells (parenchymal innervation) but not the ones innervating blood vessels. Therefore, leptin only induces the generation of parenchymal innervation in *ob/ob* mice (Figure 2.6 e). Additionally, we show that leptin is necessary to maintain WT level innervation in adipose tissue. Three weeks after withdrawal of leptin treatment from chronic leptin treated *ob/ob* mice resulted in a loss of innervation to pre-treatment level (Figure 2.6 f).

**Figure 2.6. Leptin delivery in *ob/ob* mice increase SNS innervation in adipose tissue.**
(a-b) Subcutaneous leptin delivery at 400ng/hr through an osmotic pump increases SNS innervation level in *ob/ob* mice. Sympathetic innervation density visualized by TH immunolabeling in (a) iWAT and (b) BAT in *ob/ob* animals was restored to levels similar in WT. Quantification of the images presented on the right, iWAT (n=3 per group), and BAT (n=3 for WT and *ob/ob*; n=4 for all other groups). (c) Western blots of TH protein, PGP9.5 protein and loading control vinculin in iWAT. Quantification of relative levels of TH protein (left) and PGP9.5 protein (right) in iWAT normalized to vinculin (n=5 for *ob/ob*+Leptin, n=9 for all other groups). (d) Western blots of TH protein and loading control vinculin in BAT. Quantification of relative levels of TH in BAT normalized to vinculin (n=4 for WT, n=5 for all other groups). (e) TH and beta-tubulin 3 immunolabeling in delipidated BAT sections from *ob/ob* mice treated with 400 ng/hr leptin (top) or PBS (bottom) for 14 days. (f) Zoomed in optical sections of iWAT (visualized as by iDISCO) from 14-day chronic leptin treated *ob/ob* mice, WT age-matched control mice, or *ob/ob* mice treated with PBS control. Green boxes indicate parenchymal SNS innervation. Yellow arrows showing SNS innervation colocalizing with vasculature as marked by anti-CD31. (g-h) *ob/ob* mice treated with PBS, 400ng leptin for 2 weeks or 400ng leptin for 2 weeks followed by leptin withdrawal for 3 weeks to allow mice to regain body weight until above 50g, TH immunolabeling is visualized in (g) iWAT (j, n=4 per group) and (h) BAT (k, n=3 for Leptin withdraw, n=4 for all other groups). Scale bar, 1mm (a, g); 100 μm (b, e, h); 200μm (f). Data shows mean ± SEM, significant differences between treatments calculated using Student's two-tailed, unpaired t test.

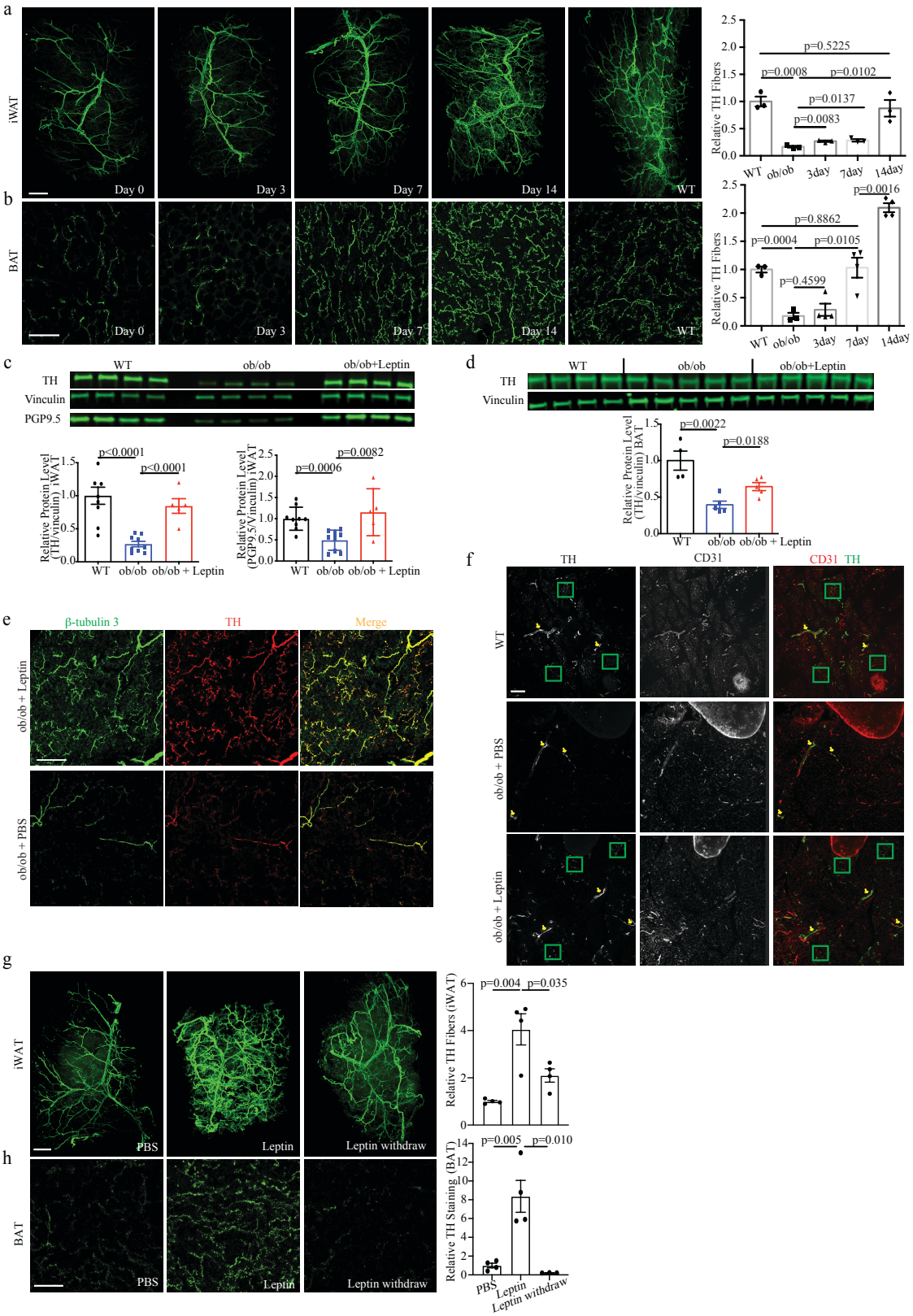


**Figure 2.6. Leptin delivery in *ob/ob* mice increase SNS innervation in adipose tissue.**

## 2.4. Leptin-induced adipose innervation is independent of anorexia

Leptin treatment of *ob/ob* mice significantly reduces daily food intake, we then tested whether the leptin's effects on innervation are secondary to anorexia. There were three groups in this experiment-*ob/ob* treated with PBS, leptin or pair-fed. The animals in the pair-fed groups were fed the same amount of food daily according to how much their leptin treated *ob/ob* littermates ate. As observed previously, *ob/ob* treated with leptin continuously lost weight throughout the 14-day treatment, however, pair-fed animals lost weight at a much slower pace (Fig. 1.8 a). At the end of the experiment, body composition of the animals was analyzed using EchoMRI machine. We found that leptin treated *ob/ob* mice have drastically reduced body fat composition, whereas pair-fed *ob/ob* mice retain the same level of body fat as their PBS treated littermates (Fig. 1.8 b). More importantly, 14-day pair-feeding of *ob/ob* mice does not have any effect on SNS innervation in iWAT or BAT (Fig. 1.8 c-d). In addition, pair-fed *ob/ob* mice still have thermogenesis defects. When exposed to cold, pair-fed *ob/ob* mice cannot defend their BAT or body temperature and succumb to cold faster than their PBS treated littermates (Fig. 1.8 e-f). In aggregate, these results show that the effect of leptin on innervation and fat utilization is independent of anorexia.

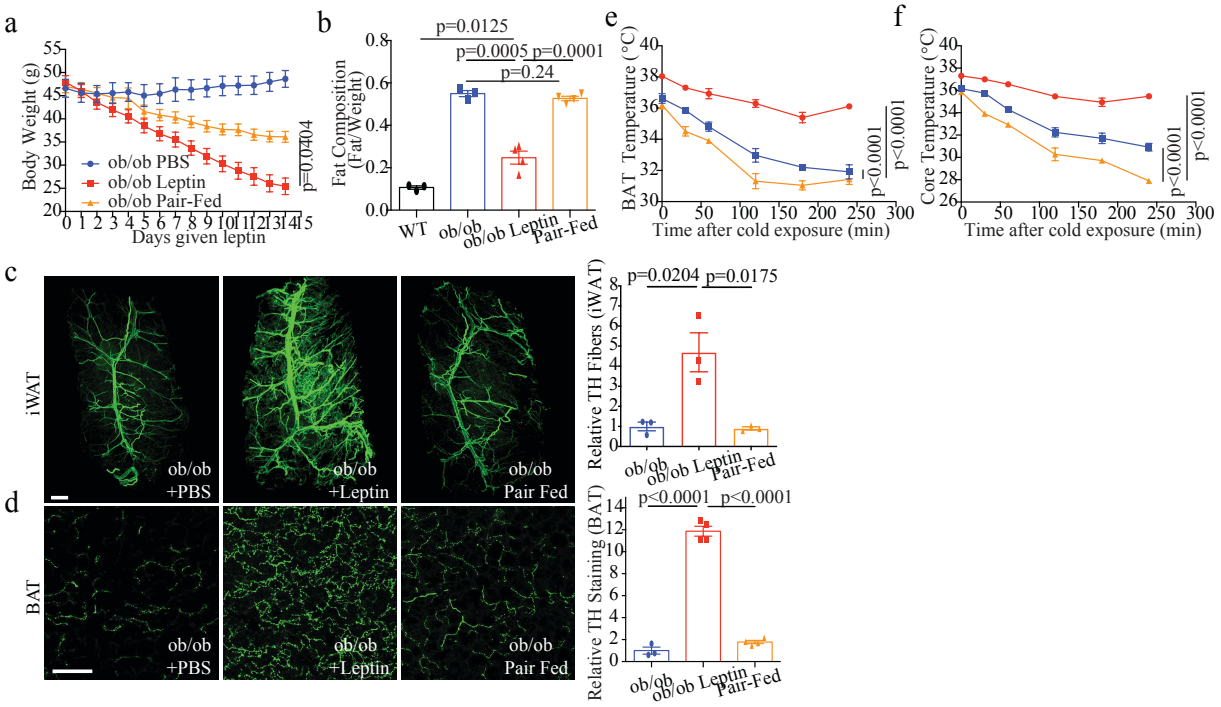


**Figure 2.7. Leptin's effect on innervation is independent of anorexia.**

a) Body weight over 14 days of *ob/ob* mice treated with leptin (red line), pair-fed to leptin treated *ob/ob* (orange line) or PBS treated *ob/ob* controls (blue line). (b) Body fat composition of mice as measured by MRI (n=3 for WT and ob/ob, n=4 for all other groups). (c-d) TH immunolabeling in iWAT (c) and BAT (d) was visualized. Quantification of images shown on the right, iWAT (n=3 per group) and BAT (n=3 for *ob/ob*, n=4 for all other groups). (e) BAT and (f) core body temperature of mice pair fed to 14-day leptin treated *ob/ob* mice as in Figure 2.2, following cold challenge (n=7 for all groups except *ob/ob* given PBS, n=6). Note that leptin treated *ob/ob* (red line) and PBS treated *ob/ob* (blue line) data shown here are the same as in Figure 2.3 a-b. Scale bar, 1mm (c); 100 µm (d). Data shows mean ± SEM, significant differences between treatments calculated using two-way ANOVA (a, e, f) or Student's two-tailed, unpaired t test (b-d).

## 2.5. Chronic leptin treatment in *ob/ob* enhances adipose metabolism

### 2.5.1. Leptin enhances SNA response to cold

Having established that leptin regulates SNS structural plasticity in the adipose tissue of *ob/ob* mice, we then ask whether leptin affects SNA in these animals. We recorded the electrophysiology of SNS in *ob/ob* adipose tissue following leptin treatment. In this experiment, we treated *ob/ob* mice with either PBS or leptin for 14 days, followed by pump removal (similarly as in Figure 2.2). Two days after pump removal, serum leptin level has dropped below detection limit. We then recorded sympathetic nerve activity (SNA) as reported in Bell et al. 2018. Briefly, animals were kept under sustained anesthesia and Core body temperature was monitored with a use of a rectal probe and continuously maintained at 37.5 ºC. Each mouse was then equipped for direct multifiber SNA from nerves innervating WAT and BAT. The mouse was first positioned on its dorsal side and the nerve sub-serving the inguinal WAT was accessed through a small incision made on the right flank near the hind limb. A bipolar platinum-iridium electrode was suspended under the nerve, and baseline WAT SNA was recorded over a 30 min period (Figure 2.8 a) under a stable isothermic (37.5 °C). Next, the mouse was re-positioned on its ventral side and the nerve sub-serving inter-scapular BAT was accessed through an incision in the nape of the neck. Baseline BAT SNA was also recorded (Figure 2.8 b). We saw a significant upregulation of baseline SNA in both iWAT and BAT of chronic leptin treated *ob/ob* mice comparing to their PBS treated littermates (Figure 2.8 a-b). Afterwards, we accessed BAT SNA response to body temperature cooling. Core body temperature of the mouse was cooled by lowering the surgical platform temperature using ice packs. This produces a slow reduction in the mouse's body temperature from 37.5 °C to 27.5 °C. During this process, chronic Leptin group also showed significantly higher SNA responses relative to baseline, compared to the controls (Figure 2.8 c). These data indicate that chronic leptin not only induces a structure change on adipose tissue sympathetic nerves but also increases basal SNA and enhances SNA response to cold; both structural and functional effects on the sympathetic nerves last a couple days after serum leptin is removed from the animal. The enhanced SNA response to cold exposure in BAT also partially explains why chronic leptin treated animals in Figure 2.3 defended their body temperature well.

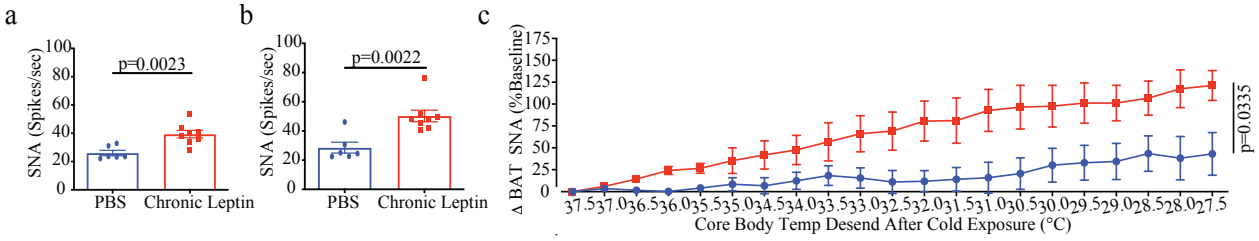


**Figure 2.8. Leptin enhances SNA.**

(a-b) Basal sympathetic nerve activity measured by electrophysiology into (a) iWAT and (b) BAT of Chronic leptin treated *ob/ob* mice compared to PBS treated *ob/ob* mice (n=6 for PBS, n=8 for Chronic leptin). (c) Relative increase in BAT SNA following cooling of mice. (n=6 for PBS; n=8 for Chronic leptin). Data shows mean ± SEM, significant differences between treatments calculated using two-way ANOVA (c) or Student's two-tailed, unpaired t test (a-b).

### 2.5.2. Leptin promotes adipose tissue metabolism

Tissue respiration or oxygen consumption is a measurement of the basal metabolic activity of a tissue; therefore, we would like to know whether leptin alters that in adipose tissue. In this experiment we included four groups, WT, *ob/ob* mice treated with PBS, leptin or pair-fed. Fresh tissues were removed from animals and tissue respiration was measured using a Clark electrode. We found that oxygen consumption in explants of BAT and iWAT from leptin treated *ob/ob* mice was also significantly higher than explants from PBS treated or pair-fed littermates (Figure 2.9 a-b). These data show that leptin treatment of *ob/ob* mice upregulates adipose tissue basal metabolic rates.

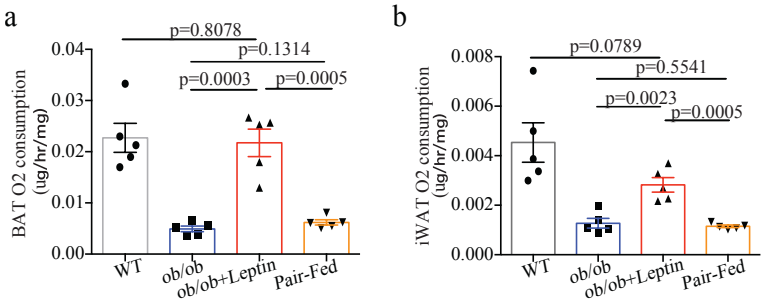


**Figure 2.9. Leptin increases adipocytes respiration.**

(a-b) $O_2$ consumption measured by a Clark electrode of BAT (a) or iWAT (b) explants from wild type, *ob/ob* mice following 14-day leptin treatment, PBS control or *ob/ob* mice pair fed to leptin treated *ob/ob* group (n=5 per group). Data shows mean ± SEM, significant differences between treatments calculated using Student's two-tailed, unpaired t test.

## 2.6. Summary and discussion

In this chapter, we set out to explore the mechanism responsible for the differential effects of acute and chronic leptin on thermogenesis (as stated in 1.2.6), and found striking plasticity of the sympathetic innervation of adipose tissue that is dependent on chronic leptin signaling. This level of neural plasticity is extreme with near absent parenchymal innervation in the absence of leptin signaling and a complete restoration of innervation after leptin treatment (Figure 2.6). More importantly, we believe that the SNS innervation structure is critical for adipose tissue functions. Chronic leptin restores SNS structural density in iWAT and BAT of *ob/ob* mice, which in turn corrects defects in both lipolysis and thermogenesis (Figure 2.3, Figure 2.4). In contrast, acute leptin treatment of *ob/ob* mice cannot restore SNS innervation density, therefore has no effects on either adipose tissue functions. Besides regulating structural plasticity, chronic leptin signaling also enhances SNA response to cold challenge (Figure 2.8), which also provides partial explanation on the cold-insensitive phenotype observed in chronic leptin treated *ob/ob* mice. In aggregate, our data reconcile the discrepancies observed on leptin's function in energy expenditure and show that leptin promotes energy expenditure in *ob/ob* mice through regulating the SNS plasticity in adipose tissues.

The dramatic leptin dependent SNS plasticity is seen in adult animals, where significant changes of peripheral innervation in general are observed only following tissue injuries (Navarro, Vivó, and Valero-Cabré 2007). Therefore, understanding the mechanisms underlying this leptin-dependent neural plasticity will provide new therapeutic insights to the treatment of both obesity and neural injuries.

## 2.7. Material and methods

### *Animals*

All animal care and experimentation were ethically performed according to procedures approved by the Institutional Animal Care and Use Committee at the Rockefeller University. Mice were housed 2–5 per cage (except cold exposure study where mice were singly caged) in a 12-hr light/12-hr dark cycle with ad libitum access to regular chow and water except in fasting studies. We used WT male C57BL/6J mice (Jackson Laboratory 000664), *ob/ob* (B6.Cg-Lepob/J, Jackson Laboratory 000632, or bred in house), db/db (BKS.Cg-Dock7m +/+ Leprdb/J, Jackson Laboratory 000642). Littermates of the same sex were randomly assigned to either experimental or control groups.

### *Leptin Treatment, Pair-feeding and Body Composition Measurements*

10-12-week old *ob/ob* mice or WT mice, were induced and maintained on isofluorane anesthesia before implanting osmotic pumps (Alzet model 1002D for 14-day treatment, 1003D for 3-day treatment, 2006D for 42-day treatment). Leptin (delivery rate of 400 ng/hr or 100ng/hr) or saline was delivered through osmotic pumps subcutaneously. Mice were housed individually for 1 week prior (for habituation) and during experiments, and body weights and food intake were measured daily. Pair-fed animals were fed with the same amount of chow diet leptin treated animals consumed the previous day. Whole-body composition was measured using NMR imaging (EchoMRI).

For cold challenge and food fasting experiments after leptin treatment, the osmotic pumps from *ob/ob* mice were removed under anesthesia after 14 days of treatment, and mice were allowed to recover for 2 days. For cold challenge, mice were subjected to acute leptin (3 mg/kg) or saline i.p. injection at 8 am on the experimental day, then placed at 4 °C for 4 hours from 10am to 2pm. For food restriction, mice were subjected to 3 doses of acute leptin (3 mg/kg) or saline i.p. injection at an interval of 12 hours starting at 7pm the first day when food was removed until mice were sacrificed 36 hours later.

### *Brown Fat, Tail, and Core Temperature Measurements*

Brown fat tissue temperature was measured using subcutaneous temperature implants (IPTT-300, Biomedic Data Systems, DE) inserted at the midline in the interscapular region under anesthesia, at least one week before start of experiment to allow animals to recover. Measurements were taken with the non-contact DAS-8007-C Wireless IPT/IPTT Reader. Tail temperature was measured using an infrared thermal camera (A325, FLIR). Snapshot images were taken at the specified time points and an average of three spot readings were taken at 1 cm from base of the tail. Core temperature was measured using a thermocouple rectal probe (Braintree Scientific).

### *Adipo-Clear and Immunofluorescence for WAT*

White adipose tissue sample collection, delipidation, permeabilization, immunolabeling and clearing were performed similarly as described previously (Chi et al. 2018) with modifications to ensure complete delipidation/immunolabeling of *ob/ob* adipose tissue.

*Sample Collection*

Mice were heavily anesthetized with an overdose of isofluorane and an intracardiac perfusion and fixation was performed with 1xPBS followed by 4% PFA at 4 °C. All harvested samples were post-fixed in 4% PFA at 4 °C for 24 hours. Fixed samples were washed in PBS for 1 hr three times.

*Delipidation and Permeabilization*

The following steps were performed at 4 °C with shaking; fixed samples were washed in 20%, 40%, 60%, 80% methanol in B1N buffer ($H_2O$/0.1% Triton X-100/0.3 M glycine, pH 7), and 100% methanol for 1 hour each. Sample were then delipidated with 100% dichloromethane (DCM; Sigma-Aldrich) for 1 hour, followed by an overnight delipidation and another 5 hours in DCM the next day for a total of three washes. Tissue samples should sink indicating complete sample equilibration between each step. After delipidation, samples were washed in 100% methanol for 1 hour twice, then in 80%, 60%, 40%, 20% methanol in B1N buffer for 1 hour each step. At this point samples can be brought to room temperature. Samples were then washed in B1N for 1 hour twice followed by PTwH buffer (PBS/0.1% Triton X-100/0.05% Tween 20/ 2 mg/ml heparin) for 1 hour twice before further staining procedures.

*Immunolabeling*

Samples were incubated in primary antibody dilutions in PTxwH for 4 days. After primary antibody incubation, samples were washed in PTxwH for 5 min, 10 min, 15 min, 30 min, 1 hr, 2 hr, 4 hr, and overnight, and then incubated in secondary antibody dilutions in PTxwH for 4 days. Samples were finally washed in PTwH for 5 min, 10 min, 15 min, 30 min, 1 hr, 2 hr, 4 hr, and overnight. In this study, CD31 (1:400, R&D Systems, AF3628) and TH (1:400, Millipore, AB1542) were used. Secondary antibodies conjugated with Alexa-568 and Alexa-647 were purchased from Invitrogen (1:400 dilution). After immunolabeling, samples were first washed three times in PBS, then embedded in 1% agarose (in PBS).

*Tissue Clearing*

Embedded samples were dehydrated in 25%, 50%, 75%, 100%, 100% methanol/$H_2O$ series for 1 hour at each step at RT. Following dehydration, samples were washed with 100% DCM for 2 hours twice, followed by an overnight clearing step in dibenzyl ether (DBE; Sigma- Aldrich). Samples were stored at RT in the dark until imaging.

***Immunofluorescence protocol for BAT***

Brown adipose tissue from mice were collected, fixed, delipidated and permeabilized the same way as for WAT. The permeabilized samples were embedded in OCT and cut into 30 µm or 15 µm sections at -20 °C. Sample sections were incubated in primary antibody dilutions in PTxwH (PBS, 0.1% Triton X-100, 0.05% Tween-20, 2 µg/ml heparin) for 4 hr at RT. After primary antibody, samples were washed in PTxwH 4 times, and then incubated in secondary antibody dilutions in PTxwH for 4 hr at RT. Samples were then washed in PTxwH 4 times and mounted with DAPI Fluoromount (Southern Biotech). In this study, CD31 (1:500, R&D System, AF3628), beta-tubulin 3 (1:250, Sigma, T2200-200UL) and TH (1:500, Millipore, AB1542) were used.

Secondary antibodies conjugated with Alexa-568 and Alexa-647 were purchased from Invitrogen (1:500).

### *Light-sheet microscopy Imaging, Processing and Sympathetic Density Quantification*

The imaging processing protocol is adapted from (Chi et al. 2018). All whole-tissue samples were imaged on a light-sheet microscope (Ultramicroscope II, LaVision Biotec) equipped with 1.3X (used for whole-tissue views with low-magnification) and 4X objective lenses (used for high-magnification views for quantification) and an sCMOs camera (Andor Neo). Images were acquired with the ImspectorPro software (LaVision BioTec). Samples were placed in an imaging reservoir filled with dibenzyl ether (DBE) and illuminated from the side by the laser light sheet. The samples were scanned with the 488, 561, and 640nm laser channels, with a step-size of 3 μm for the 1.3x objective and 3 μm for the 4X objective.

All whole-tissue images were generated using Imaris x64 software (version 8.0.1, Bitplane). 3D reconstruction was performed using the ‘‘volume rendering’’ function. Optical slices were obtained using the ‘‘orthoslicer’’ tool. To isolate a specific region of the tissue, the surface tool was used, and the mask option was selected. For tracing SNS nerve fibers, the FilamentTracer tool was applied to automatically reconstruct the neurites in 3D on images generated by the 4x objective. 3D pictures and optical sections were generated using the ‘‘snapshot’’ tool.

Regions of interest were imaged with a 4x objective lens. In each region, small cubic segments (at least 4 cubes per region) that were completely contained within lobules were created using the surface tool of Imaris. TH signal in each cube was reconstructed with the FilamentTracer tool. Regional volumes ($\mu m^3$) and total neurite length (μm) of the cubes were automatically calculated by the surface and FilamentTracer tools, respectively. Sympathetic nerve density in each cube was calculated as the ratio of total neurite length divided by regional volume.

### *Confocal Imaging and Sympathetic Density Quantification*

Representative sample regions were imaged using an inverted Zeiss LSM 780 laser scanning confocal microscope with a 20X objective lens. In each region imaged, 3 random sub-regions were picked and set to a normalized threshold for TH staining intensity. TH signal in each sub-region is quantified as the ratio of stained area to region size. Eighteen to twenty-seven sub-regions were quantified for each biological replicate.

### *RNA Preparation and Quantitative PCR (qPCR)*

Total RNA was extracted from inguinal and brown fat tissue using TRIzol (Invitrogen) along with QIAGEN RNeasy mini kits. For qPCR analysis, RNA was reverse transcribed using the QuantiTech Reverse Transcription Kit (Qiagen). cDNA was used in qPCR reactions containing SYBR-green fluorescent dye (ABI). Relative mRNA expression was determined by normalization with Tbp (TATA-box binding protein) levels using the $\Delta\Delta C_t$ method. For brains, leptin or saline treated *ob/ob* animals were perfused briefly with sterile PBS, brains were dissected out quickly and PVH region was micro-dissected under a dissection scope. RNA was isolated from the sample using PicoPure RNA isolation kit (Thermo) following manufacture’s protocol. Relative BDNF

mRNA expression was determined by normalization with RPL32 (ribosomal protein L32) levels using the $\Delta\Delta C_t$ method. Primer sequences (forward and reverse primers, 5'-> 3' respectively) are listed below.

**Table 1. Primer sequence for qPCR.**

| | Forward 5'-3' | Reverse 5'-3' |
|---|---|---|
| Ucp1 | ACT GCC ACA CCT CCA GTC ATT | CTT TGC CTC ACT CAG GAT TGG |
| Cox8b | GAA CCA TGA AGC CAA CGA CT | GCG AAG TTC ACA GTG GTT CC |
| Cidea | TGC TCT TCT GTA TCG CCC AGT | GCC GTG TTA AGG AAT CTG CTG |
| Tbp | GGGTATCTGCTGGCGGTTT | TGAAATAGTGATGCTGGGCACT |

***Western Immunoblotting***

Whole-tissue protein lysate was extracted using QIAGEN TissueLyser II and RIPA buffer containing 50mM Tris, 150mM NaCl, 1% Triton X-100, 10% glycerol, 0.1% SDS, pH 7.5, and cOmplete protease inhibitors (Roche) and PhosSTOP (Roche). The following antibodies were used for immunoblotting; UCP1 (Abcam, ab10983, 1:1000), TH (Millipore, ab152, 1:1000), p-HSL (Cell Signaling, 4126, 1:500), HSL (Cell Signaling, 4107, 1:1000), PGP9.5 (Proteintech, 14730-1-AP, 1:500) and Vinculin (Cell Signaling, 4650T, 1:1000). Following primary Ab incubation, membranes were probed with IRDye 800CW or IRDye 680RD (Licor Biosciences, 1:10000) secondary Ab and imaged using the LiCOR Odyssey system. Blots were quantified using LiCOR Image Studio software.

***Leptin ELISA***

Blood samples were collected at experimental time points through cardiac puncturing (if terminal) or tail vein bleeding. Serum was collected from blood samples using EDTA coated microcentrifuge tubes (MICROVETTE CB300 EDTA), centrifuged at 300 G for 20 minutes at 4 °C and stored at -80 °C until analysis. Plasma leptin were analyzed by Leptin ELISA according to the manufacturers protocol (R&D systems).

***Adipose sympathetic nerve activity (SNA) recording***

As described before, *ob/ob* mice were treated with leptin or saline for 14 days, followed by the removal of osmotic pumps. After 2 days of recovery, SNA recordings were performed as described previously (Bell et al. 2018). Briefly, each mouse was anesthetized with intraperitoneal administration of Ketamine (91 mg/kg body weight) and Xylazine (9.1 mg/kg body weight) and underwent intubation with PE-50 to provide an unimpeded airway for the mouse to spontaneously breathe $O_2$ enriched room air. Next, a micro-renathane tubing (MRE-40, Braintree Scientific) was inserted into the right jugular vein for infusion of the sustaining anesthetic agent, α-chloralose (initial dose: 12 mg/kg, then sustaining dose of 6 mg/kg/hr). Another MRE- 40 catheter was inserted into the left carotid artery for continuous measurement of arterial pressure and heart rate. Core body temperature was monitored with a use of a rectal probe and continuously maintained at 37.5 $^{o}$C.

Each mouse was then equipped for direct multifiber SNA from nerves innervating WAT and BAT. The mouse was first positioned on its dorsal side and the nerve sub-serving the inguinal WAT was accessed through a small incision made on the right flank near the hind limb. A bipolar platinum-iridium electrode (36-gauge, A-M Systems) was suspended under the nerve and secured with silicone gel (Kwik-Sil, WPI). The electrode was attached to a high-impedance probe (HIP-511, Grass Instruments) and the nerve signal was amplified at $10^5$ times and filtered at a 100- and 1000-Hz cutoffs with a Grass P5 AC pre-amplifier. The amplified and filtered nerve signal was routed to a speaker system and to an oscilloscope (model 54501A, Hewlett-Packard) to monitor the audio and visual quality of the WAT sympathetic nerve recordings for quantification purposes. The amplified, filtered nerve signal was also directed to a MacLab analogue-digital converter (Model 8S, AD Instruments Castle Hill, New South Wales, Australia) containing the software (MacLab Chart Pro; Version 7.0) that utilizes a cursor to analyze the number of spikes/second that exceeds the background noise threshold. Under a stable isothermic (37.5 °C) and anesthesia: baseline WAT SNA was recorded over a 30 min period. At the end this first recording period, the nerve was sectioned to determine background noise which was subtracted from the measured basal WAT SNA.

Next, the mouse was re-positioned on its ventral side and the nerve sub-serving inter-scapular BAT was accessed through an incision in the nape of the neck. The same bipolar platinum-iridium electrode (36-gauge, A-M Systems) was suspended under this nerve and secured with silicone gel (Kwik-Sil, WPI). Under a stable isothermic (37.5 °C) and anesthesia, baseline BAT SNA was recorded over a 30 min period. Core body temperature of the mouse was then cooled by lowering the surgical platform temperature using ice packs. This produces a slow reduction in the mouse's body temperature from 37.5 °C to 27.5 °C. As soon as the core body temperature reached 27.5 °C; the mouse was immediately warmed back to 37.5 °C by removing the ice packs and by exposing the mouse to a heated surgical light. Blood pressure, heart rate and BAT SNA were continuously recorded during this entire cooling/heating procedure. At the completion of the study, the mouse was euthanized and background noise was measured and subtracted from BAT SNA measurements.

### *$O_2$ respiration assay*

Tissue respiration was performed using a Clark electrode (Strathkelvin Instruments). Freshly isolated tissues were isolated from WT, *ob/ob*, leptin treated *ob/ob* (400ng/hr for 14 days) and pair-fed *ob/ob* mice. Tissues were minced and placed in respiration buffer. For each adipose depot, readings were taken with three separate pieces of tissue of equivalent size. $O_2$ consumption was normalized to tissue weight.

### *Energy expenditure measurement in metabolic home cages*

Metabolic phenotyping of mice was performed using an automated home cage phenotyping system (TSE-Systems). Briefly, the system allows for phenotyping of mice in a home-cage environment, which periodically measures a number of metabolic parameters in an automated fashion. In particular, we used a climate-controlled chamber (temperature: 22°C; humidity: 55%; 12 hr light-dark cycle). Locomotor activity is recorded as beam breaks, measuring activity in 3-D. Beam breaks are analyzed by custom software from the metabolic cage, which enables conversion

of beam breaks into distance/velocity. Additionally, an indirect gas calorimetry module determines through an open circuit oxygen consumption and carbon dioxide production. TSE software calculates respiratory exchange ratio (RER) and energy expenditure from these values. All parameters can be measured continuously and simultaneously in up to 16 animals. In our paradigm, *ob/ob* mice were first placed in the metabolic home cage and left single-housed for one week, to enable habituation to social isolation. On Day 0, *ob/ob* mice were split into 2 groups, one group implanted with osmotic pump delivering leptin (400ng/hr for 14 days) and another one with PBS. Following surgery, metabolic data were collected over the subsequent 14 days.

### *Animal study design*

No statistical methods were specifically used to calculate the sample size. Sample size was determined based on previous studies and literature in the field using similar experimental paradigms and to reach a minimum of at least three animals per group. No data were excluded, except animal subjects with deteriorating health issues after surgery or during the experiment, and the ones with "missed" or "partial" viral targeting. All experiments were performed with at least two technical replicates, each time containing the same number of biological replicates, and all attempts at replication were found to be reproducible. To randomize experimental samples, littermates of the same sex were randomly assigned to either experimental or control groups. Data were collected blind, and analysis was also performed blind to prevent any bias.

## Chapter 3. Leptin receptor (LepR) mediated regulation of SNS innervation

### 3.1. Leptin regulates innervation through a brain-mediated mechanism

After revealing that leptin can induce sympathetic plasticity in *ob/ob* mice, in this Chapter, we set out to uncover the underlying mechanisms. Leptin's primary site of action is the brain, raising the possibility that innervation is regulated by top-down efferent signals from the CNS. Therefore, the first experiment we did was to delivery leptin (or vehicle) intracerebroventricular (i.c.v.) in *ob/ob* mice for 14 days and measure their innervation level (Figure 3.1 a). We implanted a cannula targeting the lateral ventricle of *ob/ob* mice and connected the cannula with a subcutaneous osmotic pump delivering leptin at a rate of 12ng/hr, which was proved to have no obvious effect if delivered to the periphery. The body weights of the mice dropped rapidly following leptin delivery (Figure 3.1 a). At the same time, we found that i.c.v. leptin also significantly increases SNS innervation of *ob/ob* mice in both iWAT and BAT (Figure 3.1 b-c).

To test whether leptin has any direct effect on the sympathetic neurons innervating fat tissues, we dissected sympathetic ganglia from neonates, dissociated single cells from the ganglia, cultured sympathetic neurons *ex vivo*, and tested whether leptin has direct effects on these cultured neurons (Figure 3.1 d). We delivered nerve growth factor (NGF) to support neural survival and growth *ex vivo*, and found that it significantly increased cell density and axonal outgrowth in the sympathetic cell culture. We also delivered leptin at 100 ng/mL to the neuron culture with or without NGF, and found that leptin does not lead to more neural outgrowth in either condition. indicating that leptin does not directly act on neurons in sympathetic ganglia to promote their outgrowth.

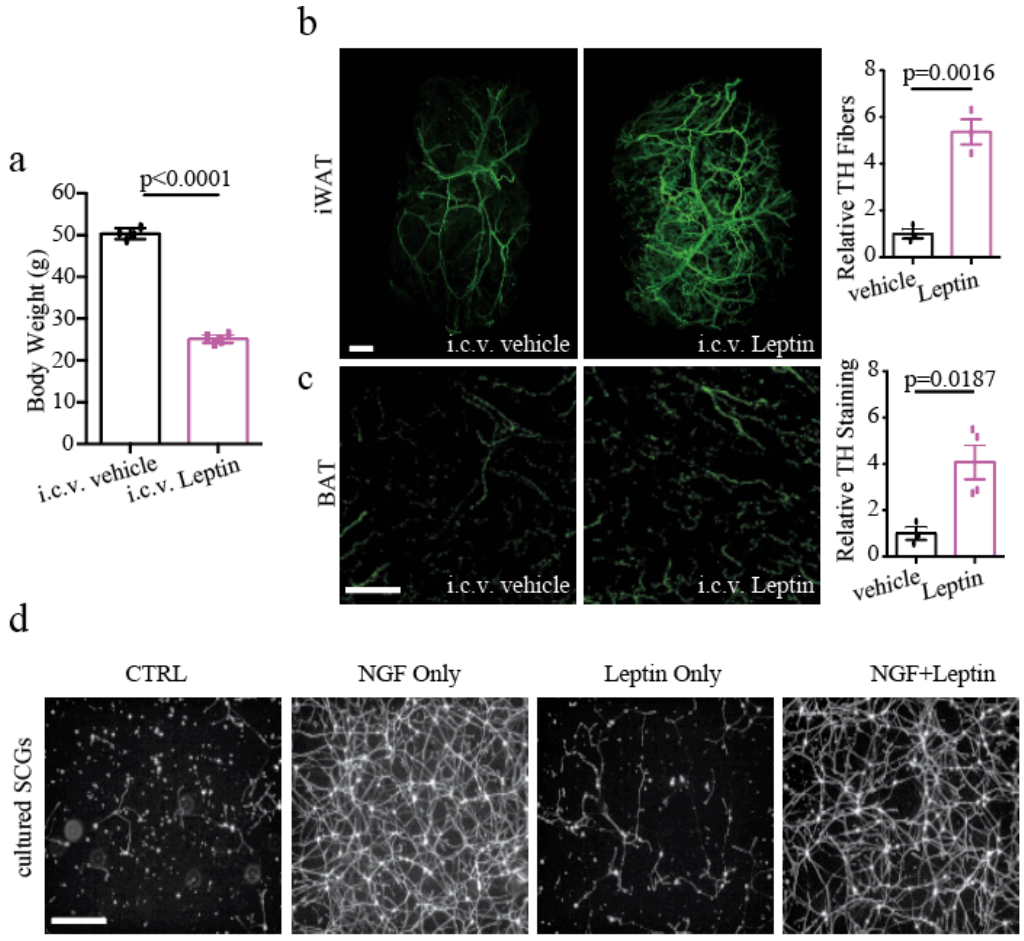


**Figure 3.1. Leptin regulates SNS innervation through the brain.**

(a) Average body weight of *ob/ob* mice after 14-day i.c.v. leptin or vehicle control (n=4 per group). SNS innervation density in (b) iWAT (n = 3 per group) and (c) BAT (n =3 for vehicle control; n=4 for Leptin) of *ob/ob* mice after a 14-day i.c.v. infusion of leptin (12 ng/hr). Graphs on right show quantification of images. (d) Leptin has negligible effects on the nerve growth of cultured superior cervical ganglia neurons. Dissociated cultured sympathetic ganglia treated with either NGF (10 ng/ul) only, leptin (100 ng/mL) only or both. Controls received neither factor. After 48 hours, sympathetic neurons were fixed with 2% PFA in PBS, permeabilized and stained with anti-tyrosine hydroxylase (TH) antibody. Scale bar, 1mm (b); 100 μm (c). Data shows mean ± SEM, significant differences between treatments calculated using Student's two-tailed, unpaired t test.

Once proved that leptin regulates SNS innervation through a brain mediated pathway, we next set out to reveal the neural mechanism underlying this phenotype. To do this, we first need to identify sites of intersection between leptin signaling and efferent pathway regulating sympathetic innervation of adipose tissue, utilizing a neurotropic pseudorabies virus (PRV, Pomeranz et al. 2017). Once injected into the adipose tissue, PRV is uptaken by the sympathetic axons and further propagates to label a series of presynaptic neurons before entering the brain. The first neurons infected by PRV, two days post-injection, are the sympathetic postganglionic neuron located in the sympathetic chain. PRV replicates in the postganglionic neurons and further infects the upstream sympathetic preganglionic neurons located in the spinal cord (Figure 3.2 a). In order to confirm that neurons in the sympathetic chain are the first order neurons innervating fat, we utilized a neurotropic toxin Cholera Toxin Subunit B (CTb) which does not replicate and therefore will not infect neurons beyond the ones directly projecting to fat. As expected, CTb only infects neurons in the sympathetic chain (Figure 3.2 a). Four days after PRV injection, we started to observe neurons labeled with PRV inside the brain. Brain regions labeled by PRV on Day 4 include the PVH and RPa, two sympathetic premotor regions which are known to project mono-synaptically to the IML (Nakamura et al. 2004; Biag et al. 2012). All the brain regions infected by PRV through day 4 to day 7 are summarized in Figure 3.2 b. We also injected PRV expressing GFP into iWAT or BAT of LepR-cre::LSL-TdTomato mice that express TdTomato fluorescent protein in LepR expressing neurons. In this experiment, co-localization of TdTomato and GFP marks leptin responsive neurons that project indirectly to adipose tissue. Starting from five days post-infection, we observed several regions containing LepR neurons infected with PRV (Figure 3.2 b, region highlighted in red). Among these regions, we noted extensive overlap of GFP (for PRV) and Tomato (for LepR) expression in neurons from the ARC (Harlan et al. 2011b; Pandit, Beerens, and Adan 2017a), the DMH (Y. Zhang et al. 2011) and medial preoptic area (MPO, Y. Zhang et al. 2011), each of which has been reported to regulate energy expenditure (Figure 3.2 c).

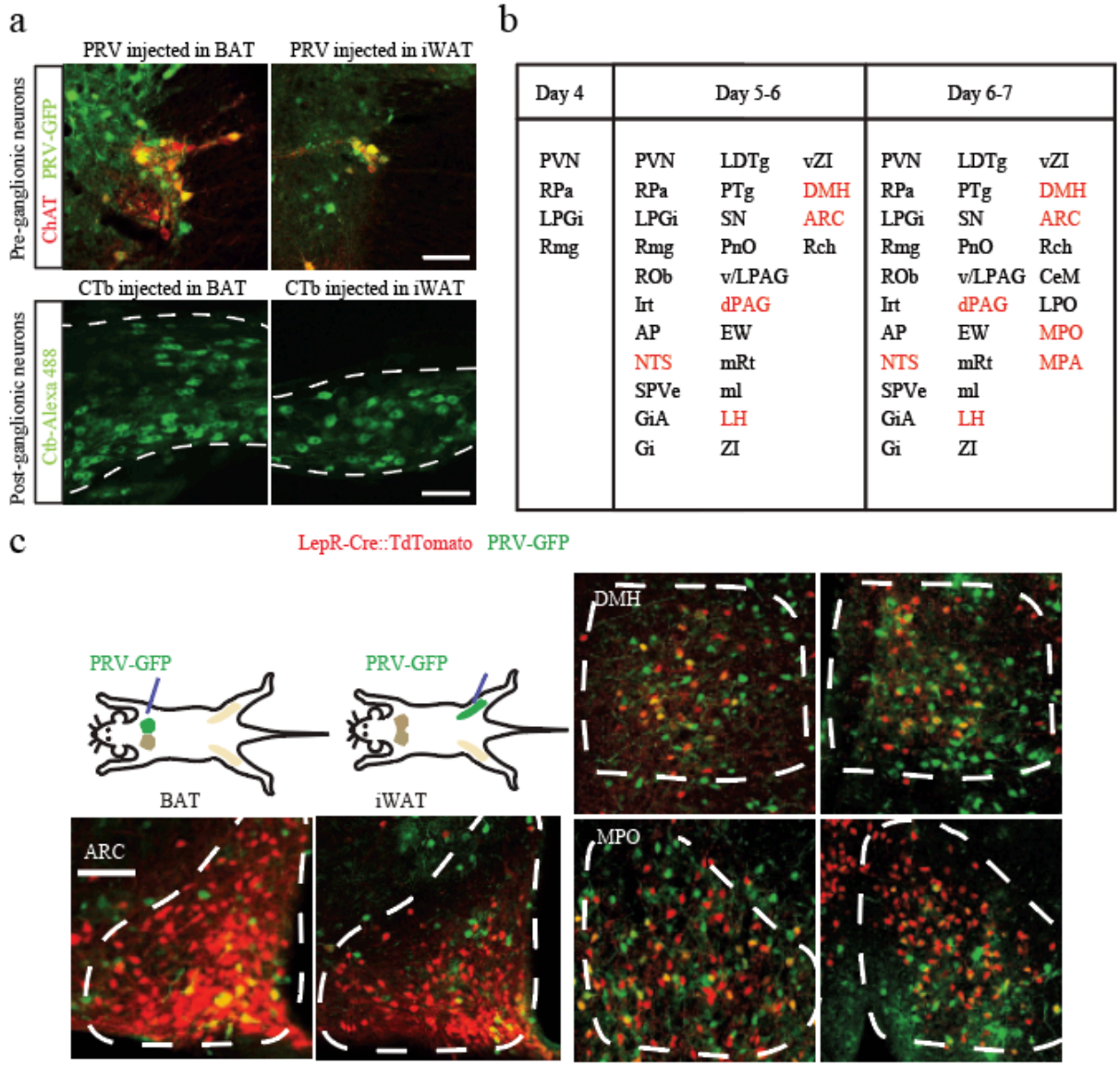


**Figure 3.2. Identification of neural pathways innervating adipose tissues.**

(a) To identify the first order neurons innervating adipose depots, cholera toxin B subunit (CTB) conjugated with Alexa 488 was injected into adipose depots. Once taken up by sympathetic axons it is transported to the cell bodies of sympathetic post-ganglionic neurons (bottom row). 2nd and subsequent order neurons were traced by injecting PRV expressing GFP into adipose depots which traveled retrogradely to infect sympathetic pre-ganglionic neurons in the IML before entering the brain (top row). (b) Table of brain regions infected by PRV from adipose depots over 4-7 days. Red text denotes regions overlapping with LepR-Tomato neurons. (c) Scheme showing PRV expressing GFP injected into BAT or iWAT of LepR-Cre::LSL-TdTomato mice. 4-7 days later, colocalization (in yellow) of PRV (in green) from either iWAT or BAT with LepR-Tomato neurons (in red) was observed in arcuate nuclei (ARC), medial preoptic area (MPO), and dorsal medial hypothalamus (DMH). Scale bar, 100 μm.

### 3.2. Leptin regulates innervation through ARC

Since LepR expressing neurons in ARC, DMH and MPO have been shown to regulate energy expenditure (Pandit, Beerens, and Adan 2017b), we hypothesized that one or multiple of these nuclei are involved in regulating leptin dependent SNS innervation. To test our hypothesis, we used a viral mediated strategy to genetically ablate leptin signaling in these neuron populations of adult mice. We injected an AAV virus expressing GFP-Cre bilaterally into the brain of $LepR^{fl/fl}$ mice, targeting ARC, DMH and MPO individually (Figure 3.3 a). Viral induced Cre expression in the indicated region will lead to a loss of LepR gene. Eight weeks post virus injection, we injected the mice with 3mg/kg leptin and perfused the mice 2 hours afterwards to check the efficiency of viral mediated LepR deletion. As expected, viral mediated LepR deletion results in a blunted responsiveness to leptin signaling, as shown by reduced pSTAT3 signaling, in the injected region only (Figure 3.3 b). Loss of leptin signaling in ARC ($LepR^{\Delta ARC}$), but not DMH ($LepR^{\Delta DMH}$) or MPO ($LepR^{\Delta MPO}$), leads to significant increase in body over eight and daily food intake in mice (Figure 3.3 c-d). Furthermore, only $LepR^{\Delta ARC}$ results in a dramatic reduction of SNS innervation in both iWAT and BAT (Figure 3.3 e-f). The innervation level of $LepR^{\Delta DMH}$ or $LepR^{\Delta MPO}$ are comparable to control animals. To confirm that simply expressing virus in the ARC does not lead to alternation in SNS innervation, we did the following experiment. We injected AAV expressing either GFP or GFP-Cre bilaterally into ARC of $LepR^{fl/fl}$ mice, and checked the efficiency of leptin receptor deletion in the ARC eight weeks post injection. Virus targeting was confirmed by visualizing GFP expression in the ARC of both groups; whereas leptin signaling loss was only observed in GFP-Cre expressing group. In the GFP-Cre injected mice, the number of cells in the ARC expressing leptin-induced p-STAT3 was reduced >95%, indicating efficient LepR deletion in these mice (Figure 3.4 a). As expected, mice in the GFP-Cre injected group continuously put on weight over eight weeks post injection and consume significantly more food, compared to those in the GFP injected group (Figure 3.4 b-c). Mice in GFP-Cre injected group also show a rising serum leptin level comparing to the controls, meaning that they have higher body fat mass (Figure 3.4 d). Similarly as shown before, LepR deletion by injecting GFP-Cre in ARC leads to loss of SNS innervation in both iWAT and BAT, whereas simply GFP expression does not (Figure 3.4 e-f). Interestingly, $LepR^{\Delta ARC}$ leads to an 85% reduction of SNS innervation in iWAT and 60% reduction in BAT. The relative level of SNS, ~6 fold reduction compared to WT, in the iWAT was similar as observed in *ob/ob* mice that does not respond to leptin at all (Figure 2.5). This suggests that LepR neurons in the ARC are the primary regulators of SNS innervation in iWAT. However, LepR deletion in ARC only leads to 60% reduction of SNS in BAT, whereas the reduction is >80% in *ob/ob* mice, suggesting that leptin signaling through other LepR neurons might also play important roles in BAT innervation (Figure 2.5). Besides the structural change of SNS in BAT, we also observed a thermogenesis defect in mice with GFP-Cre injection (Figure 3.4 g-h). When exposed the mice from both GFP and GFP-Cre injected groups to 4-degree environment, we found that mice in the GFP-Cre group exibhits a reduced thermogenic response, as shown by lower BAT and core temperature following cold exposure comparing to those in the GFP group (Figure 3.4 g-h). These functional data suggest that innervation reduction in BAT is associated with reduced BAT thermogenic capability.

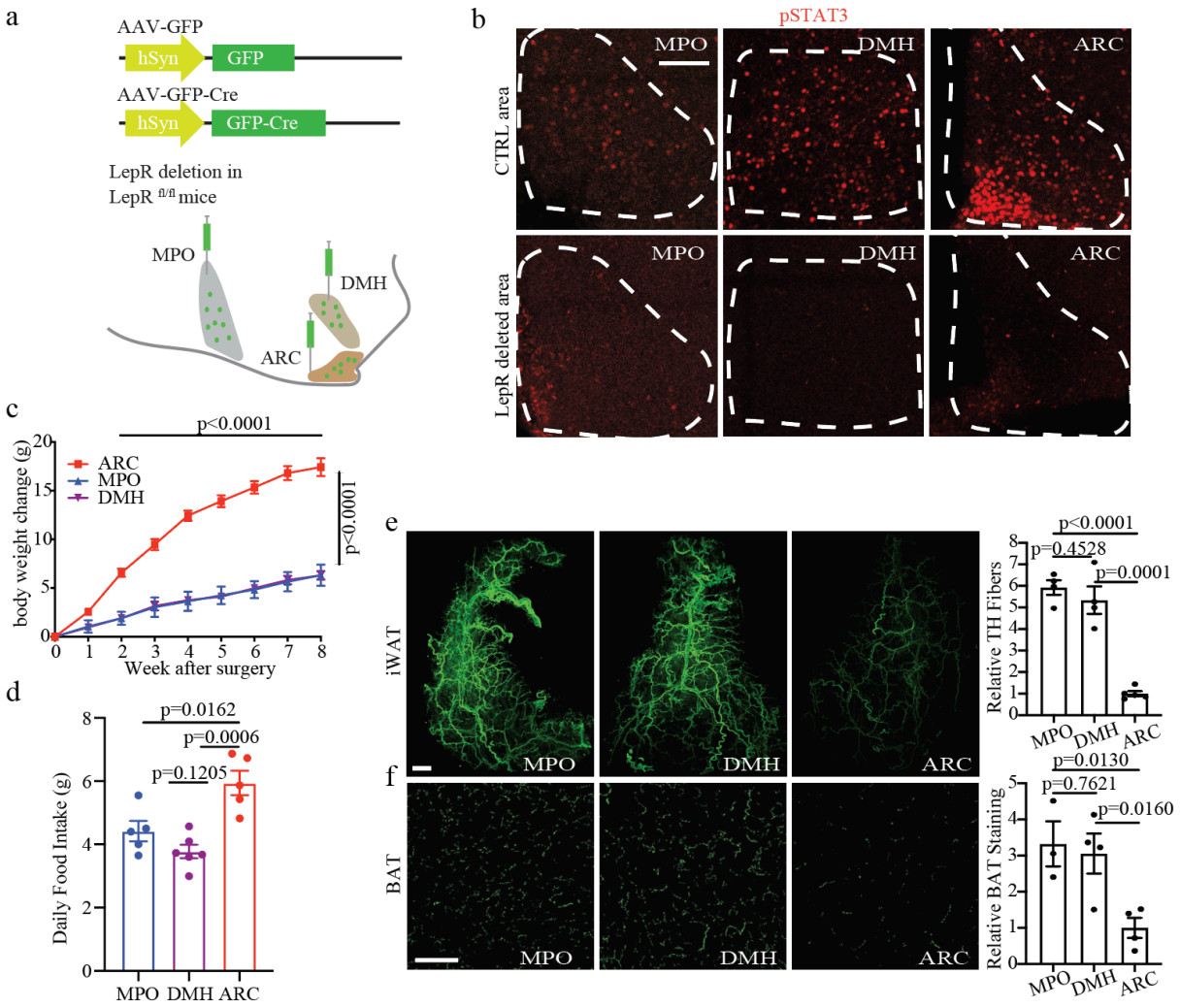


**Figure 3.3. LepR expressing neurons in the ARC, not DMH or MPO, regulate SNS innervation.**

(a) Scheme for deleting leptin receptor in these brain regions. AAV-hSyn-GFP-Cre was bilaterally injected into ARC, DMH or MPO of adult $LepR^{fl/fl}$ mice resulting in loss of LepR expression. (b) 8 weeks post-surgery of AAV-GFP-Cre delivery into brain regions shown in Fig. 2d, 3 mg/kg IP leptin induced p-STAT3 signaling in indicated area was assessed to evaluate LepR deletion. Injection of AAV-GFP-Cre in indicated area leads to depletion of p-STAT3 (bottom row), compared with the same region in brain sections from the other two groups where LepR is deleted elsewhere (top row). (c) Body weight progression and (d) daily food intake of mice treated above (n=6 for MPO, n=5 for all other groups). TH immunolabeling was visualized in (e) iWAT (n=4 per group) and (f) BAT (n=3 for MPO, n=4 for DMH and ARC) of mice after deletion of LepR in these nuclei. Scale bar, 1mm (c); 100 µm (b, f). Data shows mean ± SEM, significant differences between treatments calculated using Two Way Anova Test (c), Student's two-tailed, unpaired t test (d, e, f).

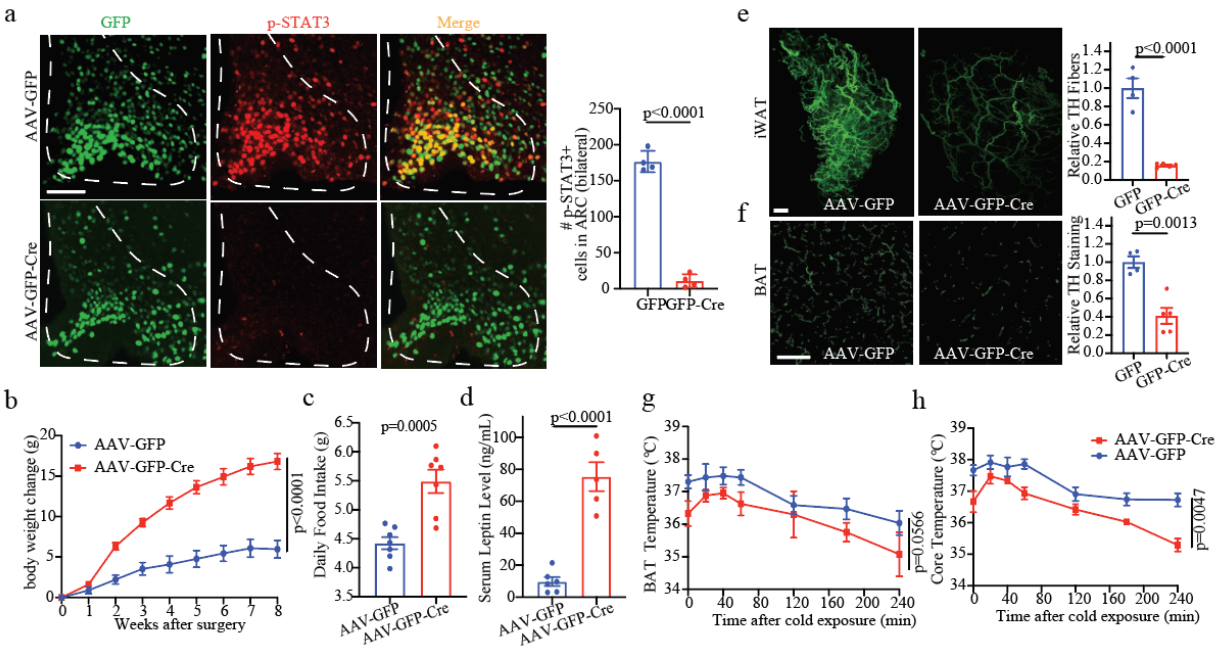


**Figure 3.4. Leptin signaling in ARC regulates SNS innervation and thermogenesis.**

(a) AAV-GFP-Cre injection (bottom row) in ARC of LepR$^{fl/fl}$ mice reduced leptin induced p-STAT3 signaling compared to AAV-GFP injected controls (top row). Quantification of imaging data shown on the right (n= 4 per group). (b) Body weight progression (n=7 per group) and (c) daily food intake of mice treated as in Fig. 2g-h (n=7 per group). (d) Serum leptin level of LepR$^{fl/fl}$ mice 8 weeks post-surgery of AAV-GFP-Cre or AAV-GFP injection (n=6 for AAV-GFP, n=5 for AAV-GFP-Cre). (e-f) TH immunolabeling was visualized in (e) iWAT and (f) BAT, quantification is shown on the right (n=4 for GFP, n=5 for GFP-Cre). Scale bar, 1mm (e); 100 μm (a, f). Data shows mean ± SEM, significant differences between treatments calculated using Two Way Anova Test (b, g, h), Student's two-tailed, unpaired t test (a, c-f).

### 3.3. Diet-induced leptin signaling loss in ARC leads to reduced innervation

So far, we have proved that genetic deletion of LepR in the ARC region leads to SNS innervation loss in both iWAT and BAT. Now we would like to know whether diet induced leptin resistance in the ARC also leads to alternation of innervation. Diet-induced obesity (DIO) is associated with leptin resistance and a partial loss of leptin signaling in the ARC (Münzberg, Flier, and Bjørbæk 2004). We fed WT mice on 60% high fat diet (HFD) for 4 months, during which time the mice gradually put on weight (Figure 3.5 a-b). These animals became increasingly leptin insensitive over the 4 months; at the end of the treatment there is only a low level of STAT3 phosphorylation after leptin treatment (Figure 3.5 e). Consistent with this loss of leptin signaling in the ARC, the DIO animals also showed a significant decrease of sympathetic innervation in subcutaneous adipose depots (Figure 3.5 c-d). However, the innervation level of HFD mice after 4 months of treatment is still lower than weight matched *ob/ob* mice (Figure 3.5 f-g). This is probably because HFD fed mice still have a low level of residual leptin signaling in the ARC, whereas *ob/ob* mice does not have any residual leptin signaling. These data demonstrated that both genetic and induced leptin signaling loss in the ARC lead to SNS innervation loss in adipose tissue. More importantly, we have shown that leptin can bidirectionally regulate SNS innervation in the adipose tissue. Giving leptin to *ob/ob* mice leads to innervation increase, and removing leptin signaling leads to innervation loss.

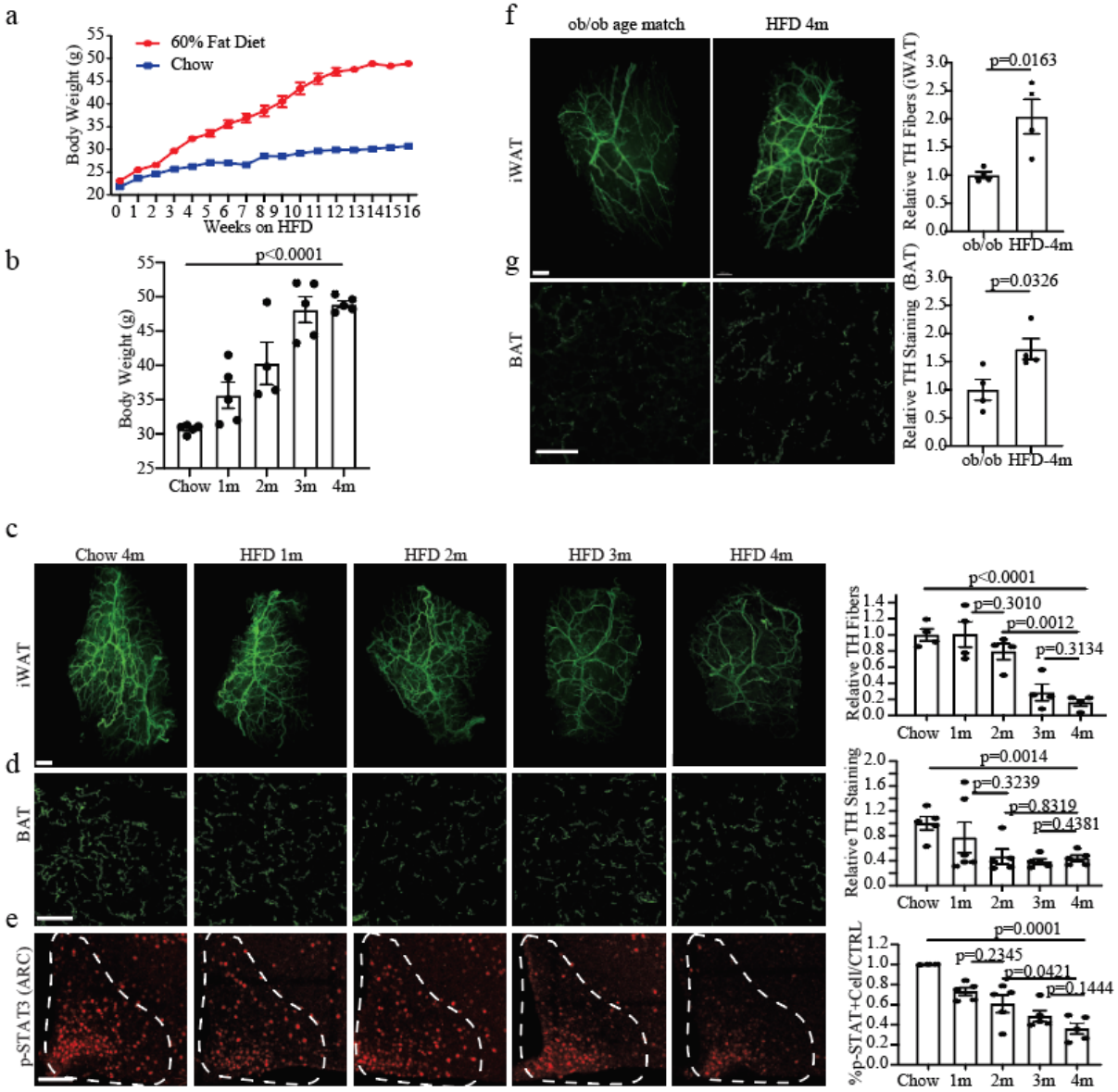


**Figure 3.5. Diet induced obesity leads to innervation loss.**

(a) Body weight progression of WT mice fed on 60% HFD (red) compared to those fed on standard chow (blue) for 4 months (n = 5 per group). (b) Body weight progression of mice fed on 60% HFD (n = 5 per group except for 2-month HFD, n = 4). (c-d) Innervation defects in DIO mice. WT mice fed on standard chow for 4 months compared with WT mice fed with 60% fat diet for 1, 2, 3 or 4 months. TH immunolabelling was visualized in iWAT (c, n = 4 per group) and BAT (n = 6 for 1-month high-fat diet (HFD 1m), d, n = 5 for all other groups). (e) Diminished leptin induced p-STAT3 signaling in the ARC of mice shown in c and d (n = 3 for chow 4m, n = 5 for all other groups). (f-g) TH immunolabelling visualized in iWAT (f) and BAT (g) of age matched *ob/ob* mice (left) compared to WT mice fed on 60% HFD for 4 months (right). Graphs on right show quantification of images (n = 4 per group). Scale bar, 1 mm (c, f); 100 µm (d, e, g). Data shows mean ± SEM, significant differences between treatments calculated using Student's two-tailed, unpaired t-test.

### 3.4. AGRP and POMC neurons regulate innervation

Leptin receptor neurons in the ARC are heterogenous, where AGRP and POMC expressing ones compose two of the major cell types (Session 1.2, Håkansson et al. 1998). AGRP and POMC neurons are both the first order leptin responsive neurons in the brain, however, leptin modulate the two groups of neurons in an opposite way. Leptin treatment inhibits AGRP activity (Baver et al. 2014; J. Xu et al. 2018), whereas leptin treatment increases POMC neuron activity (Cowley et al. 2001). Prior studies have demonstrated that leptin receptor deletion in AGRP neurons of adult animals leads to severe obesity, increased daily food consumption and decreased BAT temperature (J. Xu et al. 2018). Germline leptin receptor deletion from POMC neurons also results in mild obesity due to decreased energy expenditure (Balthasar et al. 2004).

Besides the functions we discussed above, AGRP and POMC neurons have also been shown to regulate SNS activity. First of all, leptin receptor deletion from entire ARC leads to blunted sympathetic activity after leptin treatment to BAT (Harlan et al. 2011a; Rahmouni and Morgan 2007). Moreover, LepR deletion using a Cre-Flox system from AGRP neurons leads to blunted SNA to both BAT and iWAT following leptin treatment. However, LepR deletion using Cre-Flox system from POMC neurons only leads to decreased BAT SNA following leptin administration (Bell et al. 2018). Despite the studies done on SNA, so far there has not been any study on whether AGRP or POMC neurons can modulate SNS innervation in adipose tissues. Therefore, we are going to investigate this in the following session.

#### 3.4.1. Role of AGRP neurons in regulating SNS innervation

To reveal the individual role of AGRP or POMC neurons in regulating SNS innervation, we first need to confirm whether these two population projects to the adipose tissue through a polysynaptic circuit. We injected PRV-GFP into the fat of AGRP-IRES-Cre::LSL-TdTomato mice; after 5 days, we observed colocalization of PRV with AGRP neurons in the ARC (Figure 3.6 a). The we employed a CRISPR-Cas9 based method as reported previously (J. Xu et al. 2018) to delete LepR specifically in AGRP neurons. AGRP-IRES-Cre mice were crossed with LSL-Cas9-GFP mice to express Cas9 specifically AGRP neurons, followed by bilateral injection of AAV driving a single guide RNA (sgRNA) targeting the mouse *Lepr* (sgLepR) locus or a control guide RNA (sgCtrl) (Figure 3.6 b). Specific deletion of the gene encoding LepR was validated by loss of leptin-induced p-STAT3 signaling in Cre-expressing cells (>95% reduction), compared to adjacent Cre-negative cells (Figure 3.6 c). Consistent with previous report (J. Xu et al. 2018), LepR deletion in adult AGRP neurons ($AGRP^{\Delta LEPR}$) leads to significant increase in body weight, daily food intake and serum leptin level (Figure 3.6 d-e). More importantly, $AGRP^{\Delta LEPR}$ showed a remarkable reduction of SNS innervation in both iWAT and BAT, comparing to mice injected with sgCtrl (Figure 3.6 g-h). After seeing the reduction in SNS innervation in $AGRP^{\Delta LEPR}$ mice, we asked whether this led to a alternation in cold responsiveness in mice. We exposed $AGRP^{\Delta LEPR}$ mice to 4 degree environment as previously described, and observed a modest reduction in thermogenic response in $AGRP^{\Delta LEPR}$ mice comparing to the control mice (Figure 3.6 i-j), although the data does not reach statistical significance. Overall, these results indicate that leptin signaling through AGRP neurons are necessary for maintaining WT-level innervation in mice.

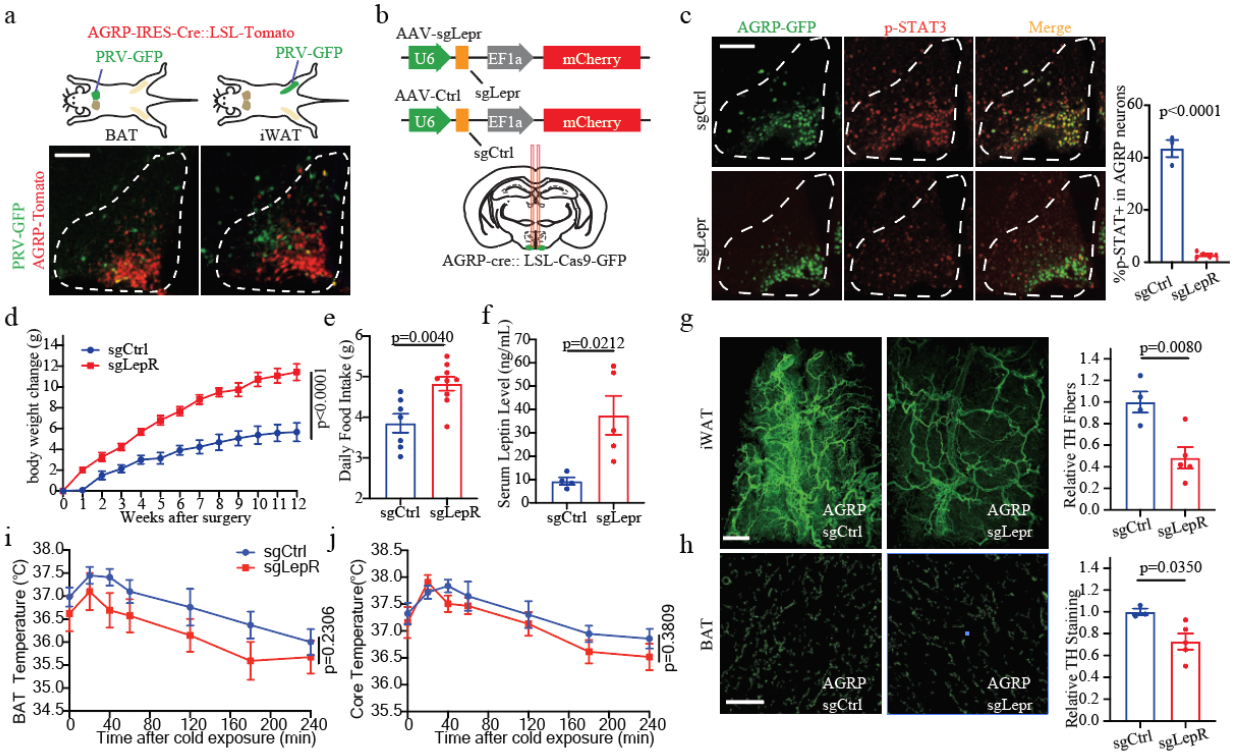


**Figure 3.6. LepR deletion in AGRP neurons leads to innervation loss in adipose tissues.**

(a) PRV-GFP tracing from BAT (left) or iWAT (right) in AGRP-IRES-Cre::LSL-TdTomato mice shows PRV (green) colocalization with AGRP in ARC neurons (red). (b) The gene encoding LepR was deleted in AGRP neurons by injecting AAV-sgLepR or AAV-sgCtrl viruses into the ARC of AGRP-IRES-Cre::LSL-Cas9-GFP mice. (c) Leptin induced p-STAT3 signalling in AGRP neurons 12 weeks after sgCtrl or sgLepR AAV delivery in the ARC of AGRP-IRES-Cre::LSL-Cas9-GFP mice (n = 3 for sgCtrl, n = 5 for sgLepR). (d-e) Body weight progression (d, *n* = 11 per group) and daily food intake (e, *n* = 11 for sgCtrl, *n* = 10 for sgLepR) of AGRP-IRES-Cre::LSL-Cas9-GFP mice. Daily food intake of each animal was calculated as an average of 3 consecutive days. (f) Serum leptin level of AGRP-IRES-Cre::LSL-Cas9-GFP mice 12 week post-surgery of the gRNA injection (*n* = 4 for sgCtrl, *n* = 5 for sgLepR). (g,h) TH immunolabelling was visualized in iWAT (g, n = 4 for sgCtrl, n = 5 for sgLepR) and BAT (h, n = 3 for sgCtrl, n = 5 for sgLepR) of AGRP-IRES-Cre::LSL-Cas9-GFP mice injected with sgLepR or sgCtrl in the ARC. (i-j) BAT temperature (i) and core temperature (j) of AGRP-Cre::LSL-Cas9-GFP mice following cold exposure at 4°C for 4 h (*n* = 10 for sgCtrl, *n* = 11 for sgLepR). Scale bars, 500 µm (g); 100 µm (a, c, h). Data show mean ± s.e.m.; significant differences between treatments were calculated using Two Way Anova Test (d, i, j), or Student's two-tailed, unpaired t-test (c, e-h).

### 3.4.2. Role of POMC neurons in regulating SNS innervation

Next we set out to reveal the role of POMC neurons innervation. Similar as before, we crossed POMC-Cre mice with LSL-Cas9-GFP mice to express Cas9 specifically in POMC neurons. We injected PRV-mCherry into the fat of POMC-Cre::LSL-TdTomato mice; after 5 days, we observed colocalization of PRV with POMC neurons in the ARC (Figure 3.7 a). To access the role of leptin signaling in POMC neurons, we selectively deleted LepR in POMC neurons using the same sgLepr as in 3.4.1 (Figure 3.7 b). Specific deletion of the gene encoding LepR was validated by loss of leptin-induced p-STAT3 signaling in Cre-expressing cells (>95% reduction), compared to adjacent Cre-negative cells (Figure 3.7 c). However, different from the phenotypes of $AGRP^{\Delta LEPR}$ mice, LepR deletion in POMC neurons ($POMC^{\Delta LEPR}$) only leads to modest weight gain (Figure 3.7 d) but has no effects on daily food intake or serum leptin levels (Figure 3.7 e-f). Despite the fact that $POMC^{\Delta LEPR}$ mice do not become severely obese, they do have a significant reduction of SNS innervation in both adipose tissues (Figure 3.7 g-h). In fact, the level of innervation reduction seen in $POMC^{\Delta LEPR}$ mice are similar as that seen in $AGRP^{\Delta LEPR}$ mice. Consistent with a reduction of SNS innervation, there is also a reduced BAT thermogenesis response to cold of $POMC^{\Delta LEPR}$ mice comparing to the controls (Figure 3.7 i-j). These data also demonstrate that leptin signaling through POMC neurons are necessary to keep WT-level SNS innervation in the adipose tissues.

Overall, we have shown that LepR deletion in either AGRP or POMC neurons leads to a significant reduction of SNS innervation in the adipose tissue. It is important to note that the magnitude of SNS innervation change observed in $POMC^{\Delta LEPR}$ or $AGRP^{\Delta LEPR}$ mice is ~50% reduction in iWAT and ~ 30% reduction in BAT (Figure 3.6, Figure 3.7); whereas the magnitude of SNS innervation change in $LepR^{\Delta ARC}$ is ~85% reduction in iWAT and ~60% reduction in BAT (Figure 3.4). This data suggests that AGRP and POMC neurons might act synergistically in regulating leptin-dependent innervation in fat.

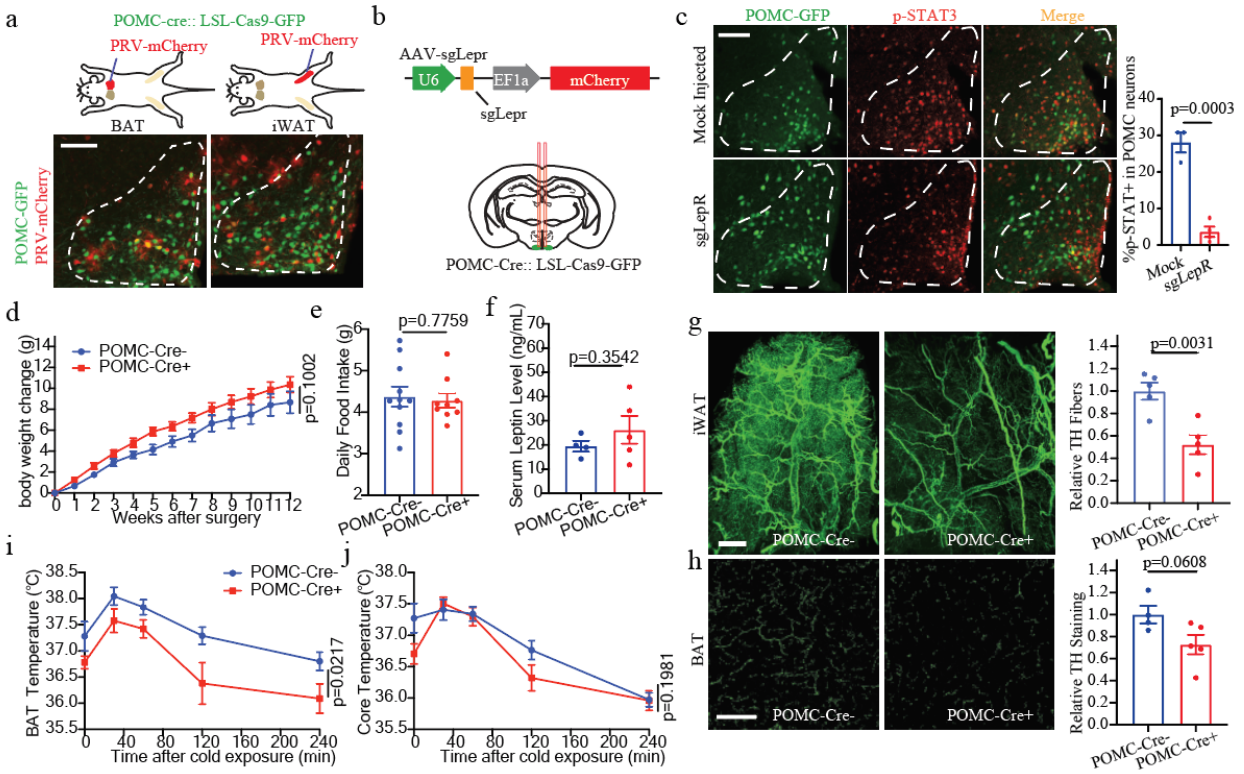


**Figure 3.7. LepR deletion in POMC neurons leads to innervation loss in adipose tissues.**

(a) PRV-mCherry tracing from BAT or iWAT in POMC-Cre::LSL-Cas9-GFP mice shows PRV (red) colocalization with POMC (green) neurons in the ARC. (b) The gene encoding LepR was deleted in POMC neurons by injecting AAV-sgLepR viruses or performing mock injection into the ARC of POMC-Cre::LSL-Cas9-GFP mice. (c) Leptin induced p-STAT3 signalling in POMC neurons after mock injection or sgLepR AAV delivery in the ARC of adult POMC-Cre::LSL-Cas9-GFP mice (n = 3 for mock, n = 4 for sgLepR). (d-e) Body weight progression (d) and daily food intake (e) of POMC-Cre::LSL-Cas9-GFP mice (n = 11 for Cre-, n = 9 for Cre+). Daily food intake of each animal was calculated as an average of 3 consecutive days. (f) Serum leptin level of POMC-Cre::LSL-Cas9-GFP mice 12 week post-surgery of AAV-gRNA injection (n = 4 for Cre-, n = 5 for Cre+). (g-h) TH immunolabelling was visualized in iWAT (g, n = 5 per group) and BAT injection (h, n = 4 for POMC-Cre−, n = 5 for POMC-Cre+) of mice from POMC-Cre−::LSL-Cas9-GFP or POMC-Cre+::LSL-Cas9-GFP mice after sgLepR ARC. (i-j) BAT temperature (i) and core temperature (j) of POMC-Cre::LSL-Cas9-GFP mice following cold exposure at 4°C for 4 h (n = 11 for Cre-, n = 9 for Cre+). Scale bars, 500 µm (g); 100 µm (a, c, h). Data show mean ± s.e.m.; significant differences between treatments were calculated using Two Way Anova Test (d, i, j), or Student's two-tailed, unpaired t-test (c, e-h).

### 3.5. Summary and discussion

In this chapter, we show that leptin regulates SNS innervation in the adipose tissue through the LepR expressing neurons in the brain. We have tested the role of LepR neurons in several nucleus which have been reported to regulate energy expenditure, including those in the DMH, MPO and ARC. We found that only the LepR neurons in the ARC have a profound role in regulating SNS innervation in the fat. Deletion of LepR from neurons in the ARC results in loss of SNS innervation in adipose tissue. Moreover, we also observed loss of innervation in adipose tissue in diet induced obese animals who have a partial loss of leptin signaling in the ARC, comparing to their chow fed littermates. These data demonstrate that active leptin signaling through the ARC are required for the maintenance of WT-level innervation in fat. Furthermore, these data show that leptin can bi-directionally regulate innervation levels in adipose tissue.

Since LepR expressing neurons in the ARC are heterogenous, it is important for us to determine which neurons populations regulate SNS innervation. AGRP and POMC neurons are two of the major populations in the ARC that mediate leptin's role in regulating behavioral and metabolic effects, therefore, we tested which of these two populations regulate leptin dependent SNS innervation. Our results demonstrated that both AGRP and POMC neurons play a role in regulating SNS innervation in fat. Deletion of LepR in either AGRP or POMC neurons results in a reduction of SNS innervation density in the adipose tissues. It is important to note that SNS innervation level we observed from either $POMC^{\Delta LEPR}$ or $AGFP^{\Delta LEPR}$ is intermediate between that from WT and $LepR^{\Delta ARC}$ mice, indicating that these two populations regulate innervation synergistically.

Overall, in this chapter we determined the role of ARC leptin responsive neurons in regulating innervation, which in part provides a mechanism on how these neurons regulate whole body energy homeostasis. In order for AGRP and POMC to regulate innervation in fat, leptin signaling through these two populations needs to reach the either the sympathetic preganglionic neurons in the spinal cord or the sympathetic postganglionic neurons in the periphery. However, both populations project mostly within the brain, leading us to hypothesize that there are downstream populations mediating leptin's effects on innervation. We will explore the possible downstream circuit in the following chapters.

### 3.6. Material and methods

#### *Animals*

All animal care and experimentation were ethically performed according to procedures approved by the Institutional Animal Care and Use Committee at the Rockefeller University. Mice were housed 2–5 per cage (except in the cold exposure study where mice were singly caged) in a 12-h light/12-h dark cycle with ad libitum access to regular chow and water except in fasting studies. We used WT male C57BL/6J mice (000664, Jackson Laboratory), *ob/ob* (B6.Cg-*Lep*$^{ob}$/J; 000632, Jackson Laboratory; or bred in-house), AGRP-IRES-Cre ($Agrp^{tm1(cre)Lowl}$/J; 012899, Jackson Laboratory), POMC-Cre (Tg(Pomc1-cre)16Lowl/J; 005965, Jackson Laboratory), LepR-Cre (B6.129(Cg)-$Lepr^{tm2(cre)Rck}$/J; 008320, Jackson Laboratory), *Lepr*$^{fl/fl}$ (B6.129P2-$Lepr^{tm1Rck}$/J; 008327, Jackson Laboratory), Rosa-LSL-TdTomato (B6.Cg-Gt(ROSA)26$Sor^{tm14(CAG-tdTomato)Hze}$/J;

007914, Jackson Laboratory) and Rosa26-Cas9 knock-in (*Gt(ROSA)26Sor*$^{tm1.1(CAG-cas9*,-EGFP)Fezh}$/J; 024858, Jackson Laboratory). Littermates of the same sex were randomly assigned to either experimental or control groups.

### *Viruses*

AAV viruses used in these studies were obtained from UNC Vector Core or generated through Janelia Viral Tools Service. For *Lepr* deletion in *Lepr*$^{fl/fl}$ mice, AAV5-hSyn-GFP-Cre or AAV5-hSyn-GFP was used. For *Lepr* deletion in AGRP-Cre and POMC-Cre mice, AAV viral vectors were cloned in-house and packaged through Janelia Viral Tools Service. The pU6-sgRNA scaffold cassettes for expressing sgLepR or sgSTOP were used in vector cloning. The sequence of sgLepR was previously reported (J. Xu et al. 2018) and the sequence of sgCtrl is 5′-TTTTTTTTTTTTTTGATATC- 3′. PRV-lp297, a variant of PRV-Bartha expressing GFP or mCherry was used for mapping multi-synaptic input to iWAT and BAT (Pomeranz et al. 2017). PRV-lp297 was made by plaque purification of PRV-Introvert-GFP after passage through Cre-expressing cells (L. Pomeranz, unpublished data). Viral aliquots were stored at −80 °C before stereotaxic or intra-fat injection.

### *Body weight measurement and Cold exposure*

For mice undergoing stereotaxic surgeries to knockout the genes encoding LepR, body weights were measured weekly post-surgery. Eight weeks or twelve weeks post-surgery, mice were implanted with subcutaneous temperature implants (as described in 2.7) and were singly housed for food intake measurements. One week after singly housing, mice were exposed to cold challenge at 4 °C for 4 h from 10:00 to 14:00 hours.

### *High-fat diet feeding*

Mice were subjected to a 60% high-fat diet (D12492, ResearchDiets) feeding starting from 6 weeks of age. Body weights were measured weekly. All mice were subjected to a 3 mg/kg leptin subcutaneous injection and sacrificed two hours later to assay leptin induced p-STAT3 signalling in the hypothalamus.

### *Immunofluorescence for brain sections*

Mice were transcardially perfused with 4% PFA and the brains were post-fixed for 1 day in 4% PFA. Brains were sectioned coronally at 50 μm using a Leica microtome (Leica SM2010R). Brain sections were washed in PBS with 0.1% Triton X-100 (PBST, pH 7.4) and blocked in 3% normal goat/donkey serum (Jackson ImmunoResearch Laboratories) and 2% BSA (Sigma) in PBST for 2 h. For p-STAT3 staining, brain slices were pre-treated with 1% $H_2O_2$ + 1% NaOH in $H_2O$ for 20 min at room temperature before blocking. Slides were then incubated overnight at 4 °C (for anti-GFP) or at room temperature in primary antibody. After washing in PBST, sections were incubated in fluorescein-conjugated goat IgG. Primary antibodies used in the current study and their dilutions are: chicken anti-GFP (1:1,000, ab 13970, Abcam), rabbit anti-p-STAT3 (1:1,000; 9145 S, Cell Signaling). Secondary antibodies conjugated with Alexa-568 and Alexa-488 were purchased from Invitrogen (1:1,000). Brain sections were mounted onto SuperFrost (Fisher

Scientific 22-034- 980) slides and then visualized with an inverted Zeiss LSM 780 laser scanning confocal microscope with a ×10 or ×20 lens. Images were imported to Fiji for further analysis. To quantitate the number of stained cells, brain slides were imaged under a ×20 objective. Regions that represent the ARC in each image were isolated and threshold for staining intensity. The number of positive cells was then counted by an observer blind to the sample identity.

### *i.c.v. cannula implantation and stereotaxic surgery*

i.c.v. cannula minipump implantation was performed as previously described (Fujikawa et al. 2010). In brief, a cannula was implanted into the cerebral lateral ventricle (anterior–posterior (AP): −0.50 mm, medial–lateral (ML): ± 1.3 mm, dorsal–ventral (DV): −2.3 mm), and a mini-osmotic pump (model 1002D, Alzet) was implanted subcutaneously via a catheter connected to the cannula for i.c.v. infusion. The mini-osmotic pump was filled with either leptin (12 ng $h^{-1}$), BDNF (24 μg/kg daily) or sterile artificial cerebrospinal fluid solution. Food intake, body weight and BAT temperature were measured daily post-surgery. Stereotaxic surgery was performed to deliver AAV into the hypothalamus of mice. Mice were anaesthetized using isoflurane anaesthesia, with induction at 3–4% and maintenance at 1.5–2%. After exposing the skull, a small hole was drilled for injection. A pulled-glass pipette with a 20–40-mm diameter tip was used for virus loading and injection, and virus was injected using NanoJect III system (Drummond 3-000-207 kit). Virus was injected at a speed of 1 nl/s (5 nl per cycle, 5-s pulse between cycles), and the pipette was held in place for another 3 min after injection to allow sufficient viral absorption. All stereotaxic injection sites were verified by immunohistochemistry. To verify *Lepr* deletion, mice were injected with 3 mg/kg leptin 2 h before being sacrificed, and p-STAT3 was visualized using immunohistochemistry. The animals with 'missed' or 'partial-targeting' were excluded from data analyses. Injection coordinates and volumes used in this study are summarized below: ARC AP: −1.50 mm, DV: −6.00 mm, ML: ±0.20 mm, 150 nl per side), DMH (AP: −1.50, DV: −4.95, ML: ±0.30, 75 nl per side), and MPO (AP: 0.5, DV: −5.25, ML: ±0.30, 100 nl per side).

Schemes describing experimental design for AAV injections in the mouse brain, with annotation of coronal brain sections, were generated using as a reference, the annotated areas in the stereotaxic atlas by Paxinos and Franklin (Paxinos and Franklin 2001).

### *PRV tracing*

For retrograde labelling of adipose-projecting neurons in the CNS, mice were maintained under anaesthesia and an incision was made above the thigh to expose iWAT, or above the intrascapular region to expose BAT. PRV-lp297, a variant of PRV-Bartha expressing GFP (or mCherry) was injected into iWAT or BAT of LepRb-TdTomato mice for mapping multisynaptic inputs to each of these depots. Injections were made using 2 μl Hamilton syringes into five different spots of iWAT (0.3 μl per injection, 1.5 μl total), and four different spots for BAT (0.2 μl per injection, 0.8 μl total). Skin incision was closed using EZ clips (Stoelting Co.). Mice were then monitored daily and sacrificed at day 7 post-infection.

### *Primary sympathetic neuron culture*

Superior cervical ganglia (SCGs) were collected from P2 WT mice. The ganglia were digested with collagenase type 4 (10 mg/ml) in Leibovitz's L-15 medium at 37 °C for 30 min, followed by inactivation with 10% FBS in DMEM/F12 medium supplemented with GlutaMAX. SCGs were then digested with 0.25% trypsin/EDTA at 37 °C for 20 min. After washing the SCGs three times with 10% FBS in DMEM/F12 medium supplemented with GlutaMAX, the ganglia were mechanically dissociated by pipetting. Neurons were resuspended in DMEM/F12 medium supplemented with GlutaMAX containing 10% FBS, 100 units/ml penicillin, and 100 μg/ml streptomycin, and seeded on 12-well plates precoated with poly-D-lysine overnight and laminin (20 μg/ml) at a density of 20,000 cells per well. Cultures were treated with either NGF (10 ng/μl) or NGF (10 ng/μl) and leptin (100 ng/ml). Controls received neither factor. After 48 h, sympathetic neurons were fixed with 4% PFA in PBS, stained with anti-TH antibody.

### *Animal study design*

No statistical methods were specifically used to calculate the sample size. Sample size was determined based on previous studies and literature in the field using similar experimental paradigms and to reach a minimum of at least three animals per group. No data were excluded, except animal subjects with deteriorating health issues after surgery or during the experiment, and the ones with "missed" or "partial" viral targeting. All experiments were performed with at least two technical replicates, each time containing the same number of biological replicates, and all attempts at replication were found to be reproducible. To randomize experimental samples, littermates of the same sex were randomly assigned to either experimental or control groups. Data were collected blind, and analysis was also performed blind to prevent any bias.

## Chapter 4. BDNF signaling mediated regulation of SNS innervation

### 4.1. Central BDNF signaling regulates SNS innervation

As we discussed in 1.4, BDNF and its receptor TrkB, is one of the most important ligand-receptor pairs in regulating energy homeostasis in mammals. Mutations in BDNF or TrkB both lead to server form of obesity in humans (B. Xu and Xie 2016). Prior studies have shown that BDNF signaling regulates energy expenditure through a brain-mediated mechanism. Deletion of BDNF in the brain leads to obesity in mice (Rios et al. 2001); i.c.v. administration of BDNF has been reported to increase noradrenaline turnover and UCP1 expression in BAT of *db/db* mice (Nonomura et al. 2001). These data make us hypothesize that central BDNF signaling might play a role in regulating SNS innervation in fat.

To test our hypothesis, we first delivered BDNF (24 μg/kg daily) i.c.v. into the lateral ventricle of *ob/ob* mice for 14 days. Surprisingly, we found a significant increase of sympathetic innervation in both iWAT and BAT (Figure 4.1 a-b). However, unlike leptin treatment, BDNF treatment only increases innervation in iWAT for 2.5-fold and in BAT for 2-fold, and does not restore innervation to WT level. We also measured body weight and BAT temperature during BDNF treatment, and found that BDNF treatment only leads to modest weight loss and modest increase in BAT temperature in *ob/ob* mice (Figure 4.1 c-d). These data show that central BDNF delivery to *ob/ob* mice can partially restore SNS innervation in adipose tissue. Since central BDNF and leptin delivery to *ob/ob* mice both lead to an increase in SNS innervation, although for different magnitudes, we next asked whether these two systems interact to control this process.

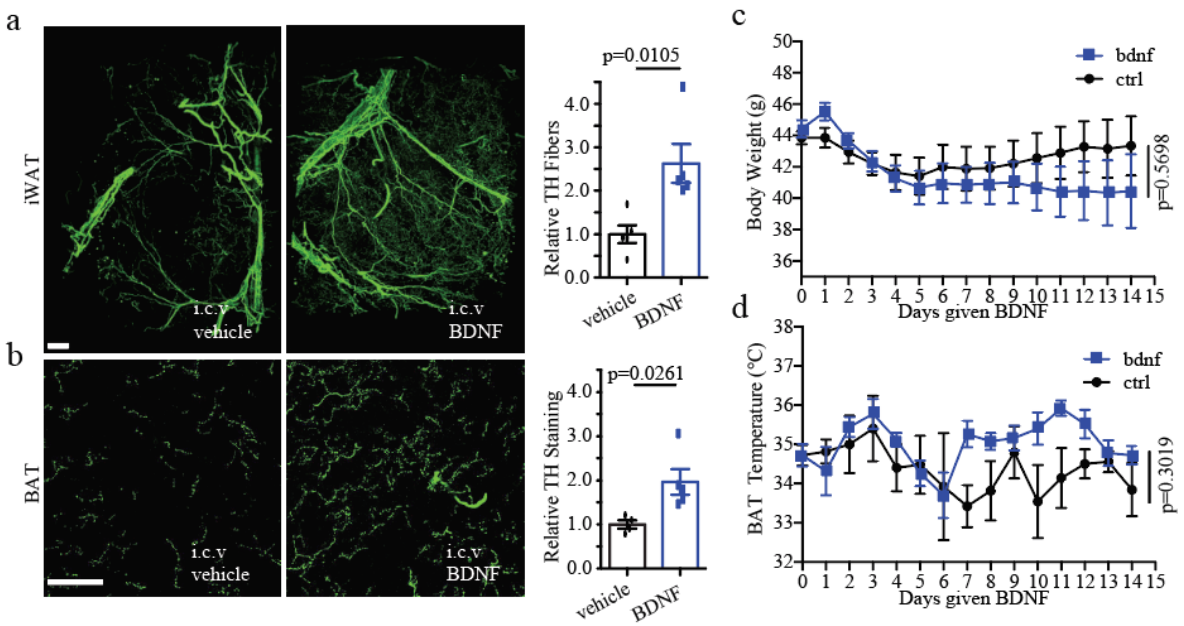


**Figure 4.1. i.c.v. BDNF in *ob/ob* mice induces SNS innervation in adipose tissue.**

(a-b) *ob/ob* mice were given i.c.v. BDNF (24 μg/kg daily) or vehicle through an osmotic pump for 14 days. TH immunolabelling in iWAT (a, $n = 5$ per group) and BAT (b, $n = 4$ for vehicle, $n = 5$ for BDNF). (c-d) Daily body weight (c) or BAT temperature (d) of mice receiving i.c.v. BDNF ($n = 5$ per group). Scale bars, 200 μm (a); 100 μm (b). Data show mean ± s.e.m.; significant differences between treatments were calculated using Two Way Anova Test (c-d), or Student's two-tailed, unpaired t-test (a-b).

### 4.2. BDNF signaling acts downstream of leptin in regulating innervation

After showing that both leptin and BDNF delivery can increase SNS innervation in adipose tissues of *ob/ob* mice, we then asked whether these two systems interact in regulating innervation. We first tested whether BDNF signaling is necessary for leptin to induce innervation change. We treated *ob/ob* animals with either PBS, leptin with or without the TrkA/B/C antagonist, K252A (Rattiner et al. 2004), delivered by i.c.v. injection twice daily. Surprisingly, we found that K525A treatment blunts leptin's effect in reducing body weight in *ob/ob* mice (Figure 4.2 a). Moreover, this BDNF antagonist significantly blunted leptin induced SNS innervation in iWAT and BAT by >50% (Figure 4.2 b-c). We next did a similar experiment using another TrkB specific antagonist, ANA12 (Cazorla et al. 2011), which was delivered intraperitoneally twice daily with or without leptin to *ob/ob* mice. This experiment leads to similar results as before, ANA12 treatment significantly blunts leptin's effect on inducing innervation (Figure 4.2 d-e). These data all indicate that BDNF regulates innervation downstream of leptin signaling. We will explore next to find which BDNF expressing neurons are responsible for this effect.

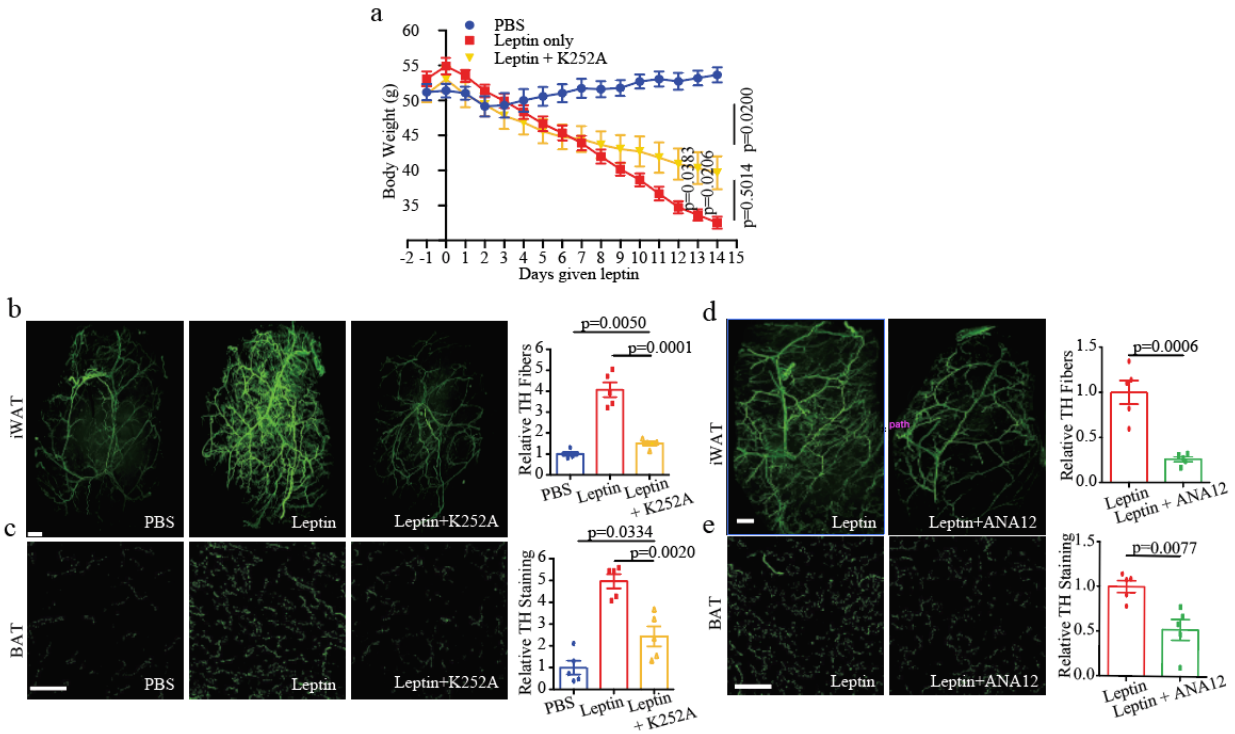


**Figure 4.2. Trk inhibitors blunt leptin induced SNS innervation in *ob/ob* mice.**

(a) Body weight of mice treated with PBS (blue), leptin (red) or leptin together with twice daily i.c.v. infusions of the TrkB antagonist K252A (orange) for 14 days. (b-c) TH immunolabelling of mice treated as in (a) was visualized in iWAT (b) and BAT (c). Quatification of data shown on the right ($n$ = 5 per group). (d-e) *ob/ob* mice were given 14 days of leptin subcutaneously by osmotic pumps, or leptin together with twice daily i.p. injections of the TrkB antagonist ANA12, TH immunolabelling was visualized in iWAT (d) and BAT (e). Panels on right show quantification of images shown on left ($n$ = 5 per group). Scale bars, 1 mm (b, d); 100 µm (c, e). Data show mean ± s.e.m.; significant differences between treatments were calculated using Two Way Anova Test (a), or Student's two-tailed, unpaired t-test (b-e).

### 4.3. BDNF$^{PVH}$ projects to adipose tissue and is downstream of leptin signaling

To identify the BDNF expressing population(s) involved in regulating adipose tissue innervation, we first conducted PRV tracing experiment. We injected PRV-mCherry into the adipose tissue of BDNF-IRES-Cre::LSL-GFPL10 mice. Similarly as shown before, we found that PRV infected PVH region in the brain four days post injection. BDNF neurons in the PVH (BDNF$^{PVH}$) were the first BDNF expressing brain population infected by PRV (Figure 4.3 a). The PVH is a known sympathetic pre-motor region in the CNS (Biag et al. 2012; Sutton, Myers, and Olson 2016; Ranson et al. 1998), and BDNF$^{PVH}$ neurons have been previously shown to project to sympathetic preganglionic neurons in the IML of the spinal cord and regulate energy expenditure (An et al. 2015). Therefore, we hypothesized that leptin acts via this neuron population to regulate innervation.

To test our hypothesis, we first treated *ob/ob* mice with leptin or PBS and assayed for neural activity in the PVH. We stained for Fos protein in the fixed brain slides and found that leptin significantly upregulates the number of Fos positive neurons in the PVH of *ob/ob* mice (Figure 4.3 b). We then asked whether these activated cells are BDNF$^{PVH}$ neurons. By performing fluorescent in situ hybridization (FISH) in fresh frozen brain sections, we also found that leptin treatment resulted in a 50% increase in the number of Fos-positive BDNF$^{PVH}$ neurons (Figure 4.3 c-d). Besides, we micro-dissected out PVH region following leptin treatment and extracted mRNA from PVH. By performing quantitative PCR assays, we found leptin induces a twofold increase in *Bdnf* mRNA expression in microdissected PVH samples (Figure 4.3 e). Taken together, these data indicate that leptin signaling activates BDNF$^{PVH}$ neurons and induces upregulation of *Bdnf* mRNA in the PVH. We then asked whether leptin activates BDNF$^{PVH}$ neurons directly. We first looked for cell bodies of LepR neurons (indicated by overlapping tomato and DAPI staining) from PVH of LepR-Cre::LSL-Tdtomato mice. However, our result show that there is no LepR expressing neurons in the PVH; instead, LepR neurons send numerous efferents to the PVH region (Figure 4.3 f). These findings suggest that leptin indirectly activates BDNF$^{PVH}$ neurons.

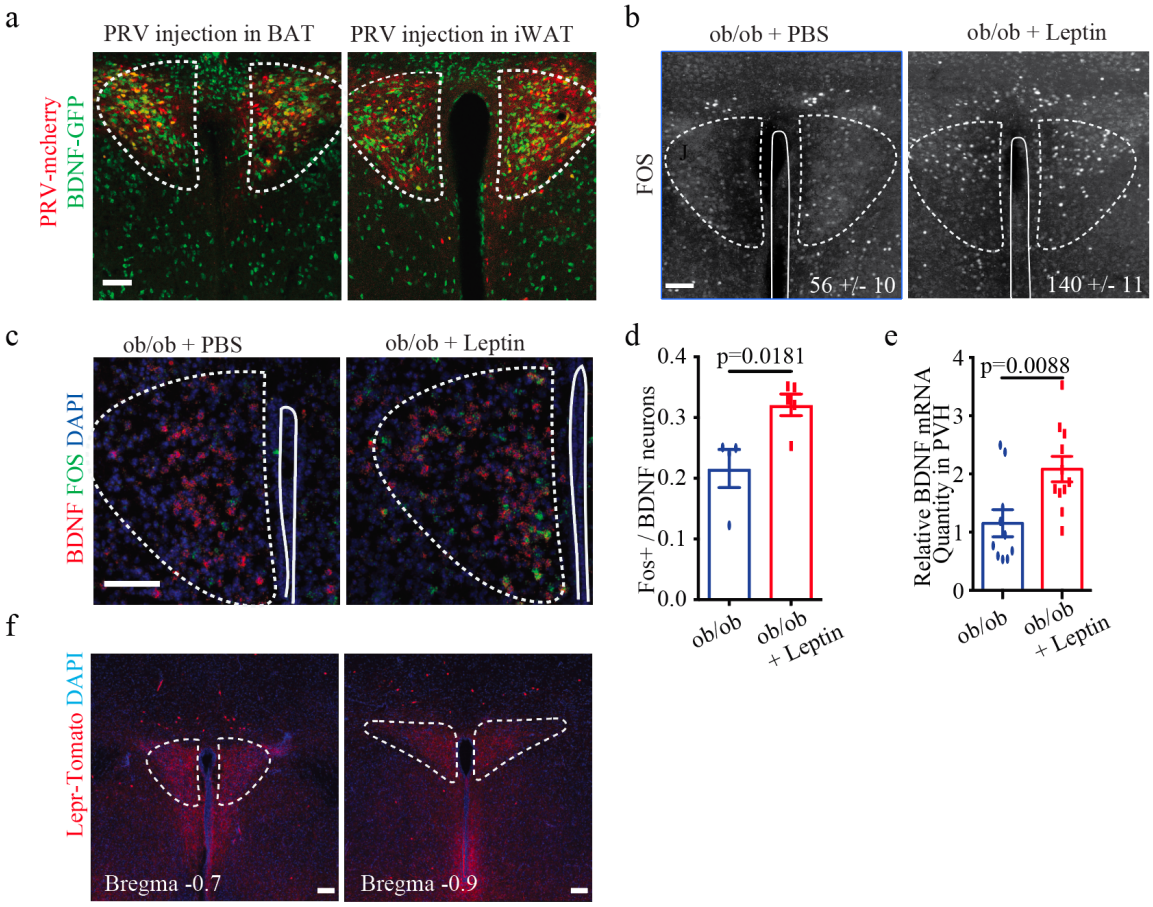


**Figure 4.3. BDNF neurons in the PVH (BDNF$^{PVH}$) project to the fat and are activated indirectly by leptin signaling.**

(a) PRV-mCherry tracing from BAT (left panel) or iWAT (right panel) in BDNF-IRES-Cre::LSL-GFPL10 mice showing PRV (red) colocalization with BDNF-expressing neurons (green) within the PVH. (b) Fluorescence microscopy showing immunolabelling of FOS in brain sections from 3-day leptin-treated *ob/ob* mice or PBS treated controls. Average number of neurons expressing FOS shown in bottom right corner of each panel ($n = 4$ per group). (c) Leptin treatment increases *Fos* RNA in BDNF$^{PVH}$ neurons of *ob/ob* mice visualized by fluorescence in situ hybridization using RNAscope. (d) Quantification of data shown in Fig. 4f ($n = 4$ for PBS, $n = 5$ for leptin). (e) Quantitative PCR measurements of *Bdnf* RNA transcript levels in microdissected PVH neurons from *ob/ob* mice following 3 days of leptin treatment versus PBS normalized to the housekeeping gene *Rpl32* ($n = 10$ for PBS, $n = 11$ for leptin). (f) Immunostaining of PVH brain slices from LepR-Cre::LSL-TdTomato mice show a lack of cell bodies of LepR neurons in the PVH region; instead LepR neurons from outside of this region send dense projections to the PVH. Scale bars, 100 µm (a, b, c, f). Data show mean ± s.e.m.; significant differences between treatments were calculated using Student's two-tailed, unpaired t-test (d, e).

Since leptin signaling indirectly regulates the activity of $BDNF^{PVH}$ neurons, we hypothesized that the first order leptin responsive neurons in the ARC might be upstream of $BDNF^{PVH}$ neurons. To test this, we employed rabies tracing strategy to identify monosynaptic inputs to $BDNF^{PVH}$ neurons (X. E. M. Callaway and Luo 2015). Rabies virus is a neurotropic virus strain wildly used for circuit mapping. Once taken up by neurons, rabies virus will travel retrogradely across multiple synaptic steps. In order to restrict the viral spread and only to label the monosynaptic inputs to genetically modified neurons, a glycoprotein (G)-deleted rabies virus (RVdG) was generated. Without G protein in the viral genome, RVdG cannot spread from their host cells, unless trans-complemented with G protein. Besides G protein deletion, the rabies virus we used was also pseudotyped to have envelope protein from avian ASLV type A (EnvA) coating, which ensures that the virus only infect cells expressing TVA receptors on their surfaces. To trace the neurons upstream of $BDNF^{PVH}$, we first injected AAV virus expressing TVA-mCherry and G protein into the PVH region of BDNF-IRES-Cre mice. We waited three weeks post AAV injection to allow sufficient virus expression in $BDNF^{PVH}$ neurons before we injected EnvA coated RVdG with GFP expression to the same area. These $BDNF^{PVH}$ cells express both TVA and G protein, allowing entry of EnvA coated rabies virus followed by efficient G-protein expressing rabies virus particle release from these cells. Because G protein coated rabies virus has broad tropism, it will infect presynaptic terminals of neurons connected to $BDNF^{PVH}$ and be transported to the cell bodies of these presynaptic neurons. The basic steps of this experiment are summarized in Figure 4.4 a. One week after rabies injection, we found extensive GFP labeled cells co-localized with mCherrry reporter in the PVH, indicating efficient viral infection of the starter cells. More importantly, we found that many cells in the ARC are labeled with rabies (GFP). To answer whether these labeled cells in the ARC are AGRP or POMC, we performed FISH to co-label mRNAs of *AGRP/POMC* with viral *GFP* on these brain sections. Interestingly, we found a small group of AGRP neurons, as well as and POMC neurons, co-express viral GFP (Figure 4.4 b-c). These data indicate that AGRP and POMC both send efferents to $BDNF^{PVH}$ neurons, raising the possibility that leptin might act via AGRP and POMC to modulate the activity of $BDNF^{PVH}$.

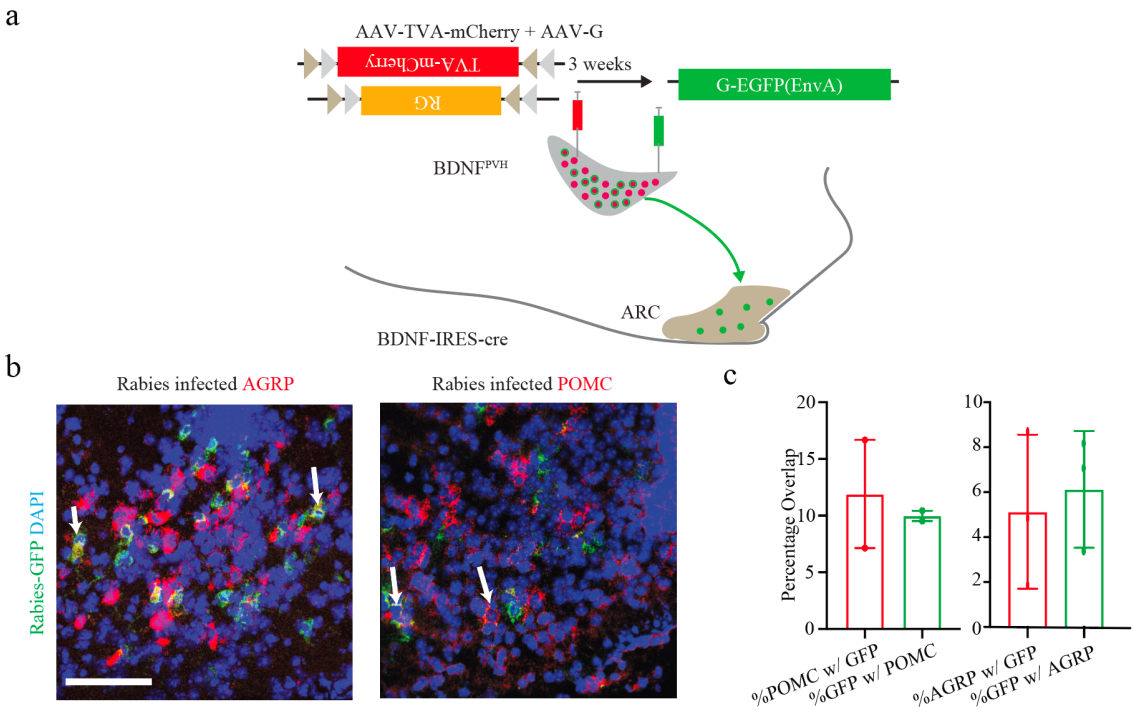


**Figure 4.4. AGRP and POMC neurons in the ARC synaptically connect to BDNF$^{PVH}$**

(a) Scheme for monosynaptic rabies tracing from BDNF$^{PVH}$ neurons. (b) One-week post rabies-EGFP injection, AGRP (left) or POMC neurons (right) in red, and rabies-GFP-infected neurons (in green) are visualized by fluorescence in situ hybridization. The white arrows indicate overlap between AGRP and POMC with rabies-GFP. (c) Quantification of data shown in Fig. 4k, l reveals around 12% of POMC neurons were infected by Rabies and around 10% of Rabies infected cells in ARC were POMC+ (left panel, $n = 2$); around 5% of AGRP neurons were infected by Rabies and around 6% of Rabies infected cells in ARC were AGRP+ (right panel, $n = 3$). Scale bars, 100 μm (b). Data show mean ± s.e.m.

## 4.4. BDNF$^{PVH}$ mediates leptin's effects on innervation

In the previous sections, we showed that 1) leptin's effects on innervation is dependent on central BDNF signaling, 2) BDNF$^{PVH}$ neurons projects to both iWAT and BAT through a polysynaptic circuit, 3) BDNF$^{PVH}$ neurons are indirectly activated by leptin signaling, likely through the AGRP and POMC neurons. These evidences lead us to hypothesize that leptin might regulates innervation through these downstream BDNF$^{PVH}$ neurons.

To test our hypothesis, we first employed a viral mediated strategy to delete *Bdnf*, gene in PVH region. As described in Figure 4.5 a, we injected either AAV expressing GFP-Cre or GFP (as controls) into PVH of BDNF$^{fl/fl}$ mice. Cre recombinase injection to these mice will lead to efficient deletion of *Bdnf*, gene from PVH region only. Twelve weeks post-surgery, the GFP-Cre injected mice show a modest weight gain comparing to the GFP injected controls (Figure 4.5 b). When we assayed their adipose tissue innervation, we found that GFP-Cre injected mice show a significant reduction in SNS innervation in both adipose tissues (Figure 4.5 c-d). These results indicate that *Bdnf*, gene deletion from PVH resulted in reduced SNS innervation from WT level. The level of SNS innervation resulted from *Bdnf* gene deletion is intermediate between WT and that from *LepR* gene deletion in the ARC.

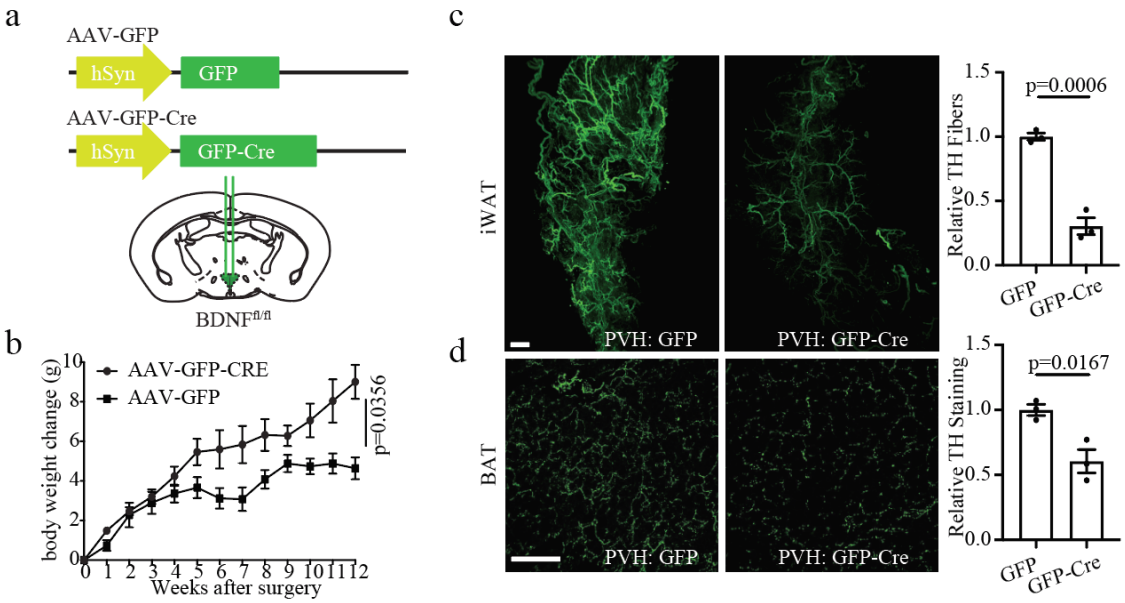


**Figure 4.5. BDNF$^{PVH}$ neurons regulates SNS innervation in fat.**

(a) Scheme describing *Bdnf* deletion in PVH. To delete *Bdnf*, AAV-GFP or AAV-GFP-Cre was injected in the PVH of *Bdnf*$^{fl/fl}$ mice. (b) Body weight progression of *Bdnf*$^{fl/fl}$ mice post-surgery ($n = 6$ for AAV-GFP-Cre, $n = 5$ for AAV-GFP). (c-d) Twelve weeks post-surgery, TH immunolabelling was visualized in iWAT (c) and BAT (d) ($n = 3$ per group). Quantification of the images shown on the right. Scale bars, 1mm (c), 100 µm (d). Data show mean ± s.e.m.; significant differences between treatments were calculated using Two Way Anova Test (b), or Student's two-tailed, unpaired t-test (c-d).

After confirming that *Bdnf* in the PVH indeed regulates innervation levels in fat, we decided to test whether these neurons mediate leptin's effects on innervation. We breed BDNF-Cre with *ob/ob* animals to generate BDNF-IRES-cre::*ob/ob* mice, and used a viral mediated strategy to deleteBDNF$^{PVH}$ neurons in these animals. As described in Figure 4.6 a, we injected AAV expressing Cre dependent diphtheria toxin A (dtA), as well as a non Cre dependent mCherry reporter to indicate virus expression, into the PVH of *ob/ob::*BDNF-IRES-Cre mice. Cre dependent dtA expression will lead to ablation of only BDNF neurons in the PVH. To confirm that viral expression leads to successful BDNF neuron deletion, we sacrificed the animals two weeks post viral infection and performed in situ hybridization using RNAscope to check for *Bdnf* expression in the PVH. As expected, our results revealed that dtA mediates an ~90% loss of BDNF$^{PVH}$ neurons (Figure 4.6 b-c). The resulting animals, *ob/ob*::BDNF$^{\Delta PVH}$, did not show alterations of body weight or food intake at baseline (Figure 4.6 d). However, when *ob/ob*::BDNF$^{\Delta PVH}$ mice were treated with leptin subcutaneously for 2.5 weeks, we found a significant decrease in the ability of leptin to induce weight loss, reduce food intake and restore BAT temperature compared to Cre-negative *ob/ob* mice (Figure 4.6 e-g). Moreover, the leptin-dependent increase of sympathetic innervation in *ob/ob* mice was significantly reduced by >50% in BAT and iWAT in *ob/ob*::BDNF$^{\Delta PVH}$ animals (Figure 4.6 h-i). Taken together, these experiments show that BDNF$^{PVH}$ neurons are necessary for leptin to restore sympathetic innervation of BAT and WAT in *ob/ob* mice.

**Figure 4.6. BDNF$^{PVH}$ neuron deletion blunts leptin-induced innervation in fat.**

(a) Scheme for ablating BDNF neurons in the PVH. AAV1-mCherry-flex-dtA virus was injected in the PVH of BDNF-IRES-cre::*ob/ob* to ablate BDNF$^{PVH}$ neurons or in Cre negative *ob/ob* littermates (as controls). (b) 2 weeks post AAV1-mCherry-flex-dtA injection, mCherry transcripts (red) indicating neurons infected by the AAV, and BDNF transcripts (green) indicating BDNF$^{PVH}$ neurons, were visualized by FISH using RNAscope. (c) Quantification of data shown in (b). AAV1-mCherry-flex-dtA virus injection leads to a reduction in BDNF expressing cells in the PVH ($n$ = 3 per group). (d) Weekly body weight of BDNF-Cre::*ob/ob* or Cre negative *ob/ob* littermates post-injection of AAV1-mCherry-flex-dtA in the PVH but before leptin treatment ($n$ = 5 for Cre-, $n$ = 6 for Cre+). (e) Daily body weight of BDNF-Cre::*ob/ob* or Cre negative *ob/ob* post leptin delivery ($n$ = 5 for Cre-, $n$ = 6 for Cre+). (f-g) Daily food intake (f) or BAT temperature (g) from BDNF-Cre::*ob/ob* or Cre negative *ob/ob* littermates post leptin delivery. Daily food intake or BAT temperature of each animal was the average of 4 consecutive days ($n$ = 5 for Cre-, $n$ = 6 for Cre+). (h-i) Four weeks post-injection of AAV with Cre-dependent diphtheria toxin A into the PVH of BDNF-IRES-Cre$^{+}$::*ob/ob* mice, the animals were treated with 14 days of leptin and compared to BDNF-IRES-Cre$^{-}$::*ob/ob* littermates treated with leptin or PBS. TH immunolabelling was visualized in iWAT ($n$ = 5 for Cre$^{-}$ with leptin, $n$ = 7 for Cre$^{+}$ with leptin, $n$ = 3 for Cre$^{-}$ without leptin) (m), and BAT ($n$ = 5 for Cre$^{-}$ with leptin, $n$ = 6 for Cre$^{+}$ with leptin, $n$ = 4 for Cre$^{-}$ without leptin) (n). Scale bars, 1 mm (h); 100 μm (b, i). Data show mean ± s.e.m.; significant differences between treatments were calculated Two Way Anova Test (d-e), or Student's two-tailed, unpaired t-test (c, f-i).

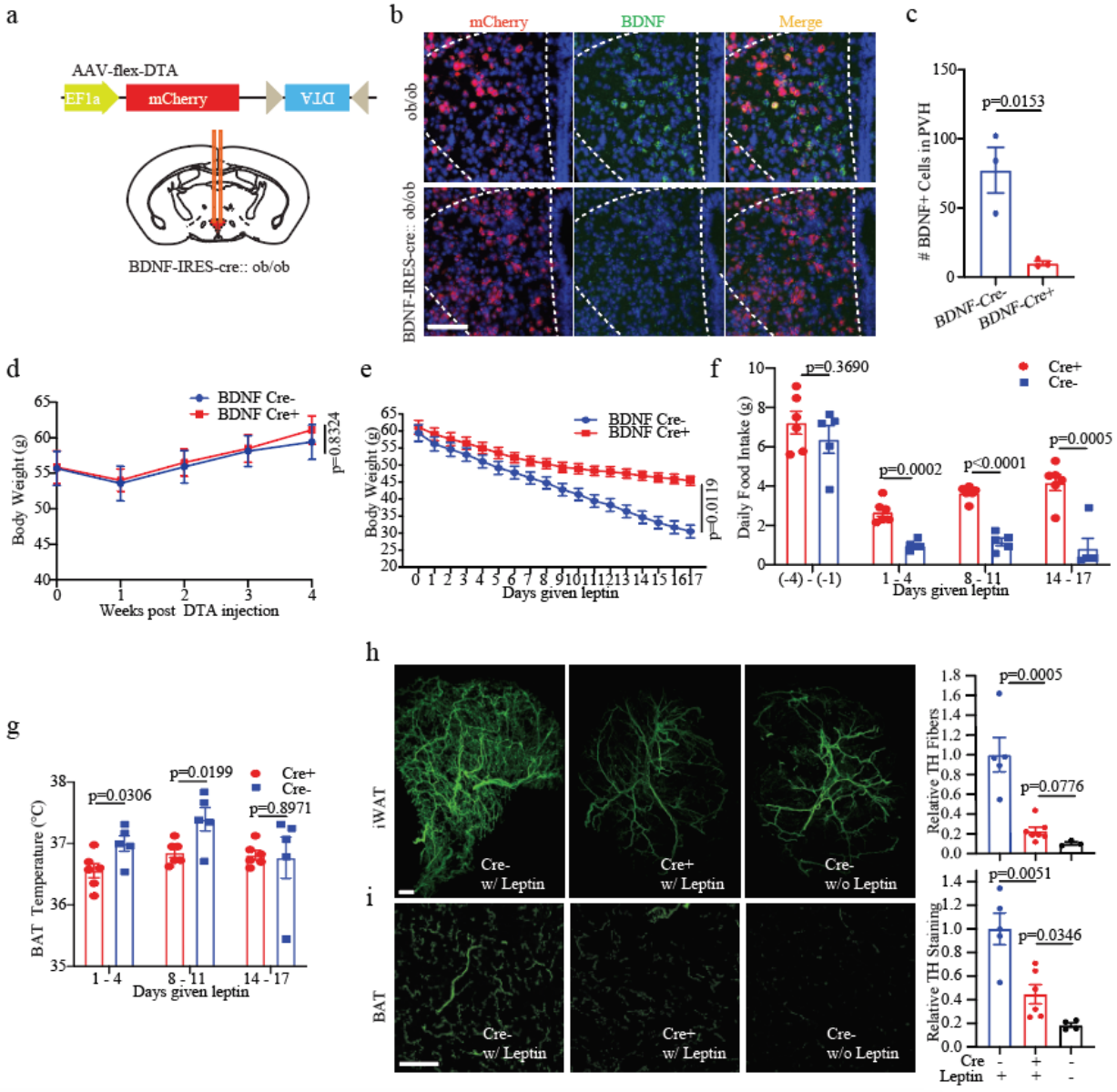


**Figure 4.6. BDNF$^{PVH}$ neuron deletion blunts leptin-induced innervation in fat.**

## 4.5. Summary and discussion

In this chapter, we first found that BDNF signaling is necessary for leptin to induce SNS innervation change in the adipose tissues. Then we identified $BDNF^{PVH}$ neurons as the mediator of leptin's effect on innervation, because $BDNF^{PVH}$ neurons 1) are downstream of leptin signaling, 2) project directly to the sympathetic presynaptic neurons in the spinal cord, and 3) are necessary for leptin to induce innervation change. These data, together with the data from Chapter 3, complete a central leptin-BDNF pathway that regulates SNS innervation in the adipose tissue (summarized in Figure 4.7).

Central BDNF signaling was previously shown to regulate energy expenditure (Han et al. 2008; B. Xu and Xie 2016; Nonomura et al. 2001), however, the underlying mechanisms were unclear. This study implicates the PVH as a source of BDNF that regulating energy expenditure depends on its ability to modulate the level of SNS innervation of WAT and BAT. In addition, leptin and BDNF signaling pathways are both the most important systems in maintaining energy homeostasis, because mutations in genes encoding leptin, BDNF, or their receptors all lead to severe obesity in human (Han et al. 2008; Yeo et al. 2004; Montague et al. 1997; Farooqi et al. 2002). However, the interaction between these two systems is not well understood. This work provides a possible mechanism that leptin depends on BDNF signaling to regulate SNS innervation level in the fat, which in turn is an important factor contributing to whole body energy expenditure.

$BDNF^{PVH}$ neurons project to sympathetic preganglionic neurons in the spinal cord (An et al. 2015), which are immediately upstream of the postganglionic sympathetic neurons (expressing TH) that directly innervate fat tissue. This connection provides a conduit for $BDNF^{PVH}$ neurons to modulate the plasticity of adipose tissue innervating neurons. How modulation of preganglionic neurons in turn lead to increased sprouting of the postganglionic neurons is unknown and currently under investigation in the lab.

Leptin acts indirectly, through the BDNF signaling pathway, to regulate SNS innervation. Manipulation of these downstream neurons may bypass central leptin resistance, which is often observed in obese patients. Therefore, understanding the cellular and molecular mechanism on how BDNF signaling regulates innervation and energy expenditure downstream of leptin will provide new cellular targets and novel therapeutic approaches to the treatment of obesity.

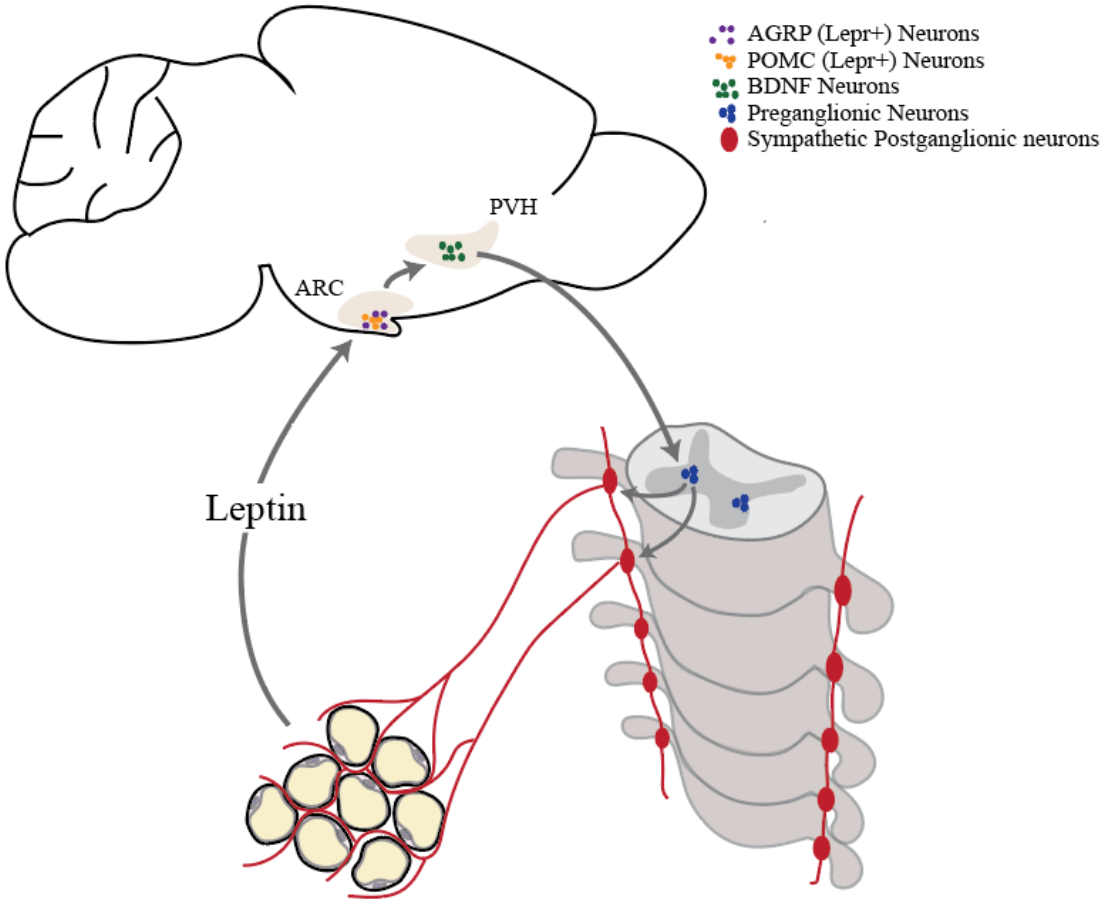


**Figure 4.7. Scheme describing the leptin-dependent CNS–SNS feedback loop that regulates adipose tissue innervation.**

## 4.6. Material and methods

### *Animals*

All animal care and experimentation were ethically performed according to procedures approved by the Institutional Animal Care and Use Committee at the Rockefeller University. Mice were housed 2–5 per cage (except in the cold exposure study where mice were singly caged) in a 12-h light/12-h dark cycle with ad libitum access to regular chow and water except in fasting studies. We used WT male C57BL/6J mice (000664, Jackson Laboratory), *ob/ob* (B6.Cg-*Lep*$^{ob}$/J; 000632, Jackson Laboratory; or bred in-house), Rosa26$^{fsTRAP}$ (B6.129S4-Gt(ROSA)26Sor$^{tm1(CAG-EGFP/Rpl10a,-birA)Wtp}$/J; 022367, Jackson Laboratory), *Bdnf*$^{fl/fl}$ (Bdnf$^{tm3Jae}$/J; 004339, Jackson Laboratory). BDNF-IRES-Cre mice (D. Wang et al. 2015) were kindly provided by W. Shen (Shanghai Institute of Technology). All mouse lines except *Bdnf*$^{fl/fl}$ are in a WT (C57BL/6J) background. Littermates of the same sex were randomly assigned to either experimental or control groups.

### *Virus*

AAV viruses used in these studies were obtained from UNC Vector Core or generated through Janelia Viral Tools Service; rabies virus was obtained from the Salk Viral Vector Core. For *Bdnf* deletion in *Bdnf*$^{fl/fl}$ mice, AAV5-hSyn-GFP-Cre or AAV5-hSyn-GFP was used. For BDNF$^{PVH}$ deletion in BDNF-IRES-Cre::*ob/ob* mice, AAV1-mCherry-flex-dtA was obtained from the UNC Vector Core. For rabies tracing, helper virus AAV1-FLEX-TVA-mCherry and AAV1-FLEX-RG was purchased from UNC Vector Core. Rabies EnvA-G deleted-eGFP were obtained from Salk Vector Core. PRV-lp297, a variant of PRV-Bartha expressing GFP or mCherry was used for mapping multi-synaptic input to iWAT and BAT (Pomeranz et al. 2017). PRV-lp297 was made by plaque purification of PRV-Introvert-GFP after passage through Cre-expressing cells (L. Pomeranz, unpublished data). Viral aliquots were stored at −80 °C before stereotaxic injection.

### *RNA preparation and quantitative PCR*

For brains, leptin or saline treated *ob/ob* animals were perfused briefly with sterile PBS, brains were dissected out quickly and the PVH region was microdissected under a dissection scope. RNA was isolated from the sample using PicoPure RNA isolation kit (Thermo) following the manufacturer's protocol. For quantitative PCR (qPCR) analysis, RNA was reverse transcribed using the QuantiTech Reverse Transcription Kit (Qiagen). cDNA was used in qPCR reactions containing SYBR-green fluorescent dye (ABI). Relative *Bdnf* mRNA expression was determined by normalization with *Rpl32* (encoding ribosomal protein L32) levels using the $\Delta\Delta C_t$ method. Primer sequences (forward and reverse primers, 5′→3′, respectively) are listed below.

| | Forward 5'-3' | Reverse 5'-3' |
|---|---|---|
| BDNF | CACTGGCTGACACTTTTGAGCAC | GCTGTGACCCACTCGCTAATACTG |
| RPL32 | ACAATGTCAAGGAGCTGGAG | TTGGGATTGGTGACTCTGATG |

### *Stereotaxic surgery*

Stereotaxic surgeries were performed as described in 3.6. Double injections were performed in rabies tracing experiments, where rabies EnvA-G deleted-eGFP was injected to the PVH 3 weeks after the helper virus injection. To verify *Bdnf* deletion or to check rabies colocalization with AGRP/POMC neurons, fresh brains were cryo-protected in OCT and sectioned into 15-µm slides. Expression of BDNF was visualized by FISH (RNAscope, see below). Injection coordinates and volumes used in this study are summarized below: PVH (AP: −0.80, DV: −4.90, ML: ±0.25, 150 nl per side).

### *Trk signalling inhibition*

*ob/ob* mice were implanted with a subcutaneous osmotic pump delivering leptin or saline for 14 days as described earlier. The pan-Trk inhibitor K252A (Rattiner et al. 2004) was delivered twice daily, centrally by i.c.v. cannula at 09:00 and 19:00 hours in a volume of 3 µl containing 48 ng of K252A in 1.5% DMSO in saline at a rate of 1 µl/min. The TrkB inhibitor ANA-12 (Cazorla et al. 2011) was delivered by i.p. injection at 09:00 and 19:00 hours daily at a dose of 0.5mg/kg body weight.

### *Multiplex FISH*

Mice were transcardially perfused with RNase-free PBS for 2 min. Brains were then quickly harvested, frozen in OCT at –20 °C and stored at –80 °C until sectioning and processing for FISH. Multiplex FISH was then performed using the RNAscope system (ACDBio). Probes for the following mRNAs were used: mm-BDNF (cat no. 424821), cFOS (cat no. 316921), eGFP (cat no. 400281), AGRP (cat no. 400711), mm-POMC (cat no. 314081) and mCherry (cat no. 431201). Briefly, RNAscope (ACDBio) was used as per the manufacturer's protocol. Fresh frozen brain tissue was sectioned using a cryostat at –20 °C. The sections obtained were attached on Superfrost Plus Adhesion Slides (Thermo Fisher), and a hydrophobic barrier was created using Immedge Hydrophobic Barrier Pen (Vector Laboratories Inc.). Pre-treatment was done by serial submersion of the slides in 1× PBS, nuclease-free water, and 100% EtOH for 2 min each, at room temperature. Probe hybridization was achieved by incubation of 35 µl mRNA target probes for 2 h at 40 °C using a HyBez oven. The signal was amplified by subsequent incubation of Amp-1, Amp-2 and Amp-3 one drop each for 30, 30 and 15 min, respectively, at 40 °C using a HyBez oven. Each incubation step was followed by two 2-min washes using RNAscope washing buffer. Nucleic acids were stained using manufacturer's supplied DAPI for 30 s followed by two washes with 1× PBS. The slides were coverslipped and mounted using Prolong Gold Antifade Mountant (Thermo Fisher). Slides were visualized with an inverted Zeiss LSM 780 laser scanning confocal microscope using a ×20 or ×40 lens. Images were imported to Fiji for further analysis.

## Chapter 5. The sympathetic circuit innervating adipose tissue

### 5.1. Overview of sympathetic nervous system

Sympathetic nervous system (SNS) and the parasympathetic nervous system are two branches of the autonomic nervous system. Both of the systems play a crucial roles in the maintenance of homeostasis (McCorry 2007). SNS is tonically active, meaning that it always provides some degree of nervous input to its target tissues. The frequency of SNS neural input to target tissues can change in response to perturbations in the environment. Sympathetic activity has often been considered as non-specific, universal throughout the body, regardless of the nature of the environmental changes. However, recent studies started to reveal that sympathetic activities can be highly specific to certain tissues under defined environmental stresses (Furlan et al. 2016). For example, in fight-or-flight response or during exercises, sympathetic inputs to the skeletal muscles will increase drastically; under starvation or during cold exposure, sympathetic input to the white and brown adipose tissue will rise. How sympathetic nervous system carries out selective and coordinated changes under various conditions is not well understood. Therefore, it is important to perform systematic studies on the organization, and the molecular features of the sympathetic nervous system.

#### 5.1.1. Sympathetic preganglionic neurons

Signals from the brain first reach sympathetic preganglionic neurons in the spinal cord, which is also the last central component of the SNS. These preganglionic neurons originate from thoracic (T) and lumbar (L) segment of the spinal cord (T1-L2), and arranged into four topographically distinct groups-the intermediolateral cell column (IML), nucleus intermediolateralis thoracolumbalis pars funicularis, intercalated nucleus, and central autonomic area (Deuchars and Lall 2015). The majority of the sympathetic preganglionic neurons locates in the IML, which is a region at the medial lateral edge of spinal cord grey matter. These neurons are cholinergic, using acetylcholine as major neurotransmitters. Most of the preganglionic neurons have short axons, and synapse with sympathetic postganglionic neurons on the ipsilateral side or directly with end organs, such as adrenal medulla. Studies have demonstrated that preganglionic neurons exit at the segment level of their soma and connect primarily with the postganglionic neurons at the same segment (Deuchars and Lall 2015).

Descending inputs from the brain have significant influences on the sympathetic pre-ganglionic neurons. Studies using retrograde tracer have identified various sympathetic premotor regions, including the paraventricular nucleus of the hypothalamus (PVH), nucleus raphe pallidus (RPa), rostral ventrolateral medulla (RVLM), etc (Nakamura et al. 2004; Sutton, Myers, and Olson 2016; Deuchars and Lall 2015). The neurochemical identities of the sympathetic premotor neurons in the above-mentioned regions have been partially revealed by immunochemistry staining of specific markers. However, it is not clear whether the neurochemical identity defines their functions or connectivity to certain types of the sympathetic preganglionic neurons. Besides, studies have demonstrated that the same neurons in the premotor regions might be dual-infected by multiple tracers injected in different organs in the periphery, suggesting that these neurons might act as central commander to enable coordinated organ activity in response to certain stimuli.

Although we have gained many understandings regarding the inputs, location and projecting patterns of the sympathetic preganglionic neurons, there are still many questions that need to be answered. Firstly, it is unclear whether the location or rostral-caudal distribution of the preganglionic neurons is associated with their functions. Secondly, the mechanism of how the preganglionic neurons integrate descending input from the brain and pass it on to the postganglionic neurons targeting designated organs remains unknown. Lastly, whether sympathetic preganglionic neuron specifically innervating different target organs show unique molecular profiles also needs to be demonstrated.

### 5.1.2. Sympathetic postganglionic neurons

Most sympathetic postganglionic neurons organize into two ganglion chains (consisting of 22 ganglia on each side), which run parallel alongside of the spinal cord (McCorry 2007). Some other postganglionic neurons locate outside of the sympathetic chain and organize into sympathetic collateral ganglia, such as celiac ganglion and superior mesenteric ganglia that innervate visceral organs. Under normal conditions, each sympathetic postganglionic neuron receives inputs primarily from single preganglionic neuron, the ratio between preganglionic neurons and postganglionic neurons is about 1:20. However, in pathological conditions, the circuit between the sympathetic pre- and postganglionic neurons may rewire, where the postganglionic neuron activities might be under modulation of multiple preganglionic neurons.

The postganglionic neurons are adrenergic, using norephedrine and epinephrine as their primary neurotransmitters. These neurons extend their long axons, alongside with the 31 pairs of spinal nerves, to innervate terminal organs. In mice, major organs all receive sympathetic innervation. In the target organ, noradrenaline binds to adrenergic receptors to activate serious of downstream target-specific pathways to modulate their functions. For example, in the heart, sympathetic activation of β1,2-adrenergic receptors leads to hart rate increase; in the adipose tissues, sympathetic activation of β3-adrenergic receptors leads to thermogenesis or lipolysis.

Although the sympathetic postganglionic neurons have been used as the model for studying peripheral nerve development, axon pathfinding, etc., the locations of target specific postganglionic neurons in adult mice are not well characterized. More importantly, our data from previous chapters show that SNS innervation in adipose tissues between WT and *ob/ob* mice is drastically different. It is worth characterizing and comparing the adipose tissue innervating sympathetic postganglionic neuron organization between these two mouse lines. Besides, although we've learned that many neurotrophies, including NT-3, NGF, and BDNF, are responsible in the axon pathfinding during sympathetic development (Glebova and Ginty 2005), we still wonder whether leptin modulates sympathetic innervation in adult mice using similar or distinct molecular programs.

### 5.1.3. Sympathetic nervous system in obesity

SNS has profound roles in promoting energy expenditure, therefore, dysregulation of SNS has been shown to be the hallmark of obesity and other metabolic diseases (Guarino et al. 2017). It is not hard to reason that targeting the sympathetic nervous system presents high therapeutic potentials in the treatment of obesity. However, the sympathetic activity blockers, adrenergic receptor blockers, have not yet been successful in clinic. Many obese patients have high tonic sympathetic activity; however, the high tonic sympathetic activities do not favor weight loss by increasing fat burning and energy expenditure, which is probably due to a selective downregulation of β adrenoceptors in the adipose tissue. On the other hand, other studies reported that obesity only leads to high SNS activity in selected tissues, such as in muscle vasculatures and in the kidneys, leading to hypertension and cardiovascular risks. Due to this ununiform SNS activity in obesity to various tissues, it is hard to use universal β blockers as a treatment of obesity.

Approaches that can selectively activate sympathetic activities in adipose tissue, sparing the cardiovascular system, would present huge therapeutic potentials in the treatment of obesity. In this Chapter, we will start to elucidate the specialized properties of the functional pathways of the sympathetic nervous system at anatomical, cellular and molecular levels.

## 5.2. Anatomical characterization of sympathetic premotor innervating adipose tissues

In order to find out the molecular mechanism driving SNS plasticity in adipose tissues, we need to first anatomically characterize the SNS innervation to adipose tissue. We employed PRV tracing methods, introduced in Chapter 3, to reveal the anatomical locations of both of the sympathetic premotor neurons and sympathetic preganglionic neurons in the central nervous system.

We first injected PRV in iWAT and BAT separately. As we have shown in Chapter 3.1, the virus should subsequently travel through sympathetic postganglionic neurons and sympathetic preganglionic neurons before reaching the brain. Since the virus travel approximately at the rate of one synapse per day, we estimate that PRV will reach postganglionic neurons by Day 2, preganglionic neurons by Day 3 and brain sympathetic premotor regions by Day 4. To characterize the sympathetic premotor regions in the brain, animals were sacrificed on Day 4 post PRV injection to harvest the brains. At this time, we found that the brain regions infected by PRV injected in iWAT and BAT are very similar. Three major regions that show the viral infection on Day 4 are in the hypothalamus, PVH, and in the hindbrain, RPa and RVLM, all of which are known to send efferents to the sympathetic preganglionic neurons in the spinal cord (Deuchars and Lall 2015).

### 5.2.1. Sympathetic premotor neurons in WT mice

As the brain regions innervating both tissues are the same, we then asked whether same neurons from PVH and RPa indirectly connect to both iWAT and BAT. To test this, we simultaneously injected PRV expressing GFP into iWAT (1.5uL) and mCherry (0.5uL) into BAT in ipsilateral side of the same animal. The inject volume was decided based on preliminary experiments. Four days post injection, we sacrificed the animals to collect the brains. PVH and hindbrain regions were identified and sectioned into 50um slides, co-stained with GFP and mCherry antibodies to label PRV infected cells originated from iWAT and BAT accordingly, followed by fluorescent confocal imaging. Since PRV injection were performed in a single side of BAT and iWAT, we expect the sympathetic postganglionic neuros and preganglionic neurons on the ipsilateral side of the injection to be infected. Interestingly, we also observed that a single side of PVH and RVLM receives much more PRV infection than the other, however, we are unable to determine whether it is the ipsilateral or contralateral side of which PRV was injected.

From this experiment, we observed a high percentage of overlap between GFP and mCherry expression in the sympathetic premotor regions (Figure 5.1). We further quantified the number of overlapping neurons in the PVH and found that there are 67% of the iWAT innervating neurons (in Green) also innervating BAT, and there are 56% of the BAT innervating neurons (in Red) also innervating iWAT (Figure 5.1 b). Besides in PVH, we also imaged hindbrain sections, and found that there were much less neurons labeled by PRV in the Rpa or RVLM region, however, almost all neurons are co-labeled by both GFP and mCherry (Figure 5.1 c,d), These data suggest that a high percentage of brain sympathetic premotor neurons in WT are connected to both BAT and iWAT. These dual-labeled neurons might be the ones enabling coordinated sympathetic response of both tissues under condition such as cold exposure.

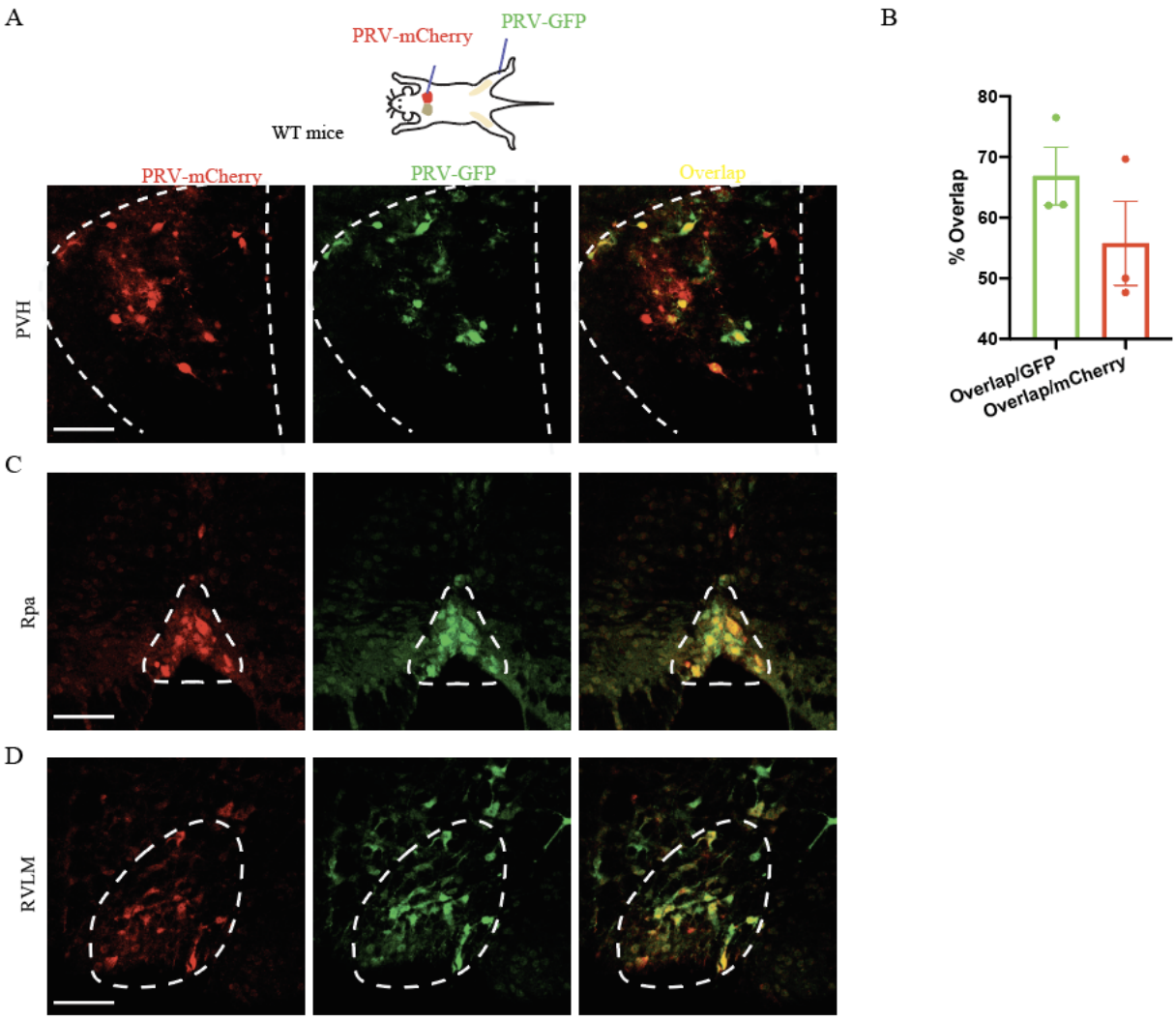


**Figure 5.1. Sympathetic premotor neurons innervating fat tissues in WT mice.**

(a) In WT mice, PRV-mCherry (0.5uL into four different sites) and PRV-GFP (1.5uL into 6 different sites) were injected into BAT and iWAT simultaneously. Four days post-injection, mice were sacrificed to collect the brains. Brains were sectioned into 50uL slides and co-stained with anti-GFP and anti-mCherry antibodies, followed by fluorescent confocal imaging. Representative images of PVH were displayed: BAT innervating neurons were labeled in Red (left most panel), iWAT innervating neurons were labeled in Green (middle panel), neurons innervating both BAT and iWAT were in yellow (right most panel). (b) Quantification of images in (a) (n=3). There are around 67% overlapping population of total iWAT innervating neurons (in green); there are around 56% overlapping population of total BAT innervating neurons. (c) Representative images of RPa. BAT innervating neurons were labeled in Red (left most panel), iWAT innervating neurons were labeled in Green (middle panel), neurons innervating both BAT and iWAT were in yellow (right most panel). (d) Representative images of RVLM. Scale bar: 100 um. Paraventricular nucleus of the hypothalamus (PVH), nucleus raphe pallidus (RPa), rostral ventrolateral medulla (RVLM).

### 5.2.2. Sympathetic premotor neurons in ob/ob mice

Since the SNS innervation level in *ob/ob* mice is around 6 fold lower than that in WT mice, we would also like to compare the anatomy of the sympathetic nervous system in the *ob/ob* mice. Therefore, we asked whether the sympathetic premotor neurons in *ob/ob* mice are at similar locations as the ones in WT mice and whether they have similar number of premotor neurons. We injected PRV-mCherry and PRV-GFP simultaneously into the BAT and iWAT of *ob/ob* mice. Since the size of fat pad of *ob/ob* is much bigger than that of WT mice, we reasoned that viral injection volume needs to be increased to allow for sufficient viral spread within *ob/ob* fat pad. Therefore, we injected 1uL PRV-mCherry in the BAT and 3uL PRV-GFP in iWAT of *ob/ob* mice. Four days post injection, animals were sacrificed to harvest the brains. At this time, we found that the brain regions infected by PRV are the same between WT and *ob/ob* mice. We saw the same three regions, PVH, Rpa and RVLM with PRV infection from both tissues in *ob/ob* mice (Figure 5.2). We next checked whether the same neurons from PVH innervate both iWAT and BAT. Similar as in WT mice, we also found that a large number of PVH neurons are both infected by PRV-mCherrry and GFP, indicating that they innervate both fat depots (Figure 5.2 b).

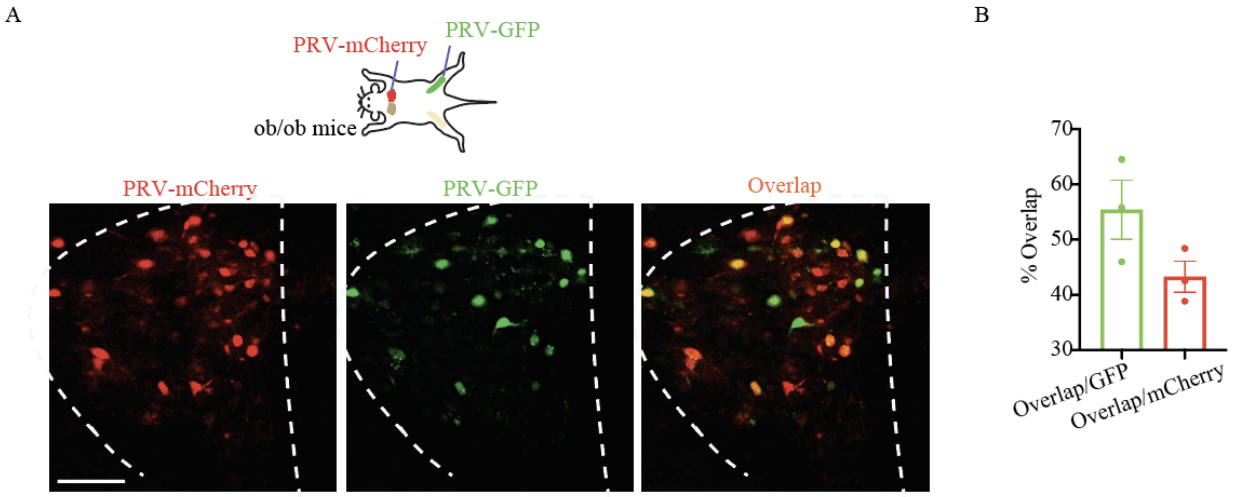


**Figure 5.2. Sympathetic preganglionic neurons innervating fat tissues in *ob/ob* mice**

(a) In *ob/ob* mice, PRV-mCherry (1 uL into four different sites) and PRV-GFP (3 uL into 6 different sites) were injected into BAT and iWAT simultaneously. Four days post-injection, mice were sacrificed to collect the brains. Brains were sectioned into 50uL slides and co-stained with anti-GFP and anti-mCherry antibodies, followed by fluorescent confocal imaging. Representative images of PVH was displayed: BAT innervating neurons were labeled in Red (left most panel), iWAT innervating neurons were labeled in Green (middle panel), neurons innervating both BAT and iWAT were in yellow (right most panel). Quantification of images are shown on the right (n=3). There are around 57% overlapping population of total iWAT innervating neurons (in green); there are around 43% overlapping population of total BAT innervating neurons. Scale bar: 100 um.

### 5.2.3. Summary

Overall, we found that the sympathetic premotor neurons innervating iWAT and BAT in both WT and *ob/ob* mice is concentrated in PVH, RPa and RVLM regions. Among the three regions, some nuclei from PVH and Rpa have been shown to have a prominent and specialized role in temperature regulations. Disinhibition of Rpa nuclei specifically activates BAT innervating sympathetic nerves while sparing the ones supplying the splanchnic nerves (Deuchars and Lall 2015). RVLM is known to primarily providing inputs to cardiovascular organs. Optogenetic activation of the adrenergic neurons in RVLM leads to a rise in blood pressure. We hypothesize that fat innervating neurons in the RVLM might be responsible to generate coordinated sympathetic response of both cardiovascular organs and adipose tissues in times of fight-or-flight reactions or during exercises.

Furthermore, we found that here are a larger number of sympathetic premotor neurons in all three regions dual labeled by PRV injected into BAT and iWAT, suggesting that these neurons might be involved in coordinating sympathetic input into both fat pads. However, there are situations where selective sympathetic activation of single fat pad is necessary. For example, during starvation, sympathetic activity to iWAT will be rising whereas that to BAT will be inhibited to conserve energy. It is possible that the sympathetic premotor neurons singly labeled by one PRV are responsible for the selective activation of single fat pad. There is evidence suggesting that sympathetic premotor neurons with distinct neurochemical identities might belong to target specific pathways. However, there is also a possibility that differential regulation of sympathetic activity to BAT and iWAT is achieved downstream of the premotor neuron level.

## 5.3. Anatomical characterization of sympathetic preganglionic neurons innervating adipose tissues

Next, we characterized the locations of sympathetic preganglionic neurons innervating BAT and iWAT. To visualize the sympathetic preganglionic neurons in the spinal cord, we used the following sample preparation method. First, we dissected out spinal cord with vertebrates and ribs attached following perfusion and fixation. We used the attached ribs to identify each spinal segment, and then separate the entire spinal cord into smaller chucks by making a cut every 2-3 vertebrate. In this way, the spinal cord is cut into segments T1-T2, T3-T5, T6-T8, T9-T11 and T12-T13. Afterwards we separated each segment of spinal cord from the bones and embedded them into 2% agarose gel as structural support for sectioning. Lastly, we sectioned spinal cord samples into free-floating 30um slides which were used for immunostaining later on.

As discussed in 5.1.1, the sympathetic preganglionic neurons are cholinergic. Therefore, we first used the spinal cord sections generated from WT mice to visualize the locations of preganglionic neruons. As expected, we observed ChAT expressing sympathetic preganglionic neurons in four distinct regions in the spinal cord, including IML: intermediolateral cell column; Ilf: nucleus intermediolateralis pars funicularis; IC: intercalated nucleus; IPPe: central autonomic area (nucleus intercalatus pars paraependymalis) (Figure 5.3 a), among which IML contains the greatest number of ChAT expressing preganglionic cells. The other groups of ChAT expressing

cells are motor neurons located at the ventral horn. Based on their distribution, we can easily exclude these cells in our analysis.

To identify the location and distribution of the fat innervating preganglionic neurons, we first injected PRV expressing mCherry into BAT of WT mice to check for PRV colocalization with ChAT expressing sympathetic preganglionic neurons in the spinal cord. Since we expect to observe PRV infection of the preganglionic neurons by Day 3, we sacrificed the animals at this time to harvest the spinal cords. By co-staining the spinal cord slides with both mCherry and ChAT antibodies, we saw that BAT innervating preganglionic neurons primarily locate in the upper thoracic segments (Figure 5.3 b) between T1-T10, among which sections from T3-T5 have the greatest number of PRV infected preganglionic neurons. Since we injected only in one side of the BAT, we also saw PRV infection primarily in one side of the spinal cord because the sympathetic preganglionic neurons are known to project only to organs on the ipsilateral side. Similar observations on BAT innervating preganglionic neurons were also made by another group (François et al. 2019).

Next we injected PRV expressing GFP into iWAT of WT mice to check the distribution of iWAT innervating preganglionic neurons. We found that iWAT innervating preganglionic neurons are in the mid-lower thoracic segments, between T5-T13, among which sections fromT9-T11 have the greatest number of PRV infected neurons (Figure 5.3 c). The locations of the sympathetic preganglionic neurons are summarized in Figure 5.3 d: sympathetic preganglionic neurons between the level of T3-T5 innervates BAT, with rostral extension to T1 and caudal extension to T10; the ones between the level of T9-T11innervates iWAT, with rostral extension to T5 and caudal extension to T13.

Other than the sympathetic preganglionic neurons, we also observed some non-ChAT expressing neurons infected by PRV in the spinal cord sections. These cells are the local interneurons, connected with the preganglionic neurons. It is known that spinal cord interneurons play an important role in sympathetic control by influencing the activity of the sympathetic preganglionic neurons (Deuchars and Lall 2015). Further studies are needed to reveal the identities and functions of these cells.

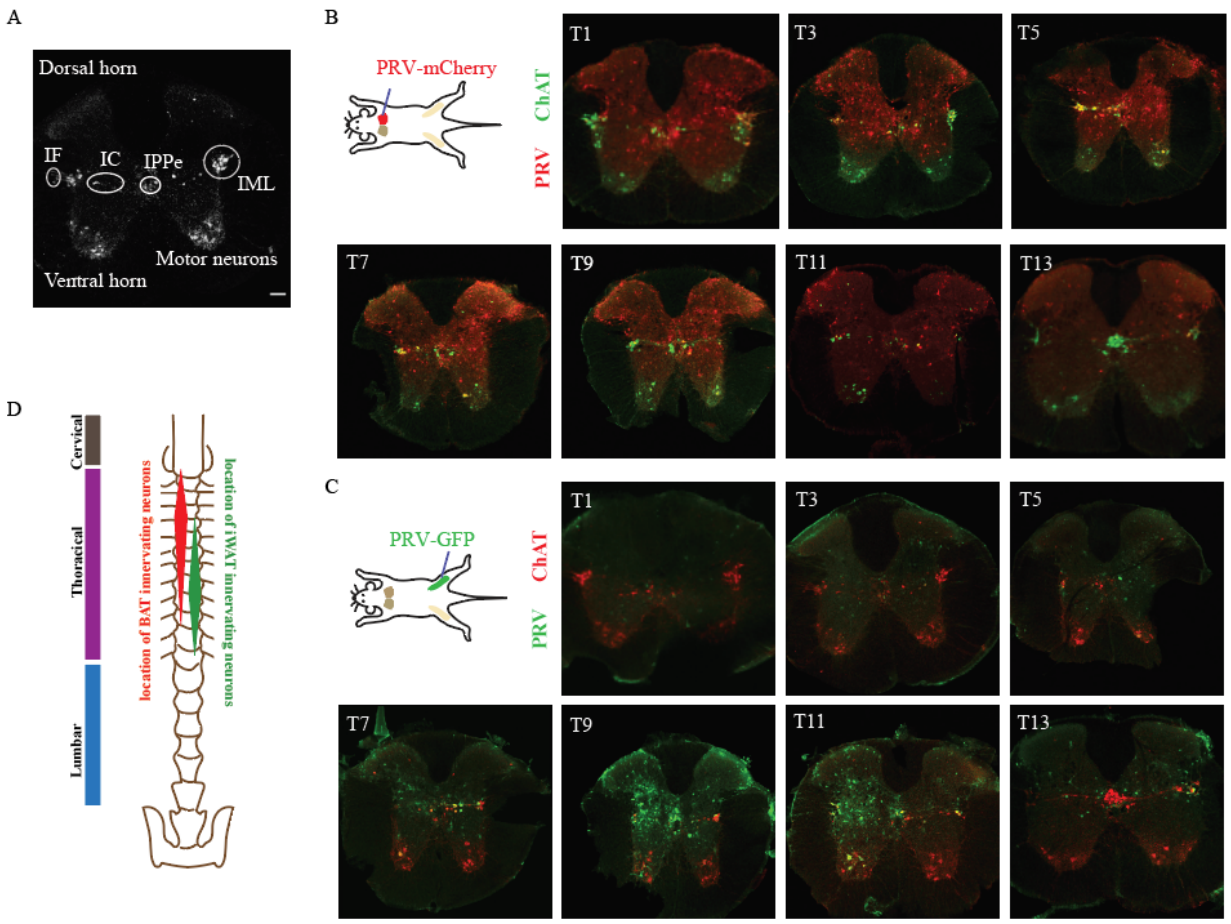


**Figure 5.3. Sympathetic preganglionic neurons innervating fat tissues.**

(a) Anatomy and distribution of ChAT+ (in grey) sympathetic preganglionic neurons in the spinal cord. IML: intermediolateral cell column; Ilf: nucleus intermediolateralis pars funicularis; IC: intercalated nucleus (nucleus intercalatus); IPPe: central autonomic area (nucleus intercalatus pars paraependymalis). Top of the image is the doral horn and the bottom of the image is the ventral horn, where most of the motor neurons locate. (b) PRV expressing mCherry was injected into the BAT (0.5uL into 4 different sites) of WT mice. On Day 3 post infection, animals were sacrificed to collect the spinal cord. Spinal cords were embedded in 2% agarose gel and sectioned into 30um slides, stained with anti-mCherry and anti-Chat antibodies, followed by fluorescent confocal imaging. We observed PRV infection in the upper thoracic channel (from T1 to T0). PRV infected cells are shown in Red, ChAT expressing neurons are shown in Green. (c) PRV expressing GFP (1.5uL into 6 different sites) was injected into the iWAT of WT mice. On Day 3 post infection, we observed PRV infection in the lower thoracic channel (from T5 to T12). PRV infected cells are shown in Green, ChAT expressing neurons are shown in Red. (d) Graphic illustration of spinal cord anatomy and distribution of preganglionic neurons innervating iWAT and BAT. The width of the bar roughly stands for the number of preganglionic neurons innervating fat depots. Scale bar: 100 um.

From the experiments above we conclude that the locations of iWAT and BAT innervating preganglionic neurons are largely distinct, however, there are still some spinal segments containing preganglionic neurons innervating both tissues. Therefore, we next asked whether there are preganglionic neurons between T5-T10 that are innervating both iWAT and BAT.

To answer this question, we injected PRV expressing mCherry into BAT and simultaneously injected PRV expressing GFP into iWAT. On Day 3 post injection, we sacrificed the animal to harvest the spinal cords. We prepared the spinal cord sections as described before, and co-stained the slides with ChAT, GFP and mCherry antibodies. Interestingly, we observed a small percentage of preganglionic neurons in the middle thoracic segments (T5-T10) expressing both GFP and mCherry, indicating that these neurons are innervating both iWAT and BAT (Figure 5.4 a). Since we divided the spinal cord into 5 segments for sectioning and imaging, we quantified the cell numbers within each region individually. In each segment, we quantified the number of ChAT expressing preganglionic neurons (in grey), BAT innervating neurons (in Red), and iWAT innervating neruons (in green) only within the four defined regions, including IML, Ilf, IPPe and IC. Then we take the ratio of the GFP or mCherry expressing cells to the total number of ChAT expressing neurons to obtain the percentage preganglionic neurons innervating different fat depots within each spinal cord region (Figure 5.4 b). It is important to note that we injected PRV into one iWAT and one BAT depots on the same side. Because the sympathetic preganglionic neurons mostly project to target organs on ipsilateral side (Deuchars and Lall 2015), we observed more PRV infected preganglionic neurons on ipsilateral spinal cord than the contralateral side. In order to be more consistent throughout our analysis, we decided to only conduct cell number quantification on single side of the spinal cord, the ipsilateral side of PRV injections.

The cell number analysis reveals that the spinal cord regions between T1-T5 contain primarily BAT innervating neurons, whereas regions between T9-T13 have primarily iWAT innervating neurons. Regions between T3-T5 have more than 40% of the preganglionic neurons sending efferents to BAT, whereas regions between T9-T11 have more than 40% of the neurons sending efferents to iWAT. Almost all preganglionic neurons double labeled with GFP and mCherry belongs to T5-T10, and T6-T8 spinal segments contain the greatest number of doubled labeled neurons (~15%). These data show that the number of preganglionic neurons simultaneously innervating both fat issues are low.

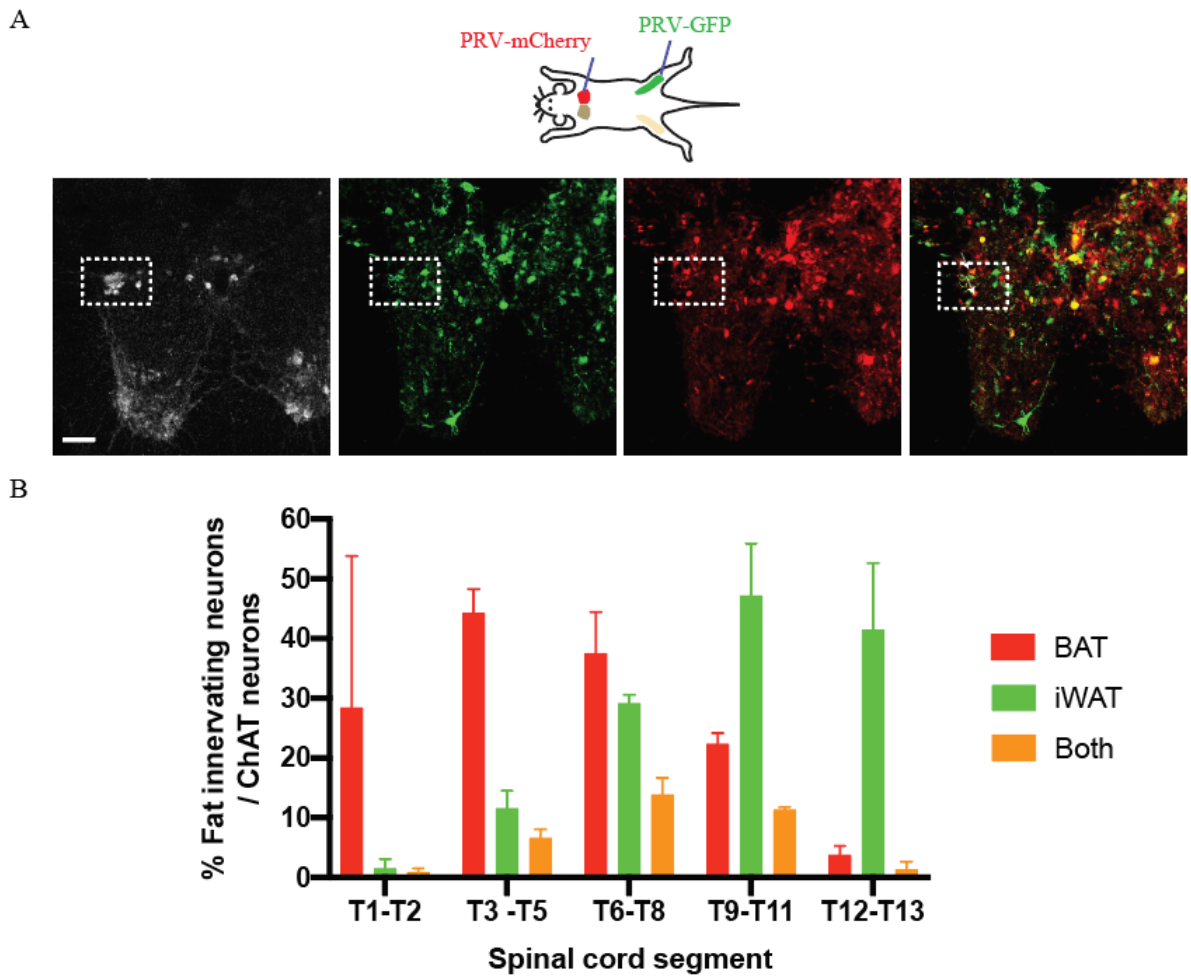


**Figure 5.4. Quantification of fat innervating preganglionic neurons across spinal segments.**

(a) We inject PRV expressing mCherry (0.5uL into 4 different sites) and GFP (1.5uL into 6 different sites) simultaneously into BAT and iWAT in the same animals. On Day 3 post infection, animals were sacrificed to collect the spinal cords. Spinal cords were embedded in 2% agarose gel and sectioned into 30um slides, co-stained with anti-mCherry, anti-GFP and anti-Chat antibodies, followed by fluorescent confocal imaging. Left most panel: ChAT staining; second to left panel: GFP staining; third to left panel: mCherry; right most panel: overlay of GFP and mCherry. We observed a few sympathetic preganglionic neurons in the middle thoracic segment, between T5-T10, that were labeled with both GFP and mCherry (indicated as white arrows). Scale bar: 100 um. (b) Quantification of the sympathetic preganglionic neurons innervating fat issues. The entire spinal cord is segmented into 5 divisions, T1-T2, T3-T5, T6-T8, T9-T11and T12-T13. The Y axis stands for the ratio of BAT/iWAT innervating neurons divided by the number of ChAT expressing preganglionic neurons in the defined spinal cord regions. Since PRV was injected into iWAT and BAT on a single side, only neurons from the ipsilateral spinal cord were included in the quantification. Red bar: percentage of BAT innervating neurons; Green Bar: percentage of iWAT innervating neurons; Orange Bar: percentage of BAT and iWAT innervating neurons.

Our data from this session show that SNS preganglionic neurons innervating BAT are located in the upper thoracic level, whereas that innervating iWAT are located in the lower thoracic level. This finding is consistent with previous knowledge that sympathetic preganglionic neurons from rostral spinal cords primarily innervate rostral organs, while those from caudal spinal cords innervates caudal organs (Deuchars and Lall 2015). More importantly, the preganglionic neurons innervating the two fat depots are largely distinct. There is with only a small number of neurons in the mid thoracic spinal segment innervating both iWAT and BAT, composing only < 5% of the total iWAT or BAT innervating preganglionic neurons. Our results suggest that most sympathetic preganglionic neurons might be specific to single target organs. Whether the preganglionic neurons innervating different organs display unique gene expression profiles remains to be discovered.

### 5.4. Anatomical characterization of sympathetic postganglionic neurons innervating adipose tissues

After revealing the anatomy of the fat innervating preganglionic neurons, we moved on to characterize the downstream fat innervating postganglionic neurons. Sympathetic postganglionic neurons receive input from preganglionic neurons in the spinal cord and extend their axons to innervate target organs. In mice, the ratio of preganglionic neuron to postganglionic neuron number is close to 1:20 (McCorry 2007). The postganglionic neurons are located in either paravertebral sympathetic ganglion chain or collateral ganglia (eg. Celiac ganglion), where the paravertebral ganglia innervate subcutaneous organs, including subcutaneous fat pads, and the collateral ganglia innervate visceral organs. To identify the sympathetic postganglionic neurons innervating both iWAT and BAT, we utilized a neurotropic tracer Cholera Toxin Subunit B (Ctb). When injected into the fat tissues, Ctb will be taken up by the nerve endings in the fat and transported to the cell bodies of the fat innervating neurons. Unlike PRV that can replicate in the infected neurons and be released to infect presynaptic neurons, Ctb will not duplicate and therefore will remain inside the first order fat innervating neurons, making it an ideal tracer of postganglionic neurons directly innervating target organs.

We first conducted several preliminary experiments to determine the logistic if the Ctb tracing experiments. In order to allow for sufficient neural uptake of Ctb from fat pads, we injected in toal 1uL (10ug/uL) of Ctb into 4 different sites in BAT and 1.5uL into 6 different sites of iWAT at the rate of 10nL/s using pulled capillaries with a NanoJect. To enable visualization of Ctb, we used Ctb conjugated with Alexa 488 or 568 (Ctb-488 or Ctb-568) for tracing. According to our polit experiments, although Ctb labeling of fat innervating neurons is detectable inside the sympathetic chain ganglia between 2-14 days post injection, the largest amount of Ctb labeled neurons were detected between 3-7 days post injection. Therefore, we sacrificed the Ctb injected animals on Day 4 post-surgery for anatomical characterization in all of the following experiments. As shown in Figure 5.5, when Ctb-568 was injected in to the iWAT of WT mice, we can see that the sympathetic chain ganglia on the ipsilateral side were infected by fluorescent Ctb. We visualized the iWAT innervating neurons located at lower thoracic segment under a fluorescent dissection scope. We can easily identify the T12 and T11 ganglia alongside the aorta and above the diaphragm. Therefore, we used T12 ganglion as the landmark, to help trace and dissect out more interconnected, iWAT innervating, ganglia in the sympathetic chain with rostral extension

to T9 and caudal extension to L3. Using a similar method, we also found that the BAT innervating neurons are mostly located in the upper thoracic segments. To trace and dissect out BAT innervating ganglia, we used the stellate ganglion, located near the first rib near the costovertebral joint, as a landmark. More BAT innervating neurons connected to the stellate ganglia, with caudal extension to T6 can be separated.

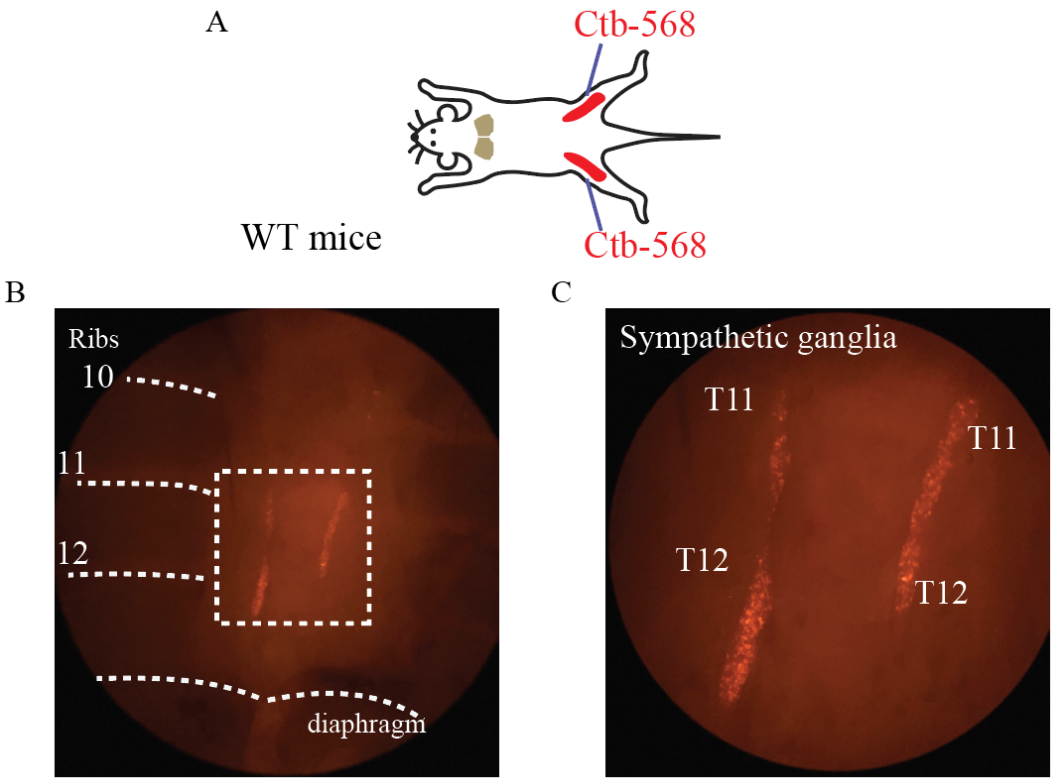


**Figure 5.5. Visualization and dissection of sympathetic ganglia using Ctb.**

(a) Scheme showing that Ctb-568 is injected into both sides of iWAT of WT mice. (b) Picture taken under the fluorescent dissection scope. In the view, the $10^{th}$-$12^{th}$ ribs from the right side can be visualized. The sympathetic ganglia T11-T12 are located near the ribs, above the diaphragm, within the dotted square. (c) Zoomed in view of the dotted square from (b). Individual neurons inside the ganglia can be visualized.

### 5.4.1. Sympathetic postganglionic neurons in WT mice

After conducting preliminary experiment to reveal the proximate location of iWAT and BAT innervating ganglia, we performed in depth analysis of the anatomy of the fat innervating ganglia, as well as the number of neurons in each ganglion innervating fat. Firstly, we injected Ctb-488 into BAT (1uL of Ctb into 4 different sites) of WT mice (Figure 5.6 a). Four days post-surgery, using stellate ganglia as a landmark, we dissected out the sympathetic chain connected to the stellate ganglia. The sympathetic chains were post fixed in 4% PFA for a couple hours and directly mounted on to microscopic slides for fluorescent confocal imaging. From this experiment, we found that BAT innervating neurons are present in many thoracic sympathetic chain ganglia, although each thoracic ganglion contains various number of BAT innervating neurons. The ganglia containing the greatest number of BAT innervating neurons are the stellate ganglion and thoracic 1 ganglion (T1), which are often fused together in B6 mice (Figure 5.6 a). More interestingly, the caudal part of stellate ganglion has much more BAT innervating neurons than the rostral part. In addition, thoracic ganglia T2-T6 also contains a large number of BAT innervating neurons (Figure 5.6 a). Although lower thoracic chain ganglia between T7-T13 all have some cells labeled by Ctb, the Ctb+ cell number is much lower compared to those in the upper thoracic chain segment (data not shown). Our results are very similar to the results from another study where the authors uses PRV to trace BAT innervating sympathetic neurons (François et al. 2019). The only difference is that we saw low number of BAT Ctb-expressing cells in T7-T13, while Francois et al. reported no BAT innervation beyond T6 ganglion.

After revealing the locations and distribution of BAT innervating neurons, we next injected Ctb-488 into iWAT of WT mice (Figure 5.6 b) and harvest the sympathetic chain four days post-surgery. We found that iWAT innervating neurons are distributed across the lower thoracic and upper lumbar sympathetic chain ganglia (Figure 5.6 b). The ganglion containing the greatest number of iWAT innervating neurons is the thoracic 12 ganglion (T12, Figure 5.6 b). In addition, the thoracic ganglia T9-T11, as well as lumbar ganglia L1 and L2, all contain large number of iWAT innervating neurons. Although the ganglia in the mid thoracic (T5-T8) and lower lumbar (L3-L4) segments also have some iWAT innervating neurons, the cell number is relatively low (data not shown). Besides, due to technical difficulties, the last ganglion in thoracic segment (T13) was hard to identify, therefore not shown in the figure. However, we believe T13 ganglion contains iWAT innervating neurons based on the fact that both T12 and L1 ganglia are heavily innervating iWAT.

Based on our findings in the above-mentioned experiments, we conclude that fat innervating sympathetic neurons resides across the sympathetic chain ganglia. BAT innervating neurons are distributed primarily in the stellate ganglia and thoracic T1-T6 ganglia, and to a lesser extent in the thoracic T7-T13 ganglia; iWAT innervating neurons are distributed primarily in the thoracic T19-T12 and lumbar L1-L2 ganglia, and to a lesser extent in the thoracic T5-T8 and lumbar L3-L4 ganglia (Figure 5.6 c, the width of the green arrow stands for the approximate number of fat innervating neurons).

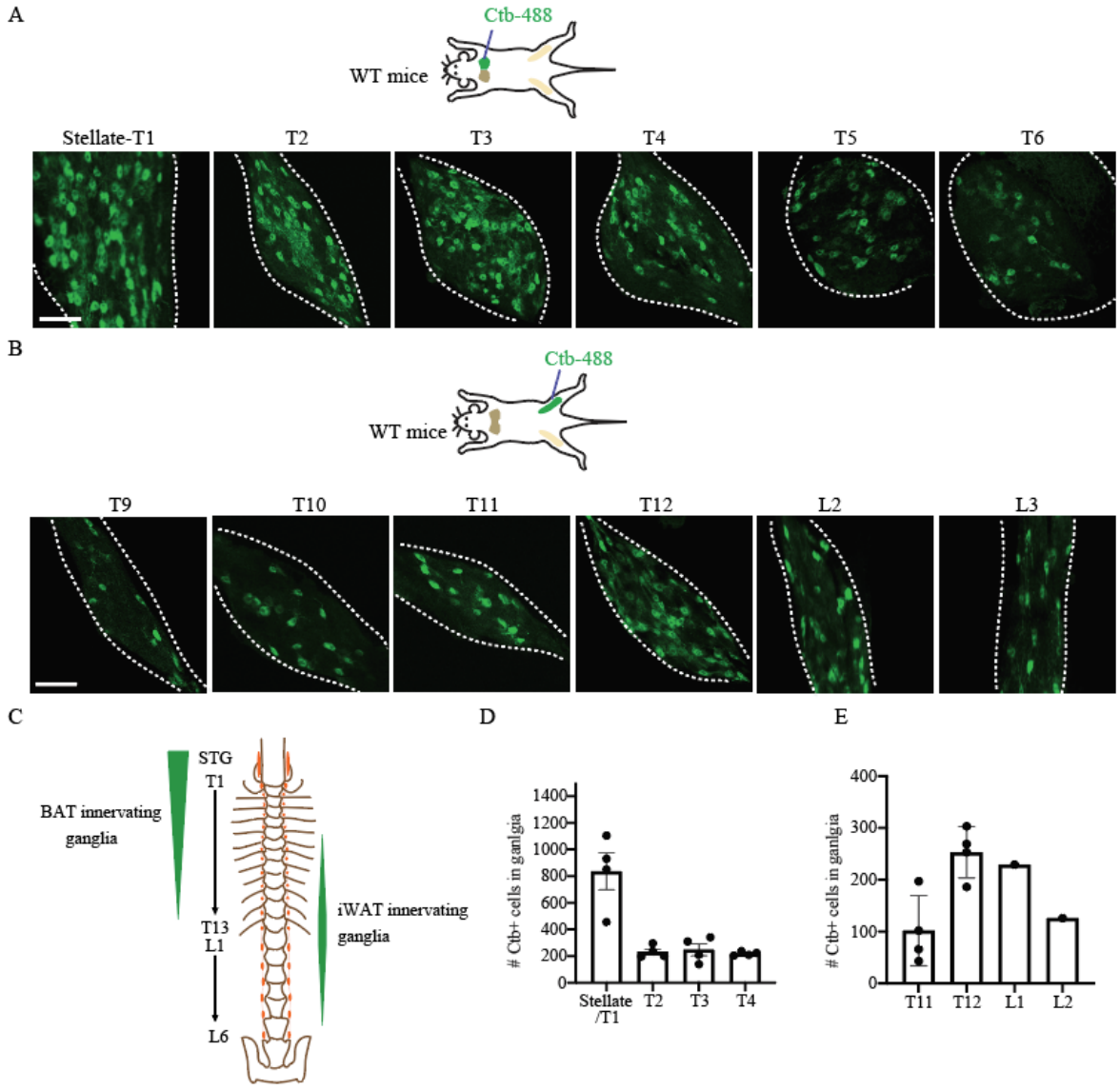


**Figure 5.6. Anatomical characterization of fat innervating sympathetic ganglia.**

(a) Ctb-488 was injected into the 4 different spots of BAT of WT mice (1uL Ctb at the concentration of 10ug/uL). Four days post-surgery, mice were sacrificed and fixed using 4%PFA and the sympathetic chain was dissected from the animal. The sympathetic ganglia were mounted and imaged by confocal microscopy. The sympathetic ganglia from stellate to T6 have the greatest number of BAT innervating neurons, therefore, the cross-section view of these ganglia was shown. (b) Ctb-488 was injected into the 6 different spots of iWAT of WT mice (1.5uL Ctb at the concentration of 10ug/uL). Four days post-surgery, sympathetic chain was dissected from the animal and imaged. The sympathetic ganglia from T9-T12, L1-L2 are displayed above. (c) Schematic describing the distribution of both iWAT and BAT innervating ganglia. (d) Quantification of the number of BAT innervating neurons (indicated as Ctb+) in the Stellate/T1, T2, T3 or T4 ganglia (n=4 for each ganglion). (e) Quantification of the number of iWAT innervating neurons (indicated as Ctb+) in the T11, T12, L1 or L2 ganglia (n=4 for T11 and T12, n=1 for L1 and L2). Scale bar: 100um.

To quantify the number of Ctb+ neurons inside each ganglion, stacked images of the entire ganglia were taken under confocal microscopy, at the step size of 1um, and analyzed using Fiji. In B6 mice, the stellate and T1 ganglia are often fused, therefore, we treated them as a single node during cell number quantification. According to our analysis, we found there are around 800 neurons in the stellate/T1 ganglia innervating BAT, while T2-T4 ganglia each contains around 200 neurons innervating BAT (Figure 5.6 d). The stellate/T1 ganglia have around half of total BAT innervating neurons. We also found that the number of iWAT innervating ganglia varies a lot among different ganglia-there are around 250 iWAT innervating neurons in the T12 and L1 ganglia, and around 100 iWAT innervating neurons in the T11 and L2 ganglia (Figure 5.6 e). It is important to note that the size and shape of the ganglia are heterogeneous among different WT animals, sometimes even within animals between two sympathetic chains. The number of Ctb+ cells within each ganglion is variable among different animals. Therefore, in the future more animals need to be quantified to provide a more accurate understanding of the number of fat innervating neurons in each ganglion. Lastly, there are much more BAT innervating neurons than iWAT innervating neurons inside the sympathetic chain ganglia, which is probably due to the fact that BAT has denser sympathetic innervation than iWAT.

The previous experiments show that the sympathetic ganglia innervating BAT or iWAT are mostly distinct – most BAT innervating ganglia are at the upper thoracic segment, whereas iWAT innervating ganglia are at the lower thoracic to lumbar segment. However, there are some sympathetic ganglia in the mid-lower thoracic segment (T5-T12) that contains neurons innervating both tissues. Therefore, we next asked whether there are neurons from sympathetic ganglia T5-T12 that innervate both tissues. In this experiment, we injected Ctb-568 into BAT and Ctb-488 into iWAT of the same animal (Figure 5.7 a). Four days post injection, animals were sacrificed, and the sympathetic chains were harvest and imaged. Interestingly, although we found both Ctb-488 (innervating iWAT) and Ctb-568 (innervating BAT) infected cells in ganglia T5-T12, there are only a very small number of neurons double positive with both Ctb-488 and 568. We visualized the sympathetic chains from 3 individual animals and found there are less then 10 cells double labeled by Ctb-488 and Ctb-568 in each animal (data not shown). This data show that BAT and iWAT innervating neurons are distinct.

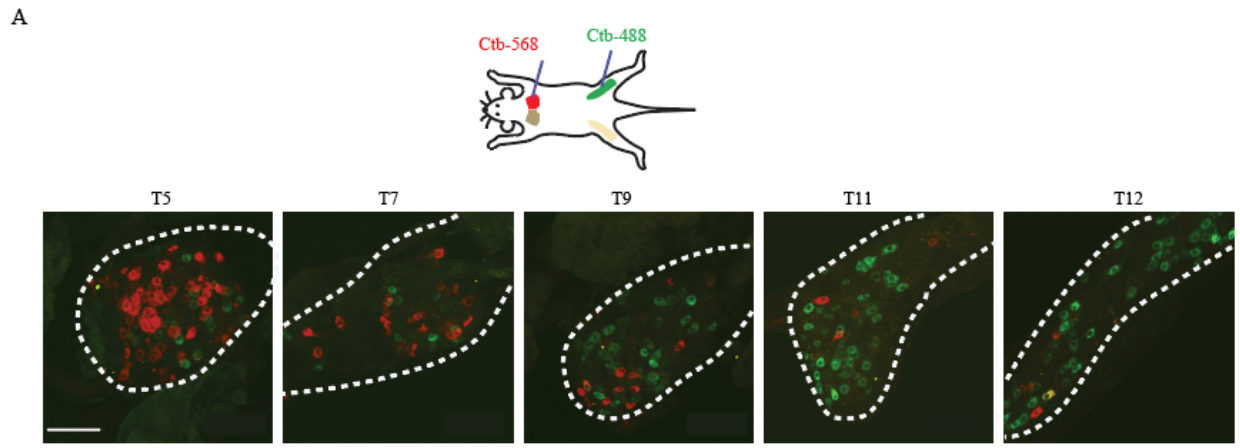


**Figure 5.7. Sympathetic neurons innervating BAT and iWAT are distinct.**

(a) Ctb-568 was injected into the 4 different spots of BAT, and Ctb-488 was injected into the 6 different spots of iWAT of WT mice (1.5uL Ctb at the concentration of 10ug/uL). Four days post-surgery, animals were sacrificed to harvest the sympathetic chain ganglia. Stacked images were taken for the individual sympathetic ganglia, at the step size of 1um; section-views of ganglia T5, T7, T9, T11 and T12 were displayed above. BAT innervating neurons are shown in Red, and iWAT innervating neurons are shown in Green; the contour of the ganglia was labeled by white dashed line. Scale bar: 100um.

### 5.4.2. Sympathetic postganglionic neurons in *ob/ob* mice

After revealing the anatomy of the fat innervating sympathetic postganglionic neurons in the WT mice, we set out to characterize that in *ob/ob* background. Since we have shown that *ob/ob* mice have significantly lower level of sympathetic innervation in both iWAT and BAT, comparing to age matched WT mice (Figure 2.5), we asked whether *ob/ob* mice also process a much lower number of fat innervating neurons in the sympathetic chain.

To compare the number of fat innervating neurons between *ob/ob* and WT mice, we decided to inject the same amount of Ctb into WT and *ob/ob* fat pads and directly compare the number of neurons labeled by Ctb in the sympathetic ganglia. Both BAT and iWAT of adult *ob/ob* mice, especially the iWAT, are much larger in size/volume compared to those from WT mice. The difference in fat pad size will likely results in variable efficiency of viral uptake between WT and *ob/ob* fat pads. Therefore, we decided to use adolescent *ob/ob* and WT mice, ~6-week-old, to perform this tracing experiment. At 6 weeks, the differences in adipose tissue sympathetic innervation between WT and *ob/ob* mice are obvious (Figure 2.5); but difference in adipose tissue size is minimum.

To decide on the amount of Ctb we inject in WT and *ob/ob* mice, we conduct preliminary experiment to decide on the optimal volume of Ctb to use. We already performed titration experiments to determine that the optimal amount of Ctb to use in WT mice is 1uL Ctb (10ug/uL) in BAT and 1.5uL in WAT. Since *ob/ob* mice have slightly larger fat pads compared to WT mice, we will perform another preliminary experiment to determine minimum amount of Ctb needed to fully label fat innervating neurons in *ob/ob* mice. To do this, we injected Ctb at two different volume in *ob/ob* mice: either 1uL in BAT and 1.5uL in iWAT, or 2uL in BAT and 3uL in iWAT. If the lower amount of Ctb (1uL Ctb in BAT and 1.5uL in WAT) is sufficient to label all fat innervating neurons in *ob/ob* mice, we would expect to see the same number of neurons labeled in both experimental paradigms. If we see the higher volume of Ctb labels more cells in the sympathetic chain, we will need to further increase the injection volume in *ob/ob* mice until we see the number of Ctb labeled fat innervating neurons plateau. From our preliminary experiments, we found that in *ob/ob* mice, both 1uL and 2uL Ctb injected in BAT labeled similar number of neurons in the stellate/T1 ganglion; both 1.5uL and 3uL Ctb injected in iWAT labeled similar number of neurons in the T12 ganglion (Data not shown). Therefore, we decided to use the lower injection volume,1uL Ctb (10ug/uL) in BAT and 1.5uL in iWAT, in the following experiment.

We first injected 1uL Ctb-568 (10ug/uL) in the BAT of 6-week-old WT or *ob/ob* mice. Four days post injection, we sacrificed the animals to harvest the sympathetic chain ganglia. Since BAT innervating neurons are located in the ganglia in the upper thoracic segment, we dissected out stellate ganglion, as well as several thoracic ganglia that are caudal to the stellate ganglion. Ganglia were post fixed in 4% PFA for 2 hrs and mounted on glass slides for fluorescent confocal imaging. Firstly, we discovered that the location of BAT innervating postganglionic neurons in *ob/ob* is very similar as WT mice. Ctb-568 injection leads to dense labeling of stellate and T2-T6 ganglia in both WT and *ob/ob* mice (Figure 5.8 a). Secondly, we found that in WT and *ob/ob* mice, Ctb-568 labeled a comparable number of BAT innervating neurons in the sympathetic chain, despite the fact that *ob/ob* mice have much less SNS innervation in BAT. Lastly, quantification of the number of Ctb labeled neurons show that, there are similar number of BAT innervating neurons in stellate/T1 ganglia and T2 ganglia of both WT and *ob/ob* mice (Figure 5.8 b).

Next, we injected 1.5uL Ctb-488 (10ug/uL) in the iWAT of 6-week-old WT or *ob/ob* mice. Four days post injection, we sacrificed the animals to harvest the sympathetic chain ganglia. This time, we used T12 as the landmark and dissected out the ganglia rostral and caudal to T12 in the sympathetic chain. Similar as what we observed in the BAT innervating ganglia, the location of iWAT innervating neurons is the same between WT and *ob/ob* mice. Ctb-488 injection leads to dense labeling of T9-T12 and L1-L2 ganglia in both WT and *ob/ob* mice (Figure 5.8 c). Moreover, quantification of cell number shows that both WT and *ob/ob* mice have similar number of iWAT innervating neurons in T12 and L1 ganglia (Figure 5.8 d). Taken together, our data show that *ob/ob* mice, although having much less SNS innervation in both iWAT and BAT, have similar amount of BAT and iWAT innervating neurons as WT mice in the sympathetic chain ganglia.

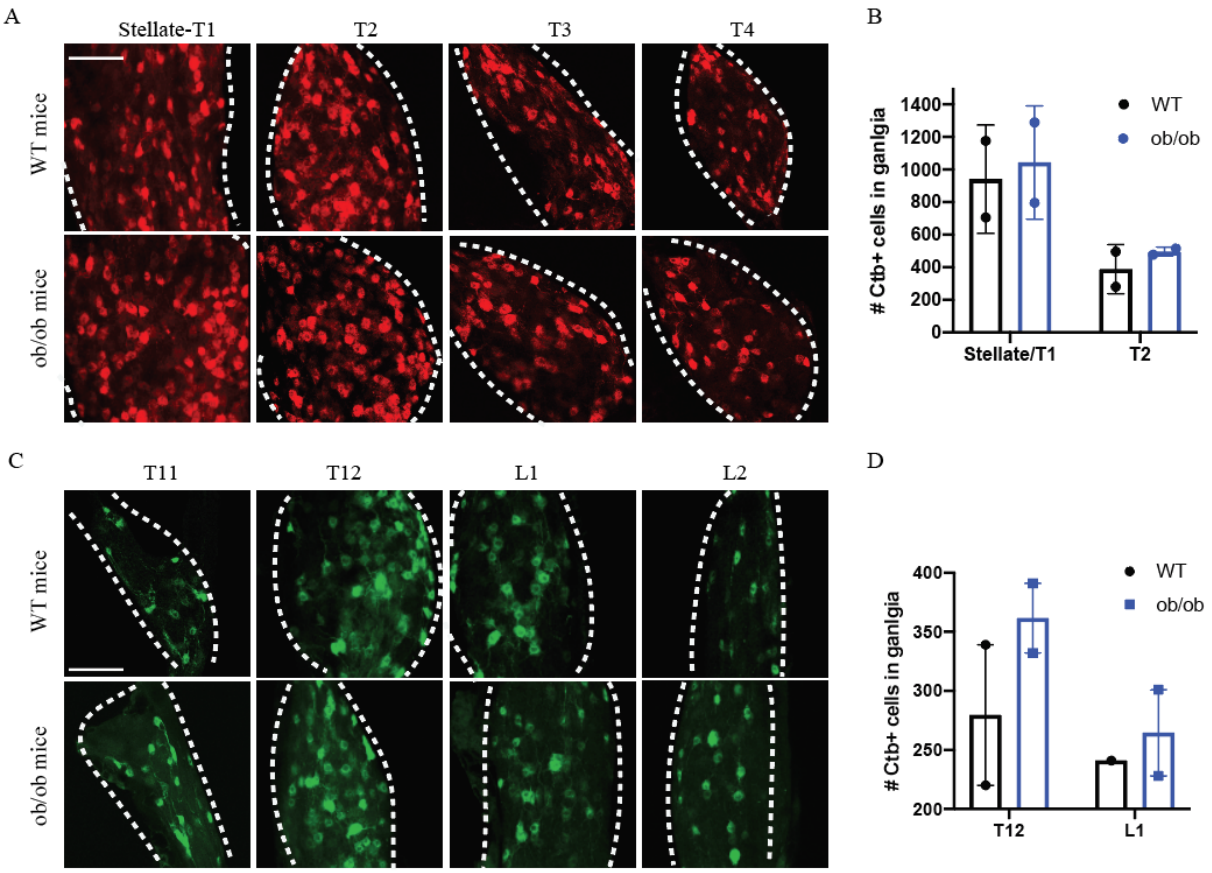


**Figure 5.8. Sympathetic postganglionic neurons innervating fat tissues in *ob/ob* mice.**

(a) Ctb-568 was injected into the 4 different spots of BAT of WT or *ob/ob* mice (1uL Ctb in total at the concentration of 10ug/uL). Four days post-surgery, mice were sacrificed to harvest the sympathetic chain. The chains were fixed using 4%PFA for a 2hrs and mounted for confocal imaging. Images were taken for stellate/T1, T2, T3 and T4 ganglia from both WT (top line) and *ob/ob* mice (bottom line). BAT innervating neurons in each ganglion are labeled in Red (Ctb-568); the contour of the ganglia was labeled by white dashed line. (b) Quantification of the number of BAT innervating neurons in stellate/T1 and T2 ganglia shown in (a) from both WT and *ob/ob* mice (n=2 for each). (c) Ctb-488 was injected into the 6 different spots of iWAT of WT or *ob/ob* mice (1.5 uL Ctb in total at the concentration of 10ug/uL). The chains were fixed using 4%PFA for a 2hrs and mounted for confocal imaging. Images were taken for T11, T12, L1 and L2 ganglia from both WT (top line) and *ob/ob* mice (bottom line). iWAT innervating neurons in each ganglion are labeled in Green (Ctb-488); the contour of the ganglia was labeled by white dashed line. (d) Quantification of the number of iWAT innervating neurons in T12 and L1 ganglia shown in (c) from both WT and *ob/ob* mice (n=2 for each). Scale bar: 100um.

### 5.4.3. Summary

The data from this session reveal the anatomy of sympathetic postganglionic neurons innervating iWAT and BAT in both WT and *ob/ob* mice. We show that in both mouse lines, BAT innervating neurons mostly locates in the stellate, T1-T6 ganglia; iWAT innervating neurons mostly locates in T9-L2 ganglia. More importantly, we demonstrated that WT and *ob/ob* mice have similar number of BAT or iWAT innervating sympathetic neurons, despite the fact that *ob/ob* mice have much less SNS innervation in the both adipose tissues. These data suggest that the lack of SNS innervation in *ob/ob* mice is not due to developmental defects that leads to low number of fat innervating neurons; it is rather due to the fact that sympathetic neurons in *ob/ob* are sending less axon projections into fat. In this case, it is worth revealing the gene expression profile of the fat innervation neurons in both WT and *ob/ob* mice to identify the molecular mechanism underlying the innervation defects in *ob/ob* mice.

Furthermore, we found that the BAT and iWAT innervating neurons in the sympathetic chain do not overlap, suggesting that sympathetic postganglionic neurons are target specific. This finding makes us wonder whether the molecular profiles of the sympathetic postganglionic neurons are also pathway/function specific. If this hypothesis is true, targeting the function-specific molecular markers in these postganglionic neurons would present tremendous therapeutic potential in various diseases, including obesity.

## 5.5. Summary and discussion

In this Chapter, we have fully characterized the anatomy of the sympathetic circuits innervating both BAT and iWAT. Briefly, we found that the sympathetic premotor neurons innervating BAT and iWAT are located primarily in three brain regions: PVH, RPa and RVLM. Among these three regions, PVH and RPa have been proved to play critical roles in thermoregulation, while RVLM is the major regulator of sympathetic activity to the cardiovascular system (Deuchars and Lall 2015). This suggest that, although the premotor neurons in all three regions can lead to sympathetic activation in fat tissues, they might be responding and integrating different environmental stimuli. Furthermore, we found that there are high percentage (>50%) of overlaps between iWAT and BAT innervating neurons in all three regions, suggesting that sympathetic activity in these two tissues are probably highly coordinated.

We also characterized the location of fat innervating sympathetic preganglionic and postganglionic neurons. Unlike the premotor neurons, the sympathetic preganglionic neurons innervating BAT and iWAT are mostly distinct (<5% overlap), with BAT innervating neurons in the rostral part of the spinal cord and iWAT innervating neurons in the caudal part. Similarly, the sympathetic postganglionic neuron innervating BAT and iWAT are distinct (no overlap). The postganglionic neurons innervating BAT are in upper thoracic sympathetic chain and the iWAT innervating ones are in the lower thoracic and upper lumbar sympathetic chain. These data suggest that the sympathetic nervous system is target specific at the level of pre- and postganglionic neuron. Further studies are needed to reveal whether there are target/function specific gene expression profiles in these sympathetic neurons. In addition, as the target innervation pattern along the rostral-caudal axis of the spinal cord/sympathetic chain are different, it is worth asking whether

there are location specific transcriptional profiles of the sympathetic neurons along the rostral-caudal axis.

The sympathetic innervation levels of WT and *ob/ob* mice are drastically different, leading us to ask whether leptin deficiency resulted in low number of fat innervating postganglionic neurons in *ob/ob* mice. However, we reveal that WT and *ob/ob* mice have similar number of fat innervating neurons. This unexpected result suggests that the *ob/ob* postganglionic neurons are sending much less axon projections to the adipose tissues. Therefore, we would like to next reveal the gene expression profile differences between WT and *ob/ob* ganglia, to identify possible molecular target that can induce axon growth in adipose tissues. Such molecular targets would have high therapeutic potential because increasing sympathetic innervation in adipose tissue can promote fat utilization and energy expenditure, both of which are key processes leading to weight loss.

## 5.6. Material and methods

### *Animals*

All animal care and experimentation were ethically performed according to procedures approved by the Institutional Animal Care and Use Committee at the Rockefeller University. Mice were housed 2–5 per cage (except in the cold exposure study where mice were singly caged) in a 12-h light/12-h dark cycle with ad libitum access to regular chow and water except in fasting studies. We used WT male C57BL/6J mice (000664, Jackson Laboratory), *ob/ob* (B6.Cg-*Lep*$^{ob}$/J; 000632, Jackson Laboratory; or bred in-house). All mouse lines are in a WT (C57BL/6J) background. Littermates of the same sex were randomly assigned to either experimental or control groups.

### *PRV tracing*

For retrograde labelling of adipose-projecting neurons in the CNS, mice were maintained under anesthesia and an incision was made above the thigh to expose iWAT, or above the intrascapular region to expose BAT. PRV-lp297, a variant of PRV-Bartha expressing GFP (or mCherry) was injected into iWAT or BAT of WT or *ob/ob* mice for mapping multisynaptic inputs to each of these depots. Injections were made using pulled-glass pipette with a 20–40-mm diameter tip coupled with NanoJect III system (Drummond 3-000-207 kit). For WT mice, PRV was injected into six different spots of iWAT (250 nl per injection at the rate of 10 nl/s, 1.5 ul total), and four different spots for BAT (125 nl per injection at the rate of 5 nl/s, 0.5 ul total). For *ob/ob* mice, PRV was injected into six different spots of iWAT (500 nl per injection at the rate of 20 nl/s, 3 ul total), and four different spots for BAT (250 nl per injection at the rate of 10 nl/s, 1 ul total). injected Skin incision was closed using EZ clips (Stoelting Co.). Mice were singly housed post injection to prevent wound opening and monitored daily. To characterize sympathetic premotor neurons in the brain, animals were sacrificed on Day 4 post-infection to collect the brains; to characterize sympathetic preganglionic neurons in the spinal cord, animals were sacrificed on Day 3 post-infection to collect the spinal cords.

### *Cholera toxin subunit B (Ctb) tracing*

For retrograde labeling of adipose innervating sympathetic postganglionic neurons, Ctb conjugated with either Alexa 488 (C22841, ThermoFisher Scientific) or Alexa 594 (C22842, ThermoFisher Scientific) were injected into the fat depots of WT or *ob/ob* mice. Mice were maintained under anesthesia and an incision was made above the thigh to expose iWAT, or above the intrascapular region to expose BAT for Ctb injection. Injections were made using pulled-glass pipette with a 20–40-mm diameter tip coupled with NanoJect III system (Drummond 3-000-207 kit). For both WT and *ob/ob* mice, Ctb was injected into six different spots of iWAT (250 nl per injection at the rate of 10 nl/s, 1.5 ul total), and four different spots for BAT (250 nl per injection at the rate of 10 nl/s, 1 ul total). Mice were singly housed post injection to prevent wound opening and monitored daily.

### *Spinal cord sectioning*

Mice were transcardially perfused with 4% PFA and the spinal cords (with bones and ribs attached) were post-fixed for 1 day in 4% PFA at 4 degree. On the second day, fixed spinal cords were washed with PBS, spinal segments were identified and cut into small chucks in the following way: T1-T2, T3-T5, T6-T8, T9-T11 and T12-T13. Spinal cords were dissected out from the vertebrates and embedded in 2% agarose (in PBS) for sectioning using Leica microtome (Leica SM2010R).

### *Immunofluorescence for brain and spinal cord sections*

Mice were transcardially perfused with 4% PFA and the brains were post-fixed for 1 day in 4% PFA. Brains were sectioned coronally at 50 μm using a Leica microtome (Leica SM2010R); spinal cords were sectioned coronally at 30 μm. Brain and spinal cord sections were washed in PBS with 0.1% Triton X-100 (PBST, pH 7.4) and blocked in 3% normal donkey serum (Jackson ImmunoResearch Laboratories) and 2% BSA (Sigma) in PBST for 2 h. Slides were then incubated overnight at room in primary antibody. After washing in PBST, sections were incubated in fluorescein-conjugated donkey IgG. Primary antibodies used in the current study and their dilutions are: chicken anti-GFP (1:1,000, ab 13970, Abcam), rabbit anti-RFP (1:1,000; 600-401-379, Rockland Immunochemicals), goat anti-ChAT (1:500, Ab144P, Millipore). Secondary antibodies conjugated with Alexa-568 and Alexa-488 were purchased from Invitrogen (1:1,000). Brain sections were mounted onto SuperFrost (Fisher Scientific 22-034- 980) slides and then visualized with an inverted Zeiss LSM 780 laser scanning confocal microscope with a ×10 or ×20 lens. Images were imported to Fiji for further analysis. To quantitate the number of stained cells, brain slides were imaged under a ×20 objective. Regions that represent the PVH, RPa or IML in each image were isolated and threshold for staining intensity. The number of positive cells was then counted by an observer blind to the sample identity.

***Sympathetic chain dissection***

Mice were transcardially perfused with 4% PFA and the internal organs were removed to expose the spine before sympathetic chain dissection. Under dissection scope, the stellate/T1 ganglion was located under the first rib near the costovertebral joint, in close proximity to the spine. T12 ganglia were located on top of the $12^{th}$ vertebrate, lateral to the descending aorta. Fine forceps and microdissection spring scissors were used to remove the stellate and T12 ganglia. To anatomically characterize the fat innervating neurons, the entire sympathetic chain from stellate to T12, L1-L4 were dissected out and post fixed in 4% PFA for 2 hours, and mounted onto SuperFrost (Fisher Scientific 22-034- 980) slides and then coverslipped for visualization with an inverted Zeiss LSM 780 laser scanning confocal microscope with a ×10 or ×20 lens. To quantitate the number of Ctb+ neurons inside the ganglia, z-stack images (1um step size) were taken to capture the entire ganglia. All images were analyzed in Image-J.

## Chapter 6. Molecular characterization of the adipose tissue innervating sympathetic postganglionic neurons

### 6.1. Overview

In Chapter 5, we characterized the anatomy of the postganglionic neurons innervating adipose tissues, enabling us to further study the molecular and functional properties of these cells. More importantly, we found that the sympathetic postganglionic neuron populations innervating BAT and iWAT are distinct, leading us to hypothesize that there might be target-specific molecular features in these sympathetic postganglionic neurons. Besides, the gene expression profiles of the sympathetic postganglionic neurons in the WT and *ob/ob* mice are most likely to be different; identifying the differential molecular profiles and revealing the factors that can promote adipose SNS target innervation will shine light on new therapeutic treatments of obesity. Therefore, in this Chapter we set out to uncover the molecular identities of these fat innervating postganglionic neurons in both WT and *ob/ob* background.

***Baseline and target specific transcriptional profiling of sympathetic postganglionic neurons***

The understandings of the complexity of the sympathetic postganglionic neurons are very limited. The cell types of the sympathetic postganglionic neurons are mostly characterized by their physiological functions, with limited number of molecular markers, such as TH, NPY, ChAT. A more systematic, unbiased characterization of cellular diversities is needed in the sympathetic chain neurons. Back in 2016, Linnarsson lab performed the first single cell sequencing experiment on the sympathetic chain ganglia (Furlan et al. 2016). In this paper, the authors dissected the stellate ganglia, as well as part of the thoracic chain ganglia, for sequencing. From their results, the thoracic sympathetic ganglia are clustered into eight subtypes (gene expression profile of each cell type is shown in Table 1), among which five cell types were adrenergic neurons (TH expressing), two cell types are cholinergic neurons (vChAT expressing) and the last one cell type expresses vGlut2. However, there were only 298 neurons passed the quality control and were included in this analysis; the number of transcripts detected in each cell were also low. Due to the quality of this data set, it might not be sufficient to fully reveal the cellular diversities in the sympathetic ganglia. In addition, this experiment only included neurons from the thoracic sympathetic chain, sparing the lumbar ganglia. Since the ganglia in lumbar segments innervates distinct sets of target organs from the thoracic segments, for example, only lumbar ganglia innervate iWAT; there is a possibility that lumbar sympathetic ganglia possess unique cell types. Thus, higher quality data sets including cells from both thoracic and lumbar segments of the sympathetic ganglia are necessary to fully reveal the cellular diversities of these neurons.

Previous studies, using bulk sequencing and immunohistochemistry coupled with viral tracing, have identified the presence of restricted set of neurochemical markers in the sympathetic postganglionic neurons innervating adipose tissues (Stefanidis et al. 2018). However, the cell type complexities among the adipose tissue innervating postganglionic neurons have not been characterized before. In this Chapter, we are interested in revealing the molecular signatures of the fat innervating neurons using single cell sequencing coupled with Ctb-tracing and Cell Hashing. Since the sympathetic activity to adipose tissues can be turned on in response to various

environmental stimuli, such as cold exposure, starvation, stress, leptin delivery, etc., it would be interesting to check whether there are function specific molecular profiles in these postganglionic neurons.

**Table 2. Cell types in thoracic sympathetic chain ganglia (adapted From Furlan et al. 2016)**

| | Cell type 1 | Cell type 2 | Cell type 3 | Cell type 4 | Cell type 5 | Cell type 6 | Cell type 7 | Cell type 8 |
|---|---|---|---|---|---|---|---|---|
| TH | + | + | + | + | + | - | - | - |
| NPY | + | + | + | - | - | - | - | - |
| Gfra2 | - | - | - | + | + | + | + | - |
| Gfra3 | + | + | + | - | - | - | - | + |
| Ret | - | + | - | + | + | + | + | - |
| Rarres1 | + | - | - | - | - | - | - | - |
| Enc1 | - | - | - | + | - | - | - | - |
| VAChT | - | - | - | - | - | + | + | - |
| Vip | - | - | - | - | - | + | + | - |
| Sst | - | - | - | - | - | - | + | - |
| vGlut2 | - | - | - | - | - | - | - | + |

TH: tyrosine hydroxylase; NPY: neuropeptide Y; Gfral2: GDNF Family Receptor Alpha 2; Gfra3: GDNF Family Receptor Alpha 3; Ret: Ret Proto-Oncogene; Rarres1: Retinoic Acid Receptor Responder 1; Enc1: Ectodermal-Neural Cortex 1; VACHT: Vesicular acetylcholine transporters ; Vip: Vasoactive Intestinal Peptide; Sst: Somatostatin; vGlut2: SLC17A6, L-glutamate transmembrane transporter.

***Differential gene expression profiles in WT and ob/ob mice***

In addition to revealing the cell type complexities of the sympathetic nervous system, we are also interested in comparing transcriptional cell state differences in these neurons between WT and *ob/ob* mice.

The sympathetic postganglionic neurons have been used as model to study peripheral nerve development for decades. Many neurotropic factors, including NT-3, NGF, and BDNF, that drive target innervation, neuron survival and synaptogenesis during sympathetic nervous system development have been identified (Glebova and Ginty 2005). However, the molecular mechanisms underlying sympathetic target innervation in adult animals, such as leptin induced axon growth in the adipose tissue, has not been demonstrated. In this Chapter, we are particularly interested in

answering the following questions: 1) Does leptin induce sympathetic innervation in adipose tissue through canonical developmental pathways? Can we target these pathways to induce axon growth in mice independently of leptin? 2) Are there cell type specific molecular mechanisms in promoting axon growth? 3) What are the dynamics of leptin-induced cell state transformation of postganglionic neurons? Is leptin able to restore the transcriptional profiles of sympathetic neurons in *ob/ob* mice back to WT level?

Methods that can selectively drive sympathetic activity in adipose tissue will likely promote fat utilization and energy expenditure, therefore, answering the above-mentioned questions will help provide valuable insights on the therapeutic potentials of these sympathetic postganglionic neurons

***Chapter summary***

In this Chapter, we will first introduce the new protocol we developed to perform single cell dissociation of the sympathetic chain ganglia. For baseline cell atlas, we will isolate single neurons from thoracic and lumbar sympathetic chain ganglia of both WT and *ob/ob* mice. Single cells are then barcoded using 10X chromium system, followed by library construction and sequencing. In addition to baseline cell type analysis, we will also sequence adipose tissue innervating neurons from both WT and *ob/ob* mice using retrograde Ctb tracing couple with Cell Hashing method (details explained in 6.2.3). Lastly, we will reveal the molecular mechanism underlying sympathetic nerve plasticity in *ob/ob* mice following leptin treatment.

## 6.2. Single cell dissociation of the sympathetic ganglia

Single cell dissociation protocol is adapted based on the published method used to dissociate sympathetic ganglia and dorsal root ganglia (Sharma et al. 2020; Furlan et al. 2016). In order to distinguish cells from BAT innervating segments (stellate to T5) and iWAT innervating segments (T10-L4) of the sympathetic chain, we utilized cell hashing approach. Briefly, we prepared single cell suspension from top thoracic (referred to as thoracic segment) and lower thoracic with lumbar sympathetic (referred to as lumbar segment) ganglia separately, incubated the two samples with Hashtag antibodies, targeting universal cell surface protein, conjugated with two unique oligo barcodes (details on cell hashing explained in 6.2.3). After barcoding, samples from two sympathetic segments were sorted separately on flow cytometer to enrich for live cells (6.2.2). Lastly, two samples were pulled together to load on 10X chromium system for single cell barcoding, followed by library preparation and sequencing.

### 6.2.1. Detailed experimental procedure

Sympathetic chain dissection:

1. Animals were transcardially perfused with ice cold, oxygenated, HBSS supplemented with tetrodotoxin (TTX) and NMDA glutamate site antagonist (AP-5).
2. Animals are positioned on ice; internal organs were removed to expose the spine before sympathetic chain dissection.
3. Both sympathetic chain from the thoracic and lumbar segments are quickly dissected out and stored temporarily in perfusion buffer (HBSS with TTX and AP-5).
4. Immediately after dissection, a fine clean-up was performed to remove attaching tissues from the ganglia, resulting in only the sympathetic ganglia remaining.
5. Afterwards, the thoracic chain ganglia, including stellate ganglia, and the lumbar chain ganglia were separately placed into oxygenated dissociation buffer (HBSS with TTX, AP-5 and transcriptional inhibitors) for short-term storage.
6. Steps 1-5 were repeated for more animals to collect enough starting material.

Single cell dissociation:

1. After all the ganglia were isolated and cleaned, samples were transferred into in to a 10KD cassette containing Step 1 dissociation solution at 37 °C for 30 min. The Step 1 dissociation solution contains HBSS, TTX, AP5, transcriptional inhibitors (actinomycin, anisomycin), and papain activators (EDTA and L-cysteine).
2. Cassettes with ganglion were transferred to Step 2 dissociation buffer and incubate at 37 °C for 30 min. Step 2 dissociation buffer contains HBSS, collagenase, dispase, TTX/AP5, and transcriptional inhibitors.
3. Ganglia were gently triturated with p1000 at 15 min and 30 min in Step 2 dissociation buffer.
4. Sample were passed through 40-μm filter to exclude undissociated materials, transferred to 15mL Conical tubes pre-coated with BSA and spined to pellet at 100g for 5 min at 4 °C.
5. Cells were resuspended in 200 uL ovomucoid buffer (DMEM:F12 + 1% pen/strep + 12.5 mM glucose, supplemented with TTX/AP-5 and transcriptional inhibitors) to quench the enzymatic activity. Cell number were counted.

Cell hashing:

1. Samples from thoracic and lumbar ganglia were separately stained with two BioLegend TotalSeq B (anti-mouse Hashtag 3 and 4) antibody cocktails, conjugated with two different barcodes, for 20 min on ice.
6. To wash off the hashing antibodies, samples were diluted with 2mL of DMEM:F12 + 1% pen/strep + 12.5 mM glucose + 0.2% BSA, supplemented with TTX/AP-5 and transcriptional inhibitors, and spined to pellet at 100g for 5 min at 4 °C.
2. Cells were then resuspended in 200 uL of flow buffer (DMEM:F12 + 1% pen/strep + 12.5 mM glucose, 0.2% BSA, TTX/AP5).
3. Cells were stained with DRAQ7 (dead cell exclusion) and Calcein violet (live cell stain) for at least 10 min on ice.
4. Live cells were sorted using flower cytometer.
5. Cell number ratio between thoracic and lumbar sympathetic chain sample was adjusted to 1:1 and combined to load on 10X chromium system.

### 6.2.2. Enrichment for live neurons using FACS

To ensure sequencing quality in single cell sequencing experiments, it is important that we enrich for live cells before loading samples onto 10X chromium system. Therefore, at the end of the single cell preparation step, we stained the cells with both dead cell exclusion dye, DRAQ7, and live cell dye, Calcein Violet, and sorted for Calcein+ DRAQ7- live cells on FACS. Besides, we are most interested in profiling the neuron cell populations in the sympathetic ganglia. Thus, it is also crucial that we can identify neuron populations from the other cell types on FACS.

In the preliminary experiment, sympathetic ganglia from both thoracic and lumbar segments are combined and processed together following the experimental procedure listed above. After staining, sample were loaded onto BD™ LSR flow cytometer for analysis. Based on the live cell and dead cell intensity, we can identify the live cell population with high Calcein violet staining and low DRAQ7 staining, distributed on the top left conner of the flow chart (Figure 6.1 a). We can always identify three distinct live cell populations in our samples, Pop 1-3. In addition, the cell population on the far right of the plot, DRAQ7 high, represents dead cell population; the population on the lower left conner, double negative for Calcein Violet or DRAQ7, are most likely the cell debris. We next backgated the live cell Pop 1-3 on cell scatter (Figure 6.1 b). Interestingly, we found that Pop 1 and 3 contain cells with similar morphology-large and circular, which are shown in the middle of the cell scatter plot. Different from Pop 1 and 3, Pop 2 contains cell with completely different scatter, mostly small and non-circular, which are shown on the lower left of the scatter plot. In addition, Pop 2 is also made up of two very different cell populations with distinct cell scatter (Figure 6.1 b). Since these population might represent completely different cell types, we next asked which population(s) represent neurons from the sympathetic chain ganglia.

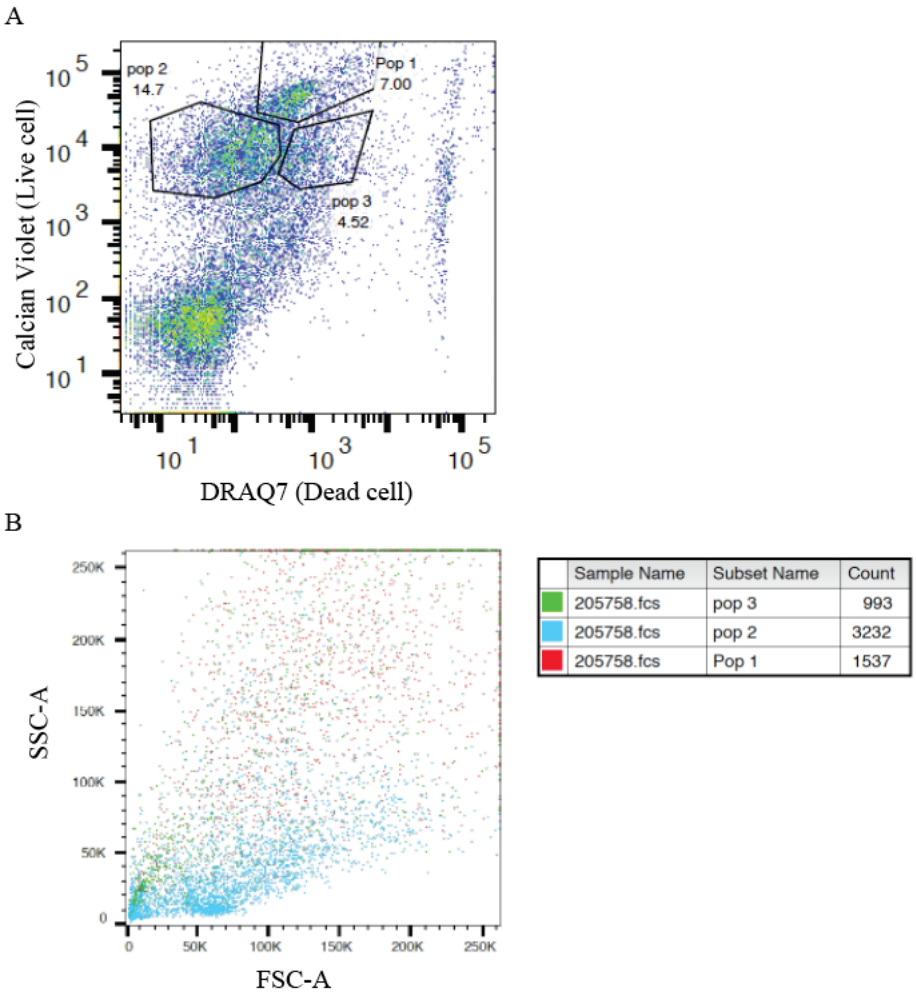


**Figure 6.1. Live cell scatter from sympathetic chain ganglia.**

(a) Based on the live and dead cell dye staining intensity, there are three distinct live cell population from the sympathetic ganglia sample. Population 1(pop 1) has the highest Calcein violet staining, is 7% of the entire scatter, pop 2 has the lowest DRAQ7 stain is 14.7% of the entire scatter, pop 3 is 4.52% of the entire scatter. In addition, the population on the far right is the dead cell population, consisting ~2% of the scatter. On the lower left conner, there is a large population, double negative in Calcein or DRAQ7, consisting ~30% of the scatter is considered as cell debris. (b) Population 1-3 are backgated to show their forward and side scattering. Pop 1 (in Red) and Pop 3 (in Green), mostly contain large, circular cells, therefore are mostly shown in the middle of the scatter; whereas Pop 2 (in Blue) contains two distinct population, both are small and non-circular cells, therefore is shown on the lower left side of the scatter. Cell number in each population is shown on the right of this panel.

To identify neurons in the sympathetic chain, we injected Ctb-488 into both BAT and iWAT of two WT mice and sacrificed the animals on Day 4 post-injection. Theoretically, only neurons will be labeled by Ctb-488 and we can identify them on FACS. Samples were prepared using the same protocol as listed in 6.2.1, and live cell populations Pop 1-3 were identified as in Figure 6.1 a. We checked the amount of Ctb-488 labeled cell in each live cell population (Figure 6.2). Interestingly, we found that Pop 1 contains 38.9% of Ctb-488 neurons and is the population with the greatest number of Ctb-488 labeled neurons. Pop 3, although has similar cell scatter as Pop1, only has around 12.5% Ctb+ neurons. Lastly, Pop 2, which has the most distinct cell scatter among the live cell population, only has 4.15% of Ctb expressing neurons.

These data show that the fat innervating sympathetic neurons are mostly in live cell Pop 1. Based on the cell scatter and the existence of high percentage of Ctb labeled neurons in Pop1, we believe Pop 1 likely represents the neuron population among the three live cell populations. In addition, since Pop 3 has the similar cell scatter as Pop 1, we think Pop 3 might also be neuron population. However, we reasoned that Pop 3 might contain different neuron cell types from Pop1 and these cell types most innervates organs other than fat. Pop 2 has the most distinct cell types from Pop 1 and 3, therefore, it might represent non-neuronal cell types in the sympathetic ganglia, such as endothelial cells, peripheral glial cells or immune cells, etc.

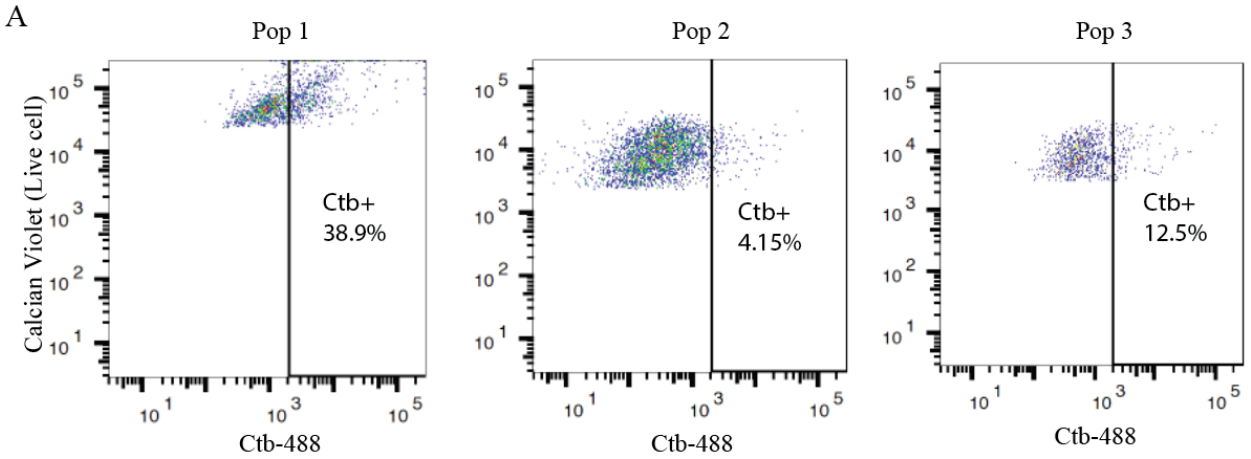


**Figure 6.2. Neuron population in the sympathetic ganglia.**

(a) Ctb-488 was injected into both iWAT and BAT of WT mice to label Part of the neurons in the sympathetic chain ganglia. After gating for three live cell populations (as shown in Figure 6.1), the percentage of Ctb-488 expressing neurons were determined in each population. Pop 1 (on the left) has the greatest percentage of Ctb+ cells; Pop 2 (in the middle) has the lowest percentage of Ctb+ cells; Pop 3 (on the right) has 12.5% Ctb+ cells.

### 6.2.3. Cell hashing with barcoded antibodies of sympathetic neurons

Furlan et al. 2016 revealed certain level of cell type diversities in the sympathetic chain along the rostro-caudal axis through imaging. In Chapter 5.4, we demonstrated that the distribution of iWAT and BAT innervating sympathetic neurons are distinct, with BAT innervating ones concentrated in the rostral thoracic chain ganglia and iWAT innervating ones in the caudal thoracic to lumbar chain ganglia. It is reasonable to hypothesize that there might be molecular diversities among neurons in different sympathetic chain segments. Therefore, we decided to include Cell Hashing technology to label neurons from two segments of the sympathetic chain (thoracic vs. lumbar), and subsequently pool the two samples for sequencing (Stoeckius et al. 2018).

This Cell Hashing approach utilizes a cocktail of antibodies recognizing ubiquitous surface proteins, such as mouse CD45 and MHC class I protein, conjugated with distinct Hashtag oligonucleotides containing barcodes which can be used for demultiplexing. When samples were incubated with Hashtag antibody cocktail, they will also be labeled with a unique sample barcode. These barcodes can be sequenced alongside the single cell gene expression library and subsequently used as a fingerprint for sample demultiplexing. In our experiments, we used two Hashtag antibody cocktails, TotalSeq™-B0303 anti-mouse Hashtag 3 and 4 Antibody, to label thoracic sympathetic ganglia and lumbar sympathetic ganglia separately.

Cell Hashing approach has been proved to work well in labeling hematopoietic cells, however, cell surface expression levels of CD45 and MHC class I protein in periphery neurons are not well documented. Therefore, we performed preliminary experiments to determine whether this is a valid approach for periphery neurons.

In the preliminary experiments, we used Hashtag antibody cocktail conjugated with PE, instead of Hashtag oligonucleotides, to visualize the percentage of sympathetic neurons labeled by these antibodies. We dissociated sympathetic chain ganglia from two mice, resuspended the cell pellets in 100 uL buffer for staining, and incubated the cells with antibody cocktail at the concentration of 1ug/ 10^6 cells or 2 ug/ 10^6 cells. Lastly, cells were stained with Calcein Violet and DRAQ7 before loading on to flow cytometer for analysis. Live cell populations were identified similarly as in Figure 6.1 a. We checked for antibody labeling efficiency in each of the three live cell populations (Figure 6.3 a-b) and found that the antibody labeling efficiency is very different among the populations. Firstly, in Pop 1, which we believe are primarily neurons, there are between 80-90% of cells labeled by the Hashtag antibody cocktail. Secondly, Pop 2 show over 50 % of antibody labeling. Additionally, within the PE+ subsets in Pop 2, there are also two separate cell populations - one with very high PE staining (on the far-right side of the plot) and the other with mid-level PE staining intensity (in the middle of the plot). Lastly, Pop 3 has the lowest staining efficiency, with only 20-30 % cells stained with Hashtag antibody. Since we tried two different staining concentration in this experiment, we found that using a higher concentration (Figure 6.3 a) of antibody results in a better coverage. More importantly, using the hashtag antibody at a concentration of 2 ug/10^6 cell leads to over 90% of the cells stained in Pop 1, which is most likely the neuron population. This ensures that the Hashtag antibodies can, at least, be used to demultiplex neuron populations from multiple samples of the sympathetic ganglia.

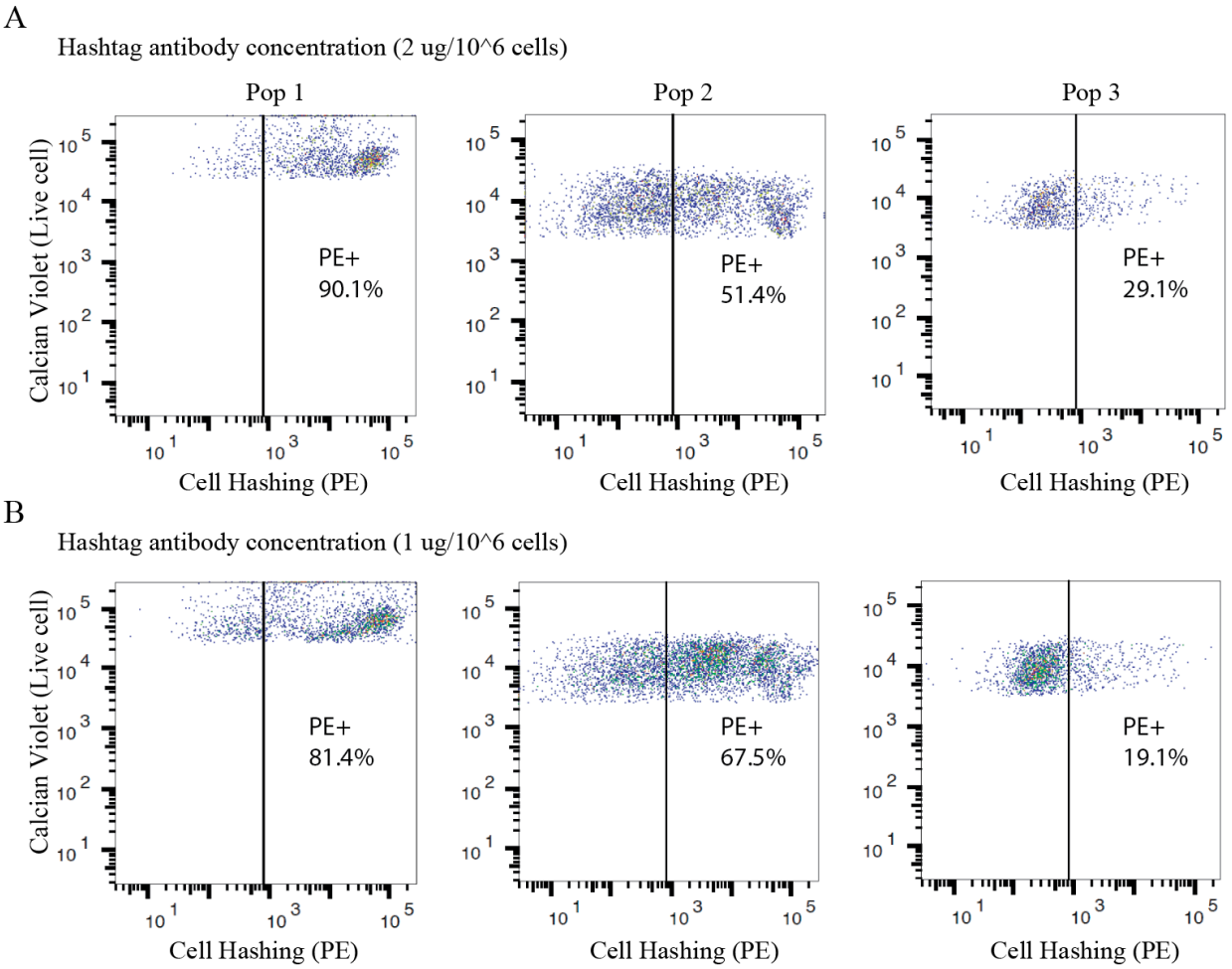


**Figure 6.3. Sympathetic labeling with Hashtag antibody cocktail.**

(a) Sympathetic cell suspension was incubated with PE conjugated Hashtag antibody cocktail at the concentration of 2 ug/10^6 cells in volume of 100 uL. Live cell populations were gated the same way as shown in Figure 6.1 a, the percentage of antibody labeled cells were shown here. Pop 1 (on the left) has the 90.1% PE+ cells; Pop 2 (in the middle) has the 51.4% Ctb+ cells; Pop 3 (on the right) has 29.1% Ctb+ cells. (b) Sympathetic cell suspension was incubated with PE conjugated Hashtag antibody cocktail at the concentration of 1 ug/10^6 cells in volume of 100 uL. Live cell populations were gated the same way as shown in Figure 6.1 a, the percentage of antibody labeled cells were shown here. Pop 1 (on the left) has the 81.4% PE+ cells; Pop 2 (in the middle) has the 67.5% Ctb+ cells; Pop 3 (on the right) has 19.1% Ctb+ cells.

### 6.2.4. Protocol summary

Based on our preliminary experiment, the single cell dissociation protocol shown in 6.2.1 works reliably in dissociating single neurons from the sympathetic chain ganglia. There are three distinct live cell populations from the single cell suspension derived from sympathetic chain ganglia (Pop 1-3, Figure 6.1). Based on the cell scatter and percentage of Ctb-488 expressing neuron in each population, we believe Pop 1 most likely represents the neurons; Pop 2 most likely represents the non-neuronal cells; Pop 3 might also be neuron cells but represents different cell types from Pop 1. In order to obtain general understanding of the cellular and molecular diversities in the sympathetic ganglia, we would include all the live cell populations for sequencing in WT and *ob/ob* mice baseline atlas experiment. Since we are mostly interested in the neuron cell populations, we would adjust the ratio among the three population after sorting to enrich Pop 1 before loading sample on 10X chromium system for single cell barcoding.

In our preliminary experiments, from two WT animals, we can approximately isolate 1500 cells from Pop 1, 3000 cells from Pop 2 and 1000 cells from Pop 3. To enrich for neuron cells in our sequencing sample, we will include all of the cells from Pop 1 (ideally >40%), and equal number of cells from Pop 2 and 3 to fill the loading capacity for 10X chromium chip. Since we can load approximately 15,000 cells on to the 10X chromium chip, we will be using 6-8 animals for the baseline sequencing experiment.

In addition, we have validated the Hashtag antibody for labeling sympathetic neurons in 6.2.3. We showed that the antibody cocktail (at the concentration of 2 ug/10^6 cell) works well in labeling >90% of cells in Pop 1, which is most likely the neuron cell population. Therefore, in the baseline sequencing experiment, we will label neurons from thoracic ganglia and lumbar ganglia using antibodies conjugated with two different Hashtag oligonucleotides, and subsequently pull the two samples together for sequencing. The unique hashtags will allow us to demultiplex neuron cells from thoracic chain and lumbar chain, providing additional information on the molecular diversity in different segments of the sympathetic chain ganglia.

## 6.3. Single cell profiling of the sympathetic ganglia from WT and *ob/ob* mice

### 6.3.1. WT sample preparation

We first performed single cell analysis of WT animals. From seven WT animals, we processed sample from thoracic chain and lumbar chain ganglia separately, stained them with TotalSeq B Hashtag 3 antibody and Hashtag 4 antibody accordingly (

Table 3). The two set of samples were sorted separately using FACS. The same three live cell populations were identified, based on Calcein Violet and DRAQ7 staining, of cell suspension derived from both thoracic chain and lumbar chain ganglia. However, the ratio of cell number between each population is slightly different between thoracic and lumbar sympathetic chain samples. From the thoracic chain single cell suspension, we sorted out 1748 cells from Pop1, 7963 cells from Pop 2, and 2502 cells from Pop 3. From the lumbar chain single cell suspension, we sorted out 2115 cells from Pop 1, 6570 cells from Pop 2, and 5096 cells from Pop 3.

Afterwards, the two samples were pooled at a ratio of 1:1, 10,000 cells from each sample. To enrich for neuron cells, in each sample, we included all cells from Pop 1, and added same number of cells from Pop 2 and 3 to reach a total number of 10,000 cells. Finally, due to the loading volume limit for 10X chromium system, we concentrated the samples before loading. We spined the sample gently at 100g for 5min to pellet the cells, took out excessive buffer volume from the top and resuspend cells in no more than 33 uL of buffer. The last spin will lead to some cell loss, therefore, we expect to load around 15,000 cells on the 10X chip for single cell barcoding. Currently we are waiting on the sequencing data.

**Table 3. Hashtag antibody information.**

| Name | Barcode sequence | Sample labeled |
|---|---|---|
| TotalSeq™-B0303 anti-mouse Hashtag 3 Antibody | CTTGCCGCATGTCAT | Thoracic chain ganglia (stellate, T1-T5) |
| TotalSeq™-B0304 anti-mouse Hashtag 4 Antibody | AAAGCATTCTTCACG | Lumbar chain ganglia (T10-L4) |

## 6.4. Leptin induces plasticity changes in sympathetic postganglionic neurons

In Chapter 2 - 4 of this thesis, we described a profound, leptin induced sympathetic nerve plasticity in the adipose tissue of adult mice. We have shown that long term, but not acute, leptin treatment of *ob/ob* mice increases the SNS density in both BAT and iWAT to match the WT levels. The level of sympathetic plasticity that appears in adult mice following leptin treatment is very surprising, because this level of sympathetic plasticity it is normally only observed during development or tissue injuries. Therefore, we would like to further reveal the molecular mechanisms underlying this leptin induced sympathetic plasticity using single cell sequencing approaches. Since we would like to treat *ob/ob* mice with leptin to assay transcriptional cell state changes, we would like to first determine the dynamics of leptin induced sympathetic plasticity changes in the ganglia before proceeding to sequencing.

### 6.4.1. Leptin's effects on WT ganglia

We first used WT animals to test whether leptin treatment lead to neural plasticity changes in the fat innervating sympathetic neurons. In this experiment, we first injected Ctb-568 into BAT and Ctb-488 into iWAT to label the fat innervating neurons in the ganglia. To allow optimal Ctb labeling and to ensure that mice fully recover from the surgery, we sacrificed the mice 7 days post Ctb injection to harvest the ganglia for immunostaining and imaging. Leptin treatment of the animals were conducted between 3-7 days post Ctb injection. From all the sympathetic chain, we specifically collected stellate/T1 and T12 ganglia to check for leptin induced changes, because the stellate/T1 and T12 ganglia are the ones containing the greatest number of BAT or iWAT innervating cells accordingly (Figure 5.6). In addition, the stellate and T12 ganglia can be easily identified according to their location and morphology, ensuring consistent sample collection across animals. The entire ganglia samples were then permeabilized and stained with anti-Fos antibody, a canonical neural plasticity marker, to reveal leptin's effect on postganglionic neurons.

Previous study, conducting sympathetic nerve recordings, showed that single leptin injection leads increased sympathetic activity to both BAT and iWAT within hours (Harlan et al. 2011a; Rahmouni and Morgan 2007; Bell et al. 2018). We first decided to test whether acute leptin treatment can cause plasticity changes in the WT ganglia. We gave WT mice a single injection of leptin (3mg/kg) or PBS as control on day 7 post Ctb injection (Figure 6.4 a) and sacrificed them 6hr post leptin injection to harvest the sympathetic ganglia. Afterwards, the ganglia were permeabilized and stained with anti-Fos antibody, followed by fluorescent confocal microscopy. To allow cell number quantification of the ganglia, we took stacked images of the entire stellate and T12 ganglia. From the analysis, we found that on a baseline level, WT animals do not have much Fos expressing neurons in either ganglia; neither does acute leptin treatment significantly upregulate Fos expression in these ganglia (Figure 6.4 b). This data show that, although acute leptin treatment increases sympathetic nerve activity, it is not sufficient to induce plasticity in these sympathetic neurons.

Next, we accessed whether leptin treatment for longer period time (3 days) induces neural plasticity in the ganglia. We first injected Ctb-568 into BAT and Ctb-488 into iWAT of WT mice, as described before; on Day 4 post Ctb injection we implanted an osmotic pump to the animals delivering leptin at the rate of 500ng/hr or PBS as control; on Day 7 we sacrificed the animals to

**Figure 6.4. Long-term leptin treatment activates postganglionic neurons in WT mice.**

(a-d) To quantify the number of Fos positive cells among the fat innervating postganglionic neurons, we injected Ctb-568 into BAT (1uL Ctb into 4 different sites) and simultaneously injected Ctb-488 into iWAT (1.5uL Ctb into 6 different sites) of WT mice to label the fat innervating neurons. All animals were sacrificed on Day 7 post Ctb injection for sufficient Ctb labeling of ganglia. (a) To reveal the effects of acute leptin treatment on sympathetic ganglia, on Day 7 post Ctb injection, WT mice receive a single injection of either PBS or Leptin (3mg/kg). To access the effects of acute leptin treatment on the ganglia, animals were sacrificed 6hr post injection and the sympathetic ganglia were dissected, stained with anti-Fos antibody and imaged using confocal microscopy. Representative images of the stellate ganglion (innervating BAT) are shown in the top row, and T13 (innervating iWAT) are shown in the bottom row. PBS treated ganglia were on the left, leptin treatment ganglia were on the right. Ctb-568 labeled neurons are in Red, Ctb-488 labeled neurons are in Green, Fos expressing neurons are in Grey. (b) Quantification of images in (a). The Y axis stands for the percentage Fos expressing cells over all the Ctb+ cells. Left side is the quantification of Fos expressing neurons in BAT innervating stellate/T1 ganglion, and the right side is Fos expressing neurons in iWAT innervating T13 ganglion. (c) On Day 4 post Ctb injection, WT mice were implanted with a subcutaneous osmotic pump delivering either PBS or Leptin (500ng/hr). To access the effects of long-term leptin treatment on the ganglia, all animals were sacrificed 3-day post pump implantation (on Day 7 post Ctb injection) and the sympathetic ganglia were dissected, stained with anti-Fos antibody and imaged using confocal microscopy. Representative images of the stellate ganglion (innervating BAT) are shown in the top row, and T13 (innervating iWAT) are shown in the bottom row. PBS treated ganglia were on the left, leptin treatment ganglia were on the right. Ctb-568 labeled neurons are in Red, Ctb-488 labeled neurons are in Green, Fos expressing neurons are in Grey. (d) Quantification of the images shown in (c). Left side is the quantification of Fos expressing neurons in BAT innervating stellate/T1 ganglion, and the right side is Fos expressing neurons in iWAT innervating T13 ganglion. Leptin treatment for 3 days significantly activates both BAT and iWAT innervating ganglia in WT mice. Scale bar: 100um.

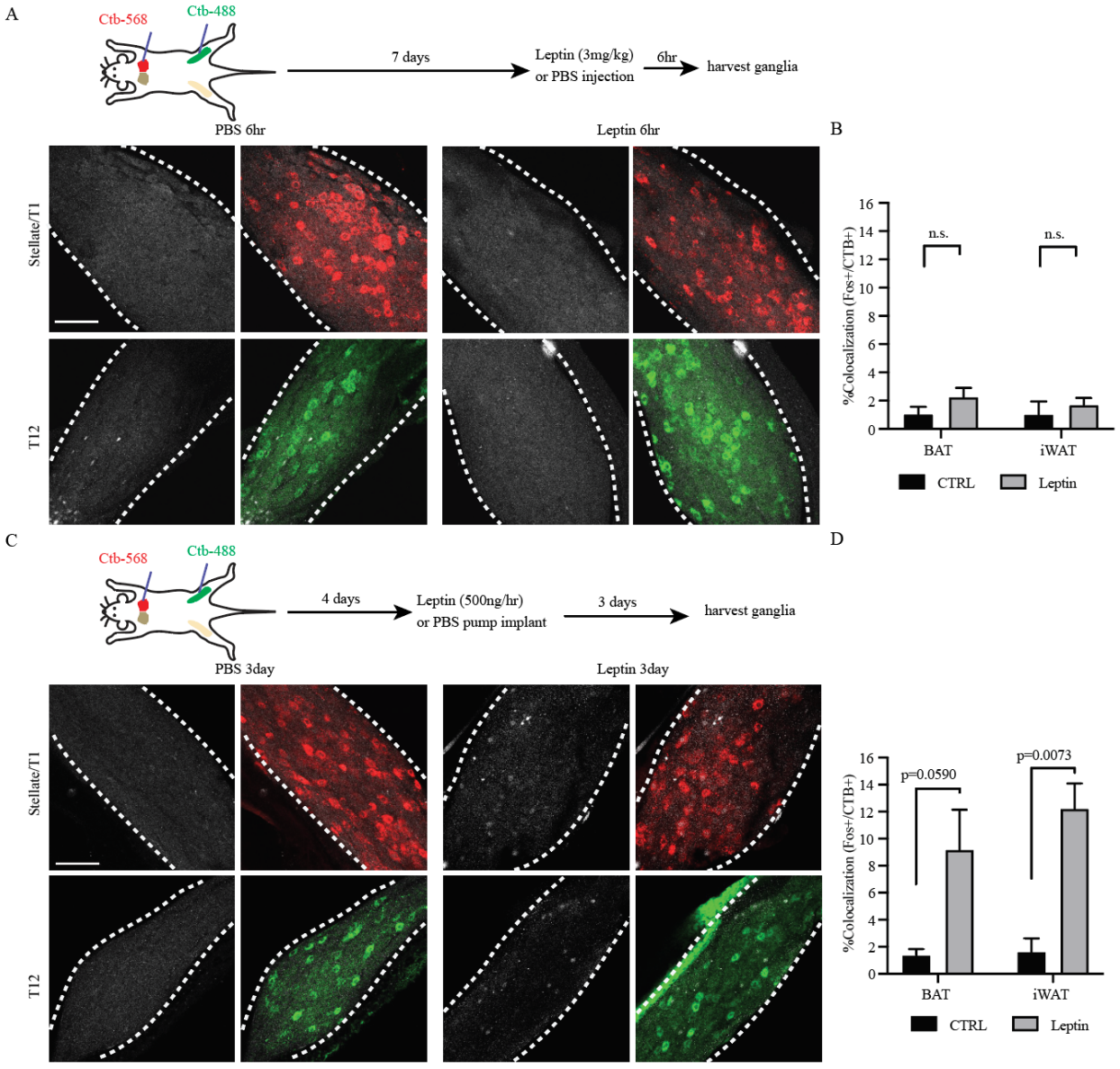


**Figure 6.4. Long-term leptin treatment activates postganglionic neurons in WT mice.**

harvest the ganglia, followed by immunostaining and imaging (Figure 6.4 c). Similar as observed in actuate PBS treated ganglia, chronic PBS treated animals does not introduce Fos activation in either stellate or T12 ganglion (Figure 6.4 c). However, chronic leptin treatment significant activated Fos in both ganglia. Following leptin treatment for 3 days, the percentage of Fos positive neurons over Ctb expressing neurons increased from 1.4% to 9.2% in BAT innervating ganglion, from 1.6% to 12.2% in iWAT innervating ganglion (Figure 6.4 d). Taken together, these data suggest that leptin induces plasticity in the sympathetic ganglia only after chronic treatment. In WT mice, 3 days of leptin treatment is sufficient to induce sympathetic neural plasticity.

### 6.4.2. Leptin's effects on *ob/ob* ganglia

After revealing the dynamics of leptin's effects on the fat innervating sympathetic ganglia in WT mice, we set out to perform similar experiments in *ob/ob* animals. Previous results on WT mice indicate that leptin only starts to induce plasticity changes in the ganglia 3 days post treatment (Figure 6.4). Therefore, we decided to first harvest the ganglia from *ob/ob* mice between 3 days post leptin treatment to check for plasticity changes in the ganglia. We delivered leptin (400ng/hr) or PBS as control to *ob/ob* mice through an osmotic pump. We sacrificed animals to harvest the ganglia 3 days post leptin treatment (Figure 6.5 a). Similar as in WT mice, we dissected out stellate/T1 and T12 ganglia for imaging. In this experiment, ganglia were fixed in 4% PFA for 2 hours, cryoprotected in 25% sucrose, and embedded in OTC for sectioning. Ganglia were sectioned into 15um slides, co-stained with TH and Fos antibodies, and imaged with fluorescent confocal microscopy. We found that there is very low number of Fos expressing neurons in either stellate or T12 ganglia of PBS treated *ob/ob* mice. To our surprise, leptin treatment of 3 days did not upregulate Fos expression in either ganglia in *ob/ob* mice (Figure 6.5 b).

Since the central leptin circuit plasticity might be different between WT and *ob/ob* mice, it might take longer for leptin to induce sympathetic plasticity in *ob/ob* mice. Therefore, we next treated *ob/ob* mice for 14 days, at which time the sympathetic innervation level in ob/ob mice is restored to WT levels. The sympathetic ganglia were processed the same way as mentioned above. At 14-day post leptin treatment, we found that leptin significantly upregulates the number of Fos expressing neurons in both ganglia. We quantified the percentage of Fos expressing cells over the TH expressing neurons, and show that in the stellate/T1 ganglia, there are around 21.7% TH neurons expressing Fos following 14-day leptin treatment compared to 0.3% following PBS treatment; in the T12 ganglion, there are 10.7% TH neurons expressing Fos following 14-day leptin treatment compared to 1.5% following PBS treatment (Figure 6.5 c).

**Figure 6.5. Chronic leptin treatment induces neural plasticity in *ob/ob* ganglia.**

(a) Scheme describing leptin or PBS delivery in *ob/ob* mice. Leptin was delivered through a subcutaneous osmotic pump at rate of 400ng/hr for 3 or 14 days. (b) Animals were sacrificed 3 days post leptin treatment, and stellate/T1 and T13 ganglia were dissected out, fixed, cryoprotected in 25% sucrose, and imbedded in OCT for sectioning. Ganglia were section into 15um slides, co-stained with anti-Fos and anti-TH antibody, followed by fluorescent confocal imaging. Representative images of the stellate/T1 ganglia were shown in the left, and the images of T13 were shown on the right. Channel with Fos (in green) is shown on the top row and overlap between Fos and TH channel (in Red) were shown on the bottom row. Contour of the ganglia is labeled by white dashed lines. Leptin treatment for 3 days does not upregulate Fos expression in *ob/ob* ganglia. (c) Animals were sacrificed 14 days post leptin treatment, and stellate/T1 and T13 ganglia were dissected out and imaged. Representative images of the stellate/T1 ganglia were shown in the left, and the images of T13 were shown on the right. Channel with Fos (in green) is shown on the top row and overlap between Fos and TH channel (in Red) were shown on the bottom row. Quantification of the images is shown on the right side. Y axis stands for the % of Fos expressing cell over TH expression sympathetic neurons. There are significantly higher percentage of Fos expressing sympathetic neurons in both ganglia in leptin treated (in Red) *ob/ob* mice compared to PBS treated ones (in Blue) (n=3 for all condition except leptin treated STGs, n=4). Scale bar, 100um.

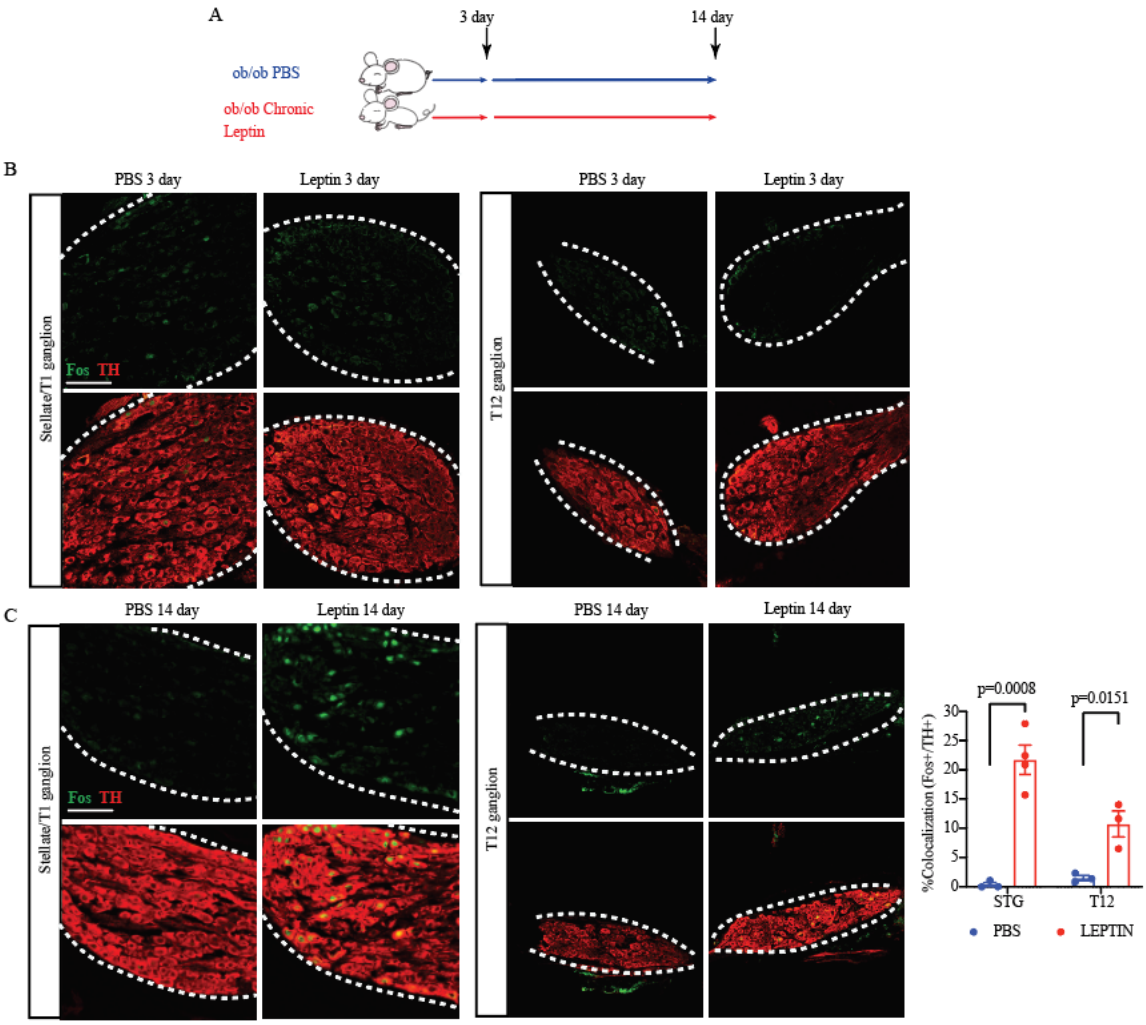


**Figure 6.5. Chronic leptin treatment induces neural plasticity in *ob/ob* ganglia.**

### 6.4.3. Summary

The data from this section demonstrate that chronic leptin treatment induces neural plasticity, shown by Fos activation, in the sympathetic postganglionic neurons of both WT and *ob/ob* mice. However, it takes much longer for leptin to induce plasticity changes, 14 days vs. 3 days, in sympathetic neurons of *ob/ob* mice compared to WT mice. According to our model in Figure 4.7, leptin signaling activates sympathetic neurons through a brain mediated pathway. The connectivity between each node of this leptin dependent CNS-SNS pathway might be different between WT and *ob/ob* mice, which might help explain why leptin activates sympathetic neurons in these animals on a different time scale.

In the future experiment, we will be treating *ob/ob* mice with leptin or PBS and assay for transcriptional cell state changes through single cell sequencing approaches. Since Fos is activated in the sympathetic ganglia between 3-14 days post leptin treatment, the transcriptional profiles within these cells are transforming during this period. Therefore, we will be taking ganglia from *ob/ob* mice for single cell analysis during this period, ideally at multiple time points.

## 6.5. Ongoing experiments

Besides the baseline atlas of WT sympathetic neurons, we will repeat the experiment in *ob/ob* mice. The experimental protocol, including Cell Hashing step, will be identical to that used for WT sample preparation (Figure 6.6 a). With the result from both WT and *ob/ob* baseline sequencing, we can compare the cell type diversities between the two mouse lines. Since we know that fat innervating neurons in the *ob/ob* mice have much less axons in the tissue, we expect to see big cell state differences, or maybe cell type differences, in the sympathetic ganglia of the two mouse lines.

In order to reveal the molecular identities of the sympathetic neurons innervating fat, we will then couple single cell sequencing experiment with retrograde Ctb tracing. Briefly, we will inject Ctb into both BAT and iWAT, and then sort out BAT and iWAT innervating neurons separately, label them with different Hashtag antibodies, and pull samples together for sequencing (Figure 6.6 b). In this experiment, we will be labeling iWAT and BAT innervating neurons from WT and *ob/ob* mice with Hashtag antibodies with 4 unique barcodes. This experiment will provide us information about the cellular diversities on the fat innervating neurons in both WT and *ob/ob* mice. By mapping the target specific dataset back to the baseline, unbiased sympathetic cell type data, we will can potentially answer whether there is target specific sympathetic pathways at the postganglionic neuron level.

Finally, we are interested in identifying the plasticity changes in the sympathetic ganglia, especially the ones directly innervating fat tissues, upon leptin treatment (Figure 6.6 c). We will treat *ob/ob* mice with leptin or PBS and subsequently dissociate and sequence the ganglia cells to reveal the transcriptional stage change of each cell type. Based on our data in Figure 6.5, we plan to sequence the sympathetic ganglia seven days post leptin treatment to reveal transcriptional cell state changes induced by leptin. We hope to identify cell type specific molecular pathways, in the fat innervating neurons, that are involved in promoting sympathetic axon target innervation. In addition, we hope to target these pathways using genetic or pharmacological approaches to promote SNS innervation in fat tissues independently of leptin. If this can be achieved, therapeutically targeting these pathways would present huge potential for the treatment of obesity.

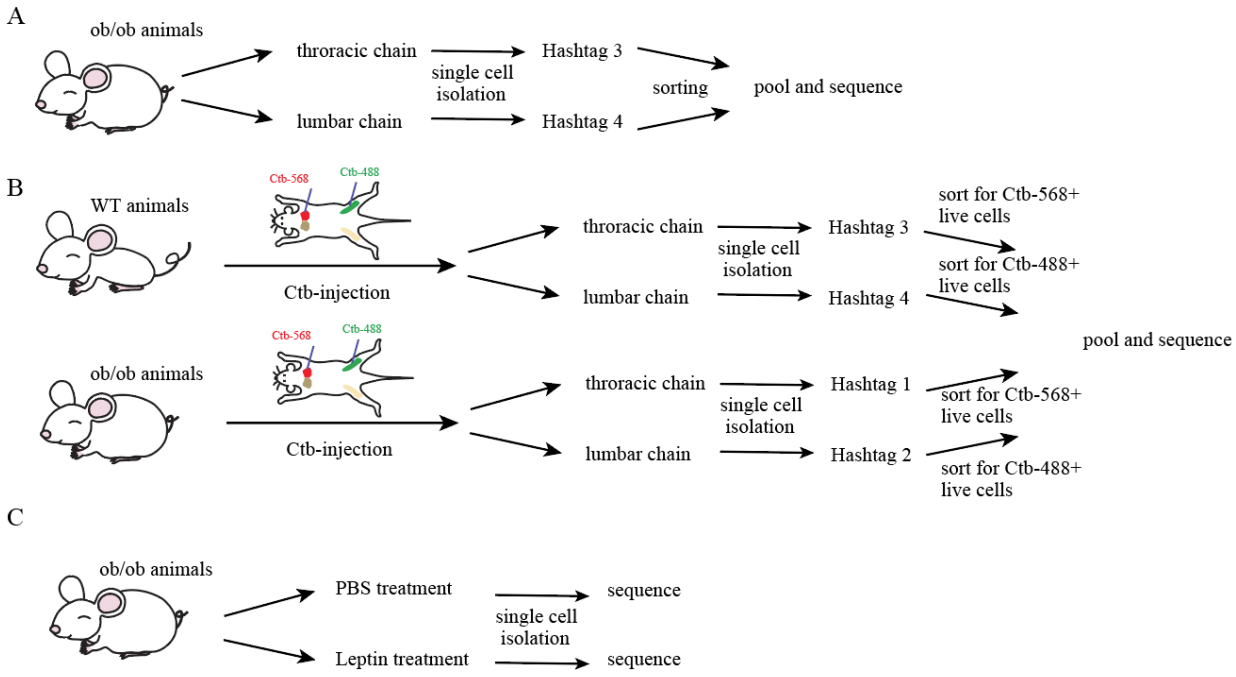


**Figure 6.6. Ongoing experiments.**

(a) Scheme describing baseline sympathetic ganglia sequencing of *ob/ob* mice. (b) Scheme describing the experimental plan for fat innervating neurons sequencing. Ctb-568 and Ctb-488 were injected into BAT and iWAT of WT and *ob/ob* mice. Seven days after Ctb injection, single cells were dissociated from the ganglia, and incubated with Hashtag antibodies with 4 unique oligonucleotide barcodes as indicated in the scheme. Samples then pooled for sequencing. (c) Scheme describing single cell sequencing experiment on *ob/ob* mice following chronic leptin or PBS control treatment.

## 6.6. Material and methods

### *Single cell dissociation and Cell Hashing*

Perfusion buffer (pH = 7.35):
HBSS (Millipore, H6648) + TTX (1uM; Tocris, 1069) + AP-5 (100uM; Hello Bio, 0105)

Dissociation buffer Step 1 (pH = 7.35):
HBSS + HEPES (10 mM, Millipore, H0887) + MgCl (4 mM, ThermoFisher, AM9530G) + d-Glucose (6.3 g/L, Millipore, G7021) + TTX (1uM) + AP-5 (100uM) + actinomycin (5 mg/mL; Sigma, A1410) + anisomycin (10 mg/mL; Sigma, A9789) + EDTA (0.5 mM, Millipore, 03690) + L-cysteine (1 mM, Sigma, A8199)

Dissociation buffer Step 2 (pH = 7.35):
HBSS + HEPES (10 mM) + MgCl (4 mM) + d-Glucose (6.3 g/L) + TTX (1uM) + AP-5 (100uM) + actinomycin (5 mg/mL) + anisomycin (10 mg/mL)

Single cell suspension buffer (pH = 7.35):
DMEM:F12 (ThermoFisher, 11-039-021) + pen/strep (1%) + d-Glucose (12.5 mM) + BSA (0.2%) + TTX (1uM) + AP-5 (100uM)

Tube coating buffer:
DMEM:F12 + pen/strep (1%) + d-Glucose (12.5 mM) + BSA (1%)

Procedures:

- Animals were perfused with ice old, oxygenated perfusion buffer.
- Fine dissections were performed to removed stellate/upper thoracic chain ganglia (thoracic sample), and lower thoracic/lumbar ganglia (lumbar sample) into oxygenated perfusion buffer.
- Attached tissue/fat were removed from ganglia, and place thoracic and lumbar samples separately into tubes filled with oxygenated dissociation buffer Step 1, cap well and store on ice.
- After all dissection and sample cleaning were finished, ganglia were transferred into 10KD cassette, filled with dissociation buffer Step 1 supplemented with sufficient Pappin (50 U for 2 animals; Worthington, LK003150) and DNase (Worthington, LK003150). Incubate at 37-degree water bath with oxygenation for 30min.
- Cassettes with sample were transfer into Dissociation buffer Step 2 supplemented with collagenase (5 mg/mL; Worthington, LS004186) + dispase (4 U/ mL; Worthington, LS002100). Incubate at 37-degree water bath with oxygenation for 30min.
- Ganglia were gently triturated with p1000 at 15 min and 30min after incubation with collagenase and dispase.
- Sample were filtered through 40 um filter into pre-coated 15 mL conical tubes, and spined at 100g for 5 min at 4-degree,
- Digestion were quenched with 20 mg/ml ovomucoid (Worthington, LK003150) in single cell suspension buffer, at volume of 100 uL.

- Cell numbers in each sample were counted and stained with Hashing antibodies (BioLegend, 155835 & 155837) at a concentration of 1ug/ 10^6 cells in 100 uL volume, for 20 min on ice.
- More single cell suspension buffer (~4 mL) was added to the sample to stop the staining.
- Sample were centrifuge at 100 g for 5 min at 4-degree to wash off the Hashtag antibody.
- After centrifugation, cells were resuspended in 250 uL of single cell suspension buffer.
- Around 1/10 of the cells were separated before staining as negative control.
- Samples were stained with DRAQ7 (1:100; Abcam, ab109202) and Calcein Violet (1:200 dilution of working solution which is 1:32 dilution of the stock, ThermoFisher, C34858).

***Sympathetic ganglia immunostaining***

For the Fos staining in the Ctb injected ganglia in Figure 6.4, the entire ganglia were used for staining. After fixation, ganglia were washed with PBS for 4 times, and permeabilized in PBS with 0.5% Triton X-100 overnight at 4 °C, blocked in PTwH buffer (PBS/0.1% Triton X-100/0.05% Tween 20/ 2 mg/ml heparin) for 4 hours, and incubated with primary antibody anti-Fos (1:1000; Cell Sign- aling Technologies, 2250S) for 48 hours at 4 °C. Ganglia were washed 4 times in PTxwH at room temperature and then stained with secondary antibody conjugated with Alexa-647 for 48 hours at 4 °C (1:1000, Invitrogen). Lastly, ganglia were washed 4 times in PTxwH, mounted onto SuperFrost (Fisher Scientific 22-034- 980) slides on and coverslipped for imaging with inverted Zeiss LSM 780 laser scanning confocal microscope. Z-stack images of the ganglia were taken to capture the entire ganglia. All images were analyzed in Image-J. For Fos quantitation, images were first threshold for staining intensity, Fos+ nuclei were defined as morphologically circular, the number of positive cells was then counted by an observer blind to the sample identity.

For Fos staining in the *ob/ob* ganglia in Figure 6.5, the ganglia were cryo-sectioned for imaging. After fixation, ganglia were washed with PBS for 4 times, and cryoprotected in 25% sucrose in PBS for 2 hours, and flash frozen in optimal cutting temperature (OCT) compound. Next, 15-µm sections of stellate or T12 ganglia were sliced on a cryostat and directly mounted onto SuperFrost (Fisher Scientific 22-034- 980) slides and stored at -20 °C before immunostaining. For staining, sample were washed and permeabilized in PBS with 0.1% Triton X-100 (PBST, pH 7.4) for at least 30min, and blocked in PBST and blocked in 3% normal donkey serum (Jackson ImmunoResearch Laboratories) and 2% BSA (Sigma) in PBST for 2 h. Hydrophobic circles were drawn over the ganglia samples on the slides, and samples were incubated in primary antibody rabbit anti-Fos (1:1000; Cell Sign- aling Technologies, 2250S) and sheep anti-TH (1:500; ab1542, Millipore) overnight at room temperature. The next day, samples were washed in PBST for 3 times and incubated with secondary antibody conjugated with Alexa-488, 568 or 547 (1:1000; Invitrogen) for 2 hours at room temperature. Lastly, slides were washed 4 times in PBST and coverslipped for imaging with inverted Zeiss LSM 780 laser scanning confocal microscope using x20 lens. To quantitate the number of TH or Fos stained cells, images were first threshold for staining intensity, the number of positive cells was then counted by an observer blind to the sample identity.

## REFERENCES


Ahima, Rexford S, and Jeffrey S Flier. 2000. "Leptin." *Annu. Rev. Physiol.* 62: 413–37.

Ahima, Rexford S, Daniel Prabakaran, Christos Mantzoros, Daqing Qut, Bradford Lowell, Eleftheria Maratos-fliert, and Jeffrey S Flier. 1996. "Role of Leptin in the Neuroendocrine Response to Fasting" 382 (July): 1995–97.

An, Juan Ji, Guey-Ying Liao, Clint E. Kinney, Niaz Sahibzada, and Baoji Xu. 2015. "Discrete BDNF Neurons in the Paraventricular Hypothalamus Control Feeding and Energy Expenditure." *Cell Metabolism* 22 (1): 175–88. https://doi.org/10.1016/J.CMET.2015.05.008.

Balthasar, Nina, Roberto Coppari, Julie McMinn, Shun M Liu, Charlotte E Lee, Vinsee Tang, Christopher D Kenny, et al. 2004. "Leptin Receptor Signaling in POMC Neurons Is Required for Normal Body Weight Homeostasis." *Neuron* 42 (6): 983–91. https://doi.org/10.1016/j.neuron.2004.06.004.

Bartness, Timothy J., and C. Kay Song. 2005. "Innervation of Brown Adipose Tissue and Its Role in Thermogenesis." *Canadian Journal of Diabetes* 29 (4): 420–28.

Bartness, Timothy J, Yang Liu, Yogendra B Shrestha, and Vitaly Ryu. 2014. "Frontiers in Neuroendocrinology Neural Innervation of White Adipose Tissue and the Control of Lipolysis Q." *Frontiers in Neuroendocrinology* 35 (4): 473–93. https://doi.org/10.1016/j.yfrne.2014.04.001.

Bartness, Timothy J, and George N Wade. 1984. "Effects of Interscapular Brown Adipose Tissue Denervation on Body Weight and Energy Metabolism in Ovariectomized and Estradiol-Treated Rats" 9 (4): 674–85.

Baver, S. B., K. Hope, S. Guyot, C. Bjorbaek, C. Kaczorowski, and K. M. S. O'Connell. 2014. "Leptin Modulates the Intrinsic Excitability of AgRP/NPY Neurons in the Arcuate Nucleus of the Hypothalamus." *Journal of Neuroscience* 34 (16): 5486–96. https://doi.org/10.1523/JNEUROSCI.4861-12.2014.

Bell, Balyssa B., Shannon M. Harlan, Donald A. Morgan, Deng Fu Guo, and Kamal Rahmouni. 2018. "Differential Contribution of POMC and AgRP Neurons to the Regulation of Regional Autonomic Nerve Activity by Leptin." *Molecular Metabolism* 8 (December 2017): 1–12. https://doi.org/10.1016/j.molmet.2017.12.006.

Biag, Jonathan, Yi Huang, Lin Gou, Houri Hintiryan, Asal Askarinam, Joel D. Hahn, Arthur W. Toga, and Hong Wei Dong. 2012. "Cyto- and Chemoarchitecture of the Hypothalamic Paraventricular Nucleus in the C57BL/6J Male Mouse: A Study of Immunostaining and Multiple Fluorescent Tract Tracing." *Journal of Comparative Neurology* 520 (1): 6–33. https://doi.org/10.1002/cne.22698.

Breslow, Michael J., Kyoung Min-Lee, Daniel R. Brown, V. P. Chacko, David Palmer, and Dan E. Berkowitz. 1999. “Effect of Leptin Deficiency on Metabolic Rate in Ob/Ob Mice.” *American Journal of Physiology - Endocrinology and Metabolism* 276 (3 39-3): 443–49. https://doi.org/10.1152/ajpendo.1999.276.3.e443.

Callaway, Edward M. 2008. “Transneuronal Circuit Tracing with Neurotropic Viruses.” *Current Opinion in Neurobiology*. https://doi.org/10.1016/j.conb.2009.03.007.

Callaway, X Edward M, and Liqun Luo. 2015. “Monosynaptic Circuit Tracing with Glycoprotein-Deleted Rabies Viruses” 35 (24): 8979–85. https://doi.org/10.1523/JNEUROSCI.0409-15.2015.

Cazorla, Maxime, Joël Prémont, Andre Mann, Nicolas Girard, Christoph Kellendonk, and Didier Rognan. 2011. “Identification of a Low-Molecular Weight TrkB Antagonist with Anxiolytic and Antidepressant Activity in Mice.” *Journal of Clinical Investigation*. https://doi.org/10.1172/JCI43992.

CDC. 2019. “Data & Statistics of Obesity.” 2019. https://www.cdc.gov/obesity/data/index.html.

Chen, Hong, Olga Charlat, Louis A. Tartaglia, Elizabeth A. Woolf, Xun Weng, Stephen J. Ellis, Nathan D. Lakey, et al. 1996. “Evidence That the Diabetes Gene Encodes the Leptin Receptor: Identification of a Mutation in the Leptin Receptor Gene in Db/Db Mice.” *Cell*. https://doi.org/10.1016/S0092-8674(00)81294-5.

Chi, Jingyi, Zhuhao Wu, Chan Hee J Choi, Lily Nguyen, Saba Tegegne, Sarah E Ackerman, Audrey Crane, François Marchildon, Marc Tessier-Lavigne, and Paul Cohen. 2018. “Three-Dimensional Adipose Tissue Imaging Reveals Regional Variation in Beige Fat Biogenesis and PRDM16-Dependent Sympathetic Neurite Density.” *Cell Metabolism* 27 (1): 226-236.e3. https://doi.org/10.1016/j.cmet.2017.12.011.

Clément, Karine, Christian Vaisse, Najiba Lahlou, Sylvie Cabrol, Veronique Pelloux, Dominique Cassuto, Micheline Gourmelen, et al. 1998. “A Mutation in the Human Leptin Receptor Gene Causes Obesity and Pituitary Dysfunction.” *Nature*. https://doi.org/10.1038/32911.

Cone, Roger D. 1999. “The Central Melanocortin System and Energy Homeostasis.” *Trends in Endocrinology and Metabolism*. https://doi.org/10.1016/S1043-2760(99)00153-8.

Cowley, Michael A., James L. Smart, Marcelo Rubinstein, Marcelo G. Cerdán, Sabrina Diano, Tamas L. Horvath, Roger D. Cone, and Malcolm J. Low. 2001. “Leptin Activates Anorexigenic POMC Neurons through a Neural Network in the Arcuate Nucleus.” *Nature* 411 (6836): 480–84. https://doi.org/10.1038/35078085.

Deuchars, Susan A, and Varinder K Lall. 2015. “Sympathetic Preganglionic Neurons : Properties and Inputs” 5 (April): 829–69. https://doi.org/10.1002/cphy.c140020.

Dhillon, Harveen, Jeffrey M Zigman, Chianping Ye, Charlotte E Lee, Robert A McGovern, Vinsee Tang, Christopher D Kenny, et al. 2006. "Leptin Directly Activates SF1 Neurons in the VMH, and This Action by Leptin Is Required for Normal Body-Weight Homeostasis." *Neuron* 49 (2): 191–203. https://doi.org/10.1016/j.neuron.2005.12.021.

Elmquist, J. K., E. Maratos-Flier, C. B. Saper, and J. S. Flier. 1998. "Unraveling the Central Nervous System Pathways Underlying Responses to Leptin." *Nature Neuroscience*. https://doi.org/10.1038/2164.

Enriori, P. J., P. Sinnayah, S. E. Simonds, C. Garcia Rudaz, and M. A. Cowley. 2011. "Leptin Action in the Dorsomedial Hypothalamus Increases Sympathetic Tone to Brown Adipose Tissue in Spite of Systemic Leptin Resistance." *Journal of Neuroscience* 31 (34): 12189–97. https://doi.org/10.1523/JNEUROSCI.2336-11.2011.

Farooqi, I Sadaf, Alex M Depaoli, Stephen O Rahilly, I Sadaf Farooqi, Giuseppe Matarese, Graham M Lord, Julia M Keogh, et al. 2002. "Beneficial Effects of Leptin on Obesity." *The Journal of Clinical Investigation* 110 (8): 1093–1103. https://doi.org/10.1172/JCI200215693.Introduction.

Feldmann, Helena M., Valeria Golozoubova, Barbara Cannon, and Jan Nedergaard. 2009. "UCP1 Ablation Induces Obesity and Abolishes Diet-Induced Thermogenesis in Mice Exempt from Thermal Stress by Living at Thermoneutrality." *Cell Metabolism*. https://doi.org/10.1016/j.cmet.2008.12.014.

Fischer, Alexander W., Carolin S. Hoefig, Gustavo Abreu-Vieira, Jasper M.A. de Jong, Natasa Petrovic, Jens Mittag, Barbara Cannon, and Jan Nedergaard. 2016. "Leptin Raises Defended Body Temperature without Activating Thermogenesis." *Cell Reports* 14 (7): 1621–31. https://doi.org/10.1016/j.celrep.2016.01.041.

François, Marie, Hayden Torres, Clara Huesing, Rui Zhang, Carson Saurage, Nathan Lee, Emily Qualls-Creekmore, et al. 2019. "Sympathetic Innervation of the Interscapular Brown Adipose Tissue in Mouse." *Annals of the New York Academy of Sciences* 1454 (1): 3–13. https://doi.org/10.1111/nyas.14119.

Friedman, Jeffrey M., and Jeffrey L. Halaas. 1998. "Leptin and the Regulation of Body Weight in Mammals." *Nature* 395 (6704): 763–70. https://doi.org/10.1038/27376.

Fujikawa, Teppei, Jen Chieh Chuang, Ichiro Sakata, Giorgio Ramadori, and Roberto Coppari. 2010. "Leptin Therapy Improves Insulin-Deficient Type 1 Diabetes by CNS-Dependent Mechanisms in Mice." *Proceedings of the National Academy of Sciences of the United States of America*. https://doi.org/10.1073/pnas.1008025107.

Furlan, Alessandro, Gioele La Manno, Moritz Lübke, Martin Häring, Hind Abdo, Hannah Hochgerner, Jussi Kupari, et al. 2016. "Visceral Motor Neuron Diversity Delineates a Cellular Basis for Nipple- and Pilo-Erection Muscle Control." *Nature Neuroscience* 19 (10): 1331–40. https://doi.org/10.1038/nn.4376.

Glebova, Natalia O., and David D. Ginty. 2005. “Growth and Survival Signals Controlling Sympathetic Nervous System Development.” *Annual Review of Neuroscience* 28: 191–222. https://doi.org/10.1146/annurev.neuro.28.061604.135659.

Guarino, Daniela, Monica Nannipieri, Giorgio Iervasi, Stefano Taddei, and Rosa Maria Bruno. 2017. “The Role of the Autonomic Nervous System in the Pathophysiology of Obesity.” *Frontiers in Physiology* 8 (SEP): 1–16. https://doi.org/10.3389/fphys.2017.00665.

Håkansson, Marie Louise, Hilary Brown, Nico Ghilardi, Radek C. Skoda, and Björn Meister. 1998. “Leptin Receptor Immunoreactivity in Chemically Defined Target Neurons of the Hypothalamus.” *Journal of Neuroscience*. https://doi.org/10.1523/jneurosci.18-01-00559.1998.

Halaas, Jeffrey L., Ketan S. Gajiwala, Margherita Maffei, Steven L. Cohen, Brian T. Chait, Daniel Rabinowitz, Roger L. Lallone, Stephen K. Burley, and Jeffrey M. Friedman. 1995. “Weight-Reducing Effects of the Plasma Protein Encoded by the Obese Gene.” *Science*. https://doi.org/10.1126/science.7624777.

Han, Joan C., Qing Rong Liu, Mary Pat Jones, Rebecca L. Levinn, Carolyn M. Menzie, Kyra S. Jefferson-George, Diane C. Adler-Wailes, et al. 2008. “Brain-Derived Neurotrophic Factor and Obesity in the WAGR Syndrome.” *New England Journal of Medicine*. https://doi.org/10.1056/NEJMoa0801119.

Harlan, Shannon M, Donald A Morgan, Khristofor Agassandian, Deng-fu Guo, Martin D Cassell, Curt D Sigmund, Allyn L Mark, and Kamal Rahmouni. 2011a. “Ablation of the Leptin Receptor in the Hypothalamic Arcuate Nucleus Abrogates Leptin-Induced.” https://doi.org/10.1161/CIRCRESAHA.111.240226.

Harlan, Shannon M, Donald A Morgan, Khristofor Agassandian, Deng-Fu Guo, Martin D Cassell, Curt D Sigmund, Allyn L Mark, and Kamal Rahmouni. 2011b. “Ablation of the Leptin Receptor in the Hypothalamic Arcuate Nucleus Abrogates Leptin-Induced Sympathetic Activation.” *Circulation Research* 108 (7): 808–12. https://doi.org/10.1161/CIRCRESAHA.111.240226.

Himms-Hagen, J. 1985. “Defective Brown Adipose Tissue Thermogenesis in Obese Mice.” *International Journal of Obesity* 9 Suppl 2: 17–24.

Kaiyala, Karl J., Kayoko Ogimoto, Jarrell T. Nelson, Kenjiro Muta, and Gregory J. Morton. 2016. “Physiological Role for Leptin in the Control of Thermal Conductance.” *Molecular Metabolism*. https://doi.org/10.1016/j.molmet.2016.07.005.

Levin, N, C Nelson, A Gurney, R Vandlen, and F de Sauvage. 1996. “Decreased Food Intake Does Not Completely Account for Adiposity Reduction after Ob Protein Infusion.” *Proceedings of the National Academy of Sciences of the United States of America* 93 (4): 1726–30.

Liao, Guey Ying, Juan Ji An, Kusumika Gharami, Emily G. Waterhouse, Filip Vanevski, Kevin R. Jones, and Baoji Xu. 2012. "Dendritically Targeted Bdnf MRNA Is Essential for Energy Balance and Response to Leptin." *Nature Medicine* 18 (4): 564–71. https://doi.org/10.1038/nm.2687.

Ly, Ngoc, T Nguyen, Candace L Barr, Vitaly Ryu, Qiang Cao, Bingzhong Xue, and Timothy J Bartness. n.d. "Separate and Shared Sympathetic Outflow to White and Brown Fat Coordinately Regulates Thermoregulation and Beige Adipocyte Recruitment." Accessed February 26, 2018. http://www.physiology.org/doi/pdf/10.1152/ajpregu.00344.2016.

Mayoclinic. 2020. "Diagnosis and Treatment of Obesity." 2020.

McCorry, Laurie Kelly. 2007. "PHYSIOLOGY OF THE AUTONOMIC NERVOUS SYSTEM." *American Journal OfPharmaceutical Education* 71 (4). http://doi.wiley.com/10.1111/j.1399-6576.1964.tb00252.x.

Montague, Carl T., I. Sadaf Farooqi, Jonathan P. Whitehead, Maria A. Soos, Harald Rau, Nicholas J. Wareham, Ciaran P. Sewter, et al. 1997. "Congenital Leptin Deficiency Is Associated with Severe Early-Onset Obesity in Humans." *Nature*. https://doi.org/10.1038/43185.

Morrison, Shaun F., Christopher J. Madden, and Domenico Tupone. 2014. "Central Neural Regulation of Brown Adipose Tissue Thermogenesis and Energy Expenditure." *Cell Metabolism* 19 (5): 741–56. https://doi.org/10.1016/j.cmet.2014.02.007.

Münzberg, Heike, Jeffrey S. Flier, and Christian Bjørbæk. 2004. "Region-Specific Leptin Resistance within the Hypothalamus of Diet-Induced Obese Mice." *Endocrinology* 145 (11): 4880–89. https://doi.org/10.1210/en.2004-0726.

Nakamura, Kazuhiro, Kiyoshi Matsumura, Thomas Hübschle, Yoshiko Nakamura, Hiroyuki Hioki, Fumino Fujiyama, Zsolt Boldogköi, et al. 2004. "Identification of Sympathetic Premotor Neurons in Medullary Raphe Regions Mediating Fever and Other Thermoregulatory Functions." *The Journal of Neuroscience : The Official Journal of the Society for Neuroscience* 24 (23): 5370–80. https://doi.org/10.1523/JNEUROSCI.1219-04.2004.

Navarro, X., Meritxell Vivó, and Antoni Valero-Cabré. 2007. "Neural Plasticity after Peripheral Nerve Injury and Regeneration." *Progress in Neurobiology* 82 (4): 163–201. https://doi.org/10.1016/j.pneurobio.2007.06.005.

Nonomura, T., A. Tsuchida, M. Ono-Kishino, T. Nakagawa, M. Taiji, and H. Noguchi. 2001. "Brain-Derived Neurotrophic Factor Regulates Energy Expenditure through the Central Nervous System in Obese Diabetic Mice." *International Journal of Experimental Diabetes Research* 2 (3): 201–9. https://doi.org/10.1155/EDR.2001.201.

Pandit, R., S. Beerens, and R. A. H. Adan. 2017a. “Role of Leptin in Energy Expenditure: The Hypothalamic Perspective.” *American Journal of Physiology - Regulatory, Integrative and Comparative Physiology* 312 (6): R938–47. https://doi.org/10.1152/ajpregu.00045.2016.

Pandit, R., S. Beerens, and R. A.H. Adan. 2017b. “Role of Leptin in Energy Expenditure: The Hypothalamic Perspective.” *American Journal of Physiology - Regulatory Integrative and Comparative Physiology* 312 (6): R938–47. https://doi.org/10.1152/ajpregu.00045.2016.

Paxinos, G, and K.B.J. Franklin. 2001. *The Mouse Brain in Stereotaxic Coordinates, 2nd Edition*. *Academic Press*.

Pelleymounter, Mary Ann, Mary Jane Cullen, Mary Beth Baker, Randy Hecht, Dwight Winters, Thomas Boone, and Frank Collins. 1995. “Effects of the Obese Gene Product on Body Weight Regulation in Ob/Ob Mice.” *Science* 269 (5223): 540–43. https://doi.org/10.1126/science.7624776.

Pomeranz, Lisa E., Mats I. Ekstrand, Kaamashri N. Latcha, Gregory A. Smith, Lynn W. Enquist, and Jeffrey M. Friedman. 2017. “Gene Expression Profiling with Cre-Conditional Pseudorabies Virus Reveals a Subset of Midbrain Neurons That Participate in Reward Circuitry.” *The Journal of Neuroscience* 37 (15): 4128–44. https://doi.org/10.1523/JNEUROSCI.3193-16.2017.

Rahmouni, Kamal, and Donald A. Morgan. 2007. “Hypothalamic Arcuate Nucleus Mediates the Sympathetic and Arterial Pressure Responses to Leptin.” *Hypertension* 49 (3 PART 2 SUPPL.): 647–52. https://doi.org/10.1161/01.HYP.0000254827.59792.b2.

Ranson, R. N., K. Motawei, S. Pyner, and J. H. Coote. 1998. “The Paraventricular Nucleus of the Hypothalamus Sends Efferents to the Spinal Cord of the Rat That Closely Appose Sympathetic Preganglionic Neurones Projecting to the Stellate Ganglion.” *Experimental Brain Research*. https://doi.org/10.1007/s002210050390.

Rattiner, Lisa M., Michael Davis, Christopher T. French, and Kerry J. Ressler. 2004. “Brain-Derived Neurotrophic Factor and Tyrosine Kinase Receptor B Involvement in Amygdala-Dependent Fear Conditioning.” *Journal of Neuroscience*. https://doi.org/10.1523/JNEUROSCI.5654-03.2004.

Rios, Maribel, F. A.N. Guoping, Csaba Fekete, Joseph Kelly, Brian Bates, Ralf Kuehn, Ronald M. Lechan, and Rudolf Jaenisch. 2001. “Conditional Deletion of Brain-Derived Neurotrophic Factor in the Postnatal Brain Leads to Obesity and Hyperactivity.” *Molecular Endocrinology*. https://doi.org/10.1210/mend.15.10.0706.

Seeley, Randy J., Keith A. Yagaloff, Stewart L. Fisher, Paul Burn, Todd E. Thiele, Gertjan van Dijk, Denis G. Baskin, and Michael W. Schwartz. 1997. “Melanocortin Receptors in Leptin Effects.” *Nature* 390 (6658): 349–349. https://doi.org/10.1038/37016.

Sharma, Nikhil, Kali Flaherty, Karina Lezgiyeva, Daniel E. Wagner, Allon M. Klein, and David D. Ginty. 2020. “The Emergence of Transcriptional Identity in Somatosensory Neurons.” *Nature* 577 (7790): 392–98. https://doi.org/10.1038/s41586-019-1900-1.

Spanswick, D., M. A. Smith, V. E. Groppi, S. D. Logan, and M. L.J. Ashford. 1997. “Leptin Inhibits Hypothalamic Neurons by Activation of ATP-Sensitive Potassium Channels.” *Nature*. https://doi.org/10.1038/37379.

Spiegelman, Bruce M, and Jeffrey S Flier. 2001. “Obesity and the Regulation Review of Energy Balance.” *Cell* 104: 531–43.

Stefanidis, Aneta, Nicole M. Wiedmann, Sonika Tyagi, Andrew M. Allen, Matthew J. Watt, and Brian J. Oldfield. 2018. “Insights into the Neurochemical Signature of the Innervation of Beige Fat.” *Molecular Metabolism* 11 (February): 47–58. https://doi.org/10.1016/j.molmet.2018.01.024.

Steinmetz, Jean, Linda Loway, and Terence T T Yen. 1969. “An Analysis of the Lipolysis in Vitro of 0bese-Hyperglycaemic and Diabetic Mice.” *Diabetologia*. Vol. 5.

Stoeckius, Marlon, Shiwei Zheng, Brian Houck-Loomis, Stephanie Hao, Bertrand Z. Yeung, William M. Mauck, Peter Smibert, and Rahul Satija. 2018. “Cell Hashing with Barcoded Antibodies Enables Multiplexing and Doublet Detection for Single Cell Genomics.” *Genome Biology* 19 (1): 1–12. https://doi.org/10.1186/s13059-018-1603-1.

Sutton, Amy K, Martin G. Myers, and David P Olson. 2016. “The Role of PVH Circuits in Leptin Action and Energy Balance.” *Annual Review of Physiology* 78 (1): 207–21. https://doi.org/10.1146/annurev-physiol-021115-105347.

Takeda, Shu, Florent Elefteriou, Regis Levasseur, Xiuyun Liu, Liping Zhao, Keith L. Parker, Dawna Armstrong, Patricia Ducy, and Gerard Karsenty. 2002. “Leptin Regulates Bone Formation via the Sympathetic Nervous System.” *Cell* 111 (3): 305–17. https://doi.org/10.1016/S0092-8674(02)01049-8.

Wang, Daqing, Xiaobing He, Zhe Zhao, Qiru Feng, Rui Lin, Yue Sun, Ting Ding, Fuqiang Xu, Minmin Luo, and Cheng Zhan. 2015. “Whole-Brain Mapping of the Direct Inputs and Axonal Projections of POMC and AgRP Neurons.” *Frontiers in Neuroanatomy*. https://doi.org/10.3389/fnana.2015.00040.

Wang, Putianqi, Ken H Loh, Michelle Wu, Donald A Morgan, Marc Schneeberger, Xiaofei Yu, Jingyi Chi, et al. 2020. “A Leptin – BDNF Pathway Regulating Sympathetic Innervation of Adipose Tissue.” *Nature* 583 (July). https://doi.org/10.1038/s41586-020-2527-y.

Xu, Baoji, Evan H. Goulding, Keling Zang, David Cepoi, Roger D. Cone, Kevin R. Jones, Laurence H. Tecott, and Louis F. Reichardt. 2003. “Brain-Derived Neurotrophic Factor Regulates Energy Balance Downstream of Melanocortin-4 Receptor.” *Nature Neuroscience*. https://doi.org/10.1038/nn1073.

Xu, Baoji, and Xiangyang Xie. 2016. “Neurotrophic Factor Control of Satiety and Body Weight.” *Nature Reviews Neuroscience* 17 (5): 282–92. https://doi.org/10.1038/nrn.2016.24.

Xu, Jie, Christopher L. Bartolome, Cho Shing Low, Xinchi Yi, Cheng-Hao Chien, Peng Wang, and Dong Kong. 2018. “Genetic Identification of Leptin Neural Circuits in Energy and Glucose Homeostases.” *Nature*. https://doi.org/10.1038/s41586-018-0049-7.

Yeo, Giles S.H., Chiao Chien Connie Hung, Justin Rochford, Julia Keogh, Juliette Gray, Shoba Sivaramakrishnan, Stephen O’Rahilly, and I. Sadaf Farooqi. 2004. “A de Novo Mutation Affecting Human TrkB Associated with Severe Obesity and Developmental Delay.” *Nature Neuroscience*. https://doi.org/10.1038/nn1336.

Zeng, Wenwen, Roksana M. Pirzgalska, Mafalda M A Pereira, Nadiya Kubasova, Andreia Barateiro, Elsa Seixas, Yi Hsueh Lu, et al. 2015. “Sympathetic Neuro-Adipose Connections Mediate Leptin-Driven Lipolysis.” *Cell* 163 (1): 84–94. https://doi.org/10.1016/j.cell.2015.08.055.

Zhang, Y., I. A. Kerman, A. Laque, P. Nguyen, M. Faouzi, G. W. Louis, J. C. Jones, C. Rhodes, and H. Munzberg. 2011. “Leptin-Receptor-Expressing Neurons in the Dorsomedial Hypothalamus and Median Preoptic Area Regulate Sympathetic Brown Adipose Tissue Circuits.” *Journal of Neuroscience* 31 (5): 1873–84. https://doi.org/10.1523/JNEUROSCI.3223-10.2011.

Zhang, Yiying, Ricardo Proenca, Margherita Maffei, Marisa Barone, Lori Leopold, and Jeffrey M. Friedman. 1994. “Positional Cloning of the Mouse Obese Gene and Its Human Homologue.” *Nature* 372 (6505): 425–32. https://doi.org/10.1038/372425a0.